NASA-CR-135293
PWA-5554-3

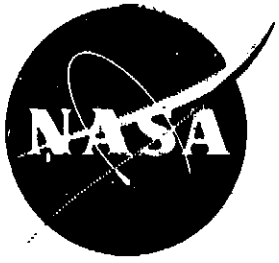

METHOD OF FAN SOUND MODE STRUCTURE DETERMINATION
FINAL REPORT

by

G. F. Pickett, T. G. Sofrin and R. A. Wells

August 1977

PRATT & WHITNEY AIRCRAFT GROUP
Commercial Products Division

prepared for

NATIONAL AERONAUTICS AND SPACE ADMINISTRATION

NASA-Lewis Research Center
Contract NAS3-20047

1. Report No.	2. Government Accession No.	3. Recipient's Catalog No.
NASA CR-135293		

4. Title and Subtitle	5. Report Date
Method of Fan Sound Mode Structure Determination Final Report	August 1977 6. Performing Organization Code
7. Author(s)	8. Performing Organization Report No.
G. F. Pickett, T. G. Sofrin, and R. W. Wells	PWA 5554-3 10. Work Unit No.
9. Performing Organization Name and Address Pratt & Whitney Aircraft Group Commercial Products Division United Technologies Corporation East Hartford, Connecticut 06108	11. Contract or Grant No. NAS3-20047
12. Sponsoring Agency Name and Address National Aeronautics and Space Administration Washington, D. C. 20546	13. Type of Report and Period Covered Contract Report 14. Sponsoring Agency Code
15. Supplementary Notes	

16. Abstract

This report presents a method for the determination of fan sound mode structure in the inlet of turbofan engines using in-duct acoustic pressure measurements. The method is based on the simultaneous solution of a set of equations whose unknowns are modal amplitude and phase. By deploying microphones equal in number to the number of modes to be calculated, the set of simultaneous equations can be solved for the amplitude and phase of each mode. A computer program for the solution of the equation set was developed. An additional computer program was developed which calculates microphone locations the use of which results in an equation set that does not give rise to numerical instabilities. Furthermore, by calculating a set of influence coefficients for each case considered, the method can be used to determine the sensitivity of the modal calculation procedure to errors in the knowledge of the measuring location and in the measured phase angles and pressure amplitudes. Also, an estimate can be obtained of the effect on the modal calculation procedure of extraneous modes not included in the modal calculation.

An experimental assessment is presented that shows that the method is reasonably accurate if either the number or the amplitudes of the extraneous modes are not too large. Based on this experimental assessment and an order-of-magnitude analysis of the influence coefficients, a procedure is presented that can be used to estimate the number of microphones and the accuracy of experimental measurements that would be required to achieve a specific accuracy in calculating the amplitudes and phases of the propagating coherent sound modes.

In addition to the development of a method for determination of coherent modal structure, experimental and analytical approaches are developed for the determination of the amplitude frequency spectrum of randomly generated sound modes for use in narrow annulus ducts. Two approaches are defined: one based on the use of cross-spectral techniques and the other based on the use of an array of microphones.

17. Key Words (Suggested by Author(s))	18. Distribution Statement
fan sound mode structures amplitude phase coherent sound modes extraneous sound modes	Unclassified - Unlimited

19. Security Classif. (of this report)	20. Security Classif. (of this page)	21. No. of Pages	22. Price*
Unclassified	Unclassified	164	

* For sale by the National Technical Information Service, Springfield, Virginia 22151

TABLE OF CONTENTS

TABLE OF CONTENTS (Cont'd)

LIST OF ILLUSTRATIONS

LIST OF ILLUSTRATIONS (Cont'd)

LIST OF TABLES

LIST OF TABLES (Cont'd)

METHOD OF FAN SOUND MODE STRUCTURE DETERMINATION FINAL REPORT

by

G. F. Pickett, T. G. Sofrin and R. A. Wells

1.0 SUMMARY

This report presents a method for the determination of fan sound mode structure in the inlet of turbofan engines using in-duct acoustic pressure measurements. The method is based on the simultaneous solution of a set of equations whose unknowns are modal amplitude and phase. By deploying microphones equal in number to the number of modes to be calculated, the set of simultaneous equations can be solved for the amplitude and phase of each mode. A computer program for the solution of the equation set was developed. An additional computer program was developed which calculates microphone locations the use of which results in an equation set that does not give rise to numerical instabilities. Furthermore, by calculating a set of influence coefficients for each case considered, the method can be used to determine the sensitivity of the modal calculation procedure to errors in the knowledge of the measuring location and in the measured phase angles and pressure amplitudes. Also, an estimate can be obtained of the effect on the modal calculation procedure of extraneous modes not included in the modal calculation.

An experimental assessment is presented that shows that the method is reasonably accurate if either the number or the amplitudes of the extraneous modes are not too large. Based on this experimental assessment and an order-of-magnitude analysis of the influence coefficients, a procedure is presented that can be used to estimate the number of microphones and the accuracy of experimental measurements that would be required to achieve a specific accuracy in calculating the amplitudes and phases of the propagating coherent sound modes.

In addition to the development of a method for determination of coherent modal structure, experimental and analytical approaches are developed for the determination of the amplitude frequency spectrum of randomly generated sound modes for use in narrow annulus ducts. Two approaches are defined: one based on the use of cross-spectral techniques and the other based on the use of an array of microphones.

2.0 INTRODUCTION

All modern high-bypass ratio, commercial transport engines incorporate noise reduction features in their design as evidenced by the blade-and-vane number selections in the fan sections of these engines. These selections along with other noise reducing features such as large blade-vane spacing, cycle selection, and improved acoustic treatment designs have resulted in significant reductions in aircraft noise compared with that from first-generation aircraft.

Despite these reductions, the aircraft industry is faced with legislative requirements to meet yet lower noise limits in the future. Also, because of the equally urgent requirement to lower fuel consumption, the impact on efficiency of new noise reducing features must be minimized.

Fan noise is predicted to be the dominant noise source for most advanced gas turbine engine designs. More specifically, fan tone noise at blade passing frequency (BPF) and its harmonics continues to be the most prominant spectral noise component from engines tested without inlet and aft duct acoustic suppression liners.

Fan tone noise can be generated by four different sources: 1) rotor wake-stator, or stator wake-rotor interaction, 2) rotor-strut, pylon, etc. potential field interactions, 3) rotor-turbulence and steady inflow distortion interactions, and 4) pressure field of the rotor alone. Experimental evidence suggests that randomly phased tone noise generated during ground static testing is caused by turbulent flows in the fan inlet that have very long axial length scales. These turbulent flows are believed to change in flight, resulting in greatly reduced turbulence intensities and length scales. These reductions significantly reduce the importance of rotor-turbulence interaction as an in-flight tone noise source, and is currently thought to explain the observations that flight fan tone noise levels from high bypass ratio turbofan engines are significantly lower than those measured during static engine tests. The remaining contribution to flight fan-tone-noise levels of randomly generated noise sources has yet to be determined. Broadband noise is, of course, generated by random noise sources and is becoming more of a contributor to overall flight fan noise levels as tone noise levels are reduced.

The dominant noise source in flight, however, is thought to be due to coherent acoustic fields generated by the pressure field of the rotor and the interaction of rotor wakes with stator vanes and vice versa. The former will be classified as "rotor locked" and is a significant source of multiple pure-tone inlet noise from fans operating at supersonic tip speeds. The latter noise source will be classified as "interaction tone" noise and can be significant, particularly for typical low-bypass-ratio turbofan engines, even at low subsonic fan tip speeds.

Fans for engines currently designed for conventional takeoff and landing (CTOL) aircraft (for example, the JT9D) exhibit acoustic duct modes generated by all of the above source types. These fans typically operate at supersonic tip speeds at takeoff (generating inlet radiated multiple pure tone noise), and at about sonic tip speeds during landing approach where, at least for the second harmonic of blade passing frequency and higher harmonics, the interaction tone mechanisms that lead to coherent modal structure are well cut on and dominate over the tone generated by the rotor/turbulence interaction, which leads to incoherent modal structure.

In all new fan designs, blade-vane interaction theory is exploited to the extent possible to minimize noise at blade passing frequency. This theory, based on an analysis that is constantly being refined, identifies the modes that can propagate, but it has not yet been developed to the extent that the amplitudes and phases of each of the propagating modes can be predicted reliably. Analytical models also exist for randomly generated tone noise and broadband noise due to rotor-inflow turbulence interaction. Again, these models identify the modes that can propagate, but are not sufficiently developed to predict reliably the expected amplitudes of the propagating modes.

Further tone and broadband noise reductions could be achieved through improved acoustic treatment design if the propagating modal structure could be quantified. Since reliable analytical predictions of modal structure are not likely to be available in the near future, a need exists to be able to measure reliably fan modal structures. These measured modal structures could then be used directly as input to analytical acoustic liner prediction systems, resulting in improved liner efficiency. The measured modal structure could also be used to check the developing theories for fan noise generation and to evaluate noise reduction design concepts. Once a valid fan noise generation model on a modal basis has been developed, it can be coupled with acoustic liner modal prediction systems so that fan and inlet treatments can be jointly optimized to minimize engine weight and performance losses while achieving specific fan noise goals.

The specific objectives of the work described in this report, and performed under NASA contract (NAS3-20047) at Pratt & Whitney Aircraft are to:

1) Develop and check out experimental and computational methods for the calculation of the amplitudes and phases of propagating coherent sound modes in the inlet of a turbofan engine using in-duct acoustic measurements as the calculation input.

2) Develop experimental and analytical methods for the determination of the expected amplitudes of propagating randomly generated sound modes in the inlet of a turbofan engine using in-duct acoustic measurements as the calculation input.

The report is organized as follows: In section 3.0 the overall program is described. After an overview of the program (section 3.1), an analytical method is presented for calculating coherent fan sound modal structures (section 3.2). In section 3.3 an analytical approach is presented for calculating random sound fields in ducts, and this is followed by an experimental assessment of the accuracy of the method for determining coherent fan sound modal structures (3.4). A discussion is then presented of the accuracy requirements for general application of the method for coherent sound fields (3.5) leading to an analysis of the method utility (3.5.6). The overall program results are reviewed in section 4.0 followed by a conclusions section (5.0) and a section recommending future work (6.0)

3.0 PROGRAM DESCRIPTION

3.1 SCOPE OF WORK CONDUCTED

Pratt & Whitney Aircraft has developed and evaluated both computational and experimental methods for calculating amplitudes and phases of coherent sound modes in the inlet of turbofan engines using in-duct measurements as the calculation input. In addition, an approach has been developed for determining the structure of incoherent duct modes.

The approach used for determining the structure of incoherent duct modes was first to formulate the concept of the modal power spectral density function of random sound fields in thin annular ducts. Secondly, a system for determining the modal power spectral density was developed that uses progressively time-delayed outputs from a circumferential array of microphones. The array performance characteristics were then defined for both random and coherent discrete-frequency sound fields.

Emphasis has been placed on the determination of coherent duct modes such as those generated by rotor-stator interaction. This emphasis is considered well placed because incoherent tone noise, generated by rotor-turbulence interaction, is greatly reduced inflight, thus diminishing the importance of rotor-turbulence interaction as an in-flight noise source. Also, at the beginning of the program, a suitable theory was not available on which to base a method for determining the structure of random sound modes. A theory was available, however, for determining the structure of coherent sound modes. To meet the requirements of this program, the governing equations and related algorithms were assembled to formulate a computational procedure for determining the amplitudes and phases of coherent modes.

The computational procedure to determine coherent sound modes was developed in the form of two computer programs. One program selects microphone locations from three dimensions in the duct to ensure that the signal averaged acoustic pressure amplitude and phase measurements from these microphones can be used as input to the second program without giving rise to numerical instabilities. These locations are initially restricted to the duct wall unless these locations do not suffice to identify all possible modes. In this situation, microphone locations are selected on radial probes at the furthest axial location. The second program calculates the amplitude and phase of coherent duct modes using the in-duct pressure measurements and the corresponding duct locations as input. Additionally, this program has an option that permits calculation of overall pressure amplitude and phase at specific duct locations given the modal structure either arbitrarily, or as output from an analytical prediction deck. The computational method is, in principle, capable of determining all coherent modes that can propagate at a frequency of interest. In practice, the number of modes that can be determined is limited by the time, accuracy, and storage limitations of present-day computers and the accuracy with which the modal amplitude and phase is desired. These computer programs were developed with sufficient storage to accommodate a group of fifty coherent modes.

A study was performed to define the error in the calculated mode amplitudes and phases due to errors caused by tolerances in measuring microphone locations and inaccuracies in the measurement of acoustic pressure amplitudes and phases. As part of this study, equa-

tions were derived for the influence coefficients or partial derivatives of the modal coefficients with respect to first-order errors in pressure measurement and microphone location. These influence coefficients were incorporated in the second computer program and are evaluated as a part of the computational procedure for each data case that is run. Upon multiplication by a particular measurement error, the corresponding error in the mode amplitude and phase can be determined. In addition, errors in the calculated modes were assessed due to the effects of a multiplicity of extraneous modes that propagate at the frequency of interest, but are not included in the calculation procedure.

These two computer programs are written entirely in FORTRAN IV and are fully operative on the NASA computers. A user's manual was written for each program. These manuals define the algorithm and corresponding subroutines that were developed to meet the computer program objectives. Also, the input parameters and output format are discussed for each option.

The method and computer programs were assessed in an experimental program approved by the NASA Project Manager to determine the modal structure of the inlet duct sound field in the P&WA 25 cm (10 inch) diameter compressor rig. During the course of these experiments, measured acoustic pressure signals were obtained for six different modal structures. Four modal structures were generated by the wakes from a 34 rod stator interacting with a 32 bladed rotor. For two rotor speeds, different modal structures existed at both blade passing and twice blade passing frequency. The final two modal structures simulated steady inflow distortion by placing a single rod assembly upstream of the rotor. For this configuration, the rotor was operated at two speeds and data were acquired at only BPF. The measured acoustic pressures were filtered and then signal enhanced to provide amplitude and phase information at each microphone location. Then the pressure signals were used as input to the calculation procedure, yielding amplitudes and phases of the specific modes.

The method utility and measurement accuracy were assessed by using the calculated mode amplitudes and phases to predict the overall sound field measured by microphones at other duct locations not used to provide input to the calculation procedure. This study demonstrated that the method could be used within a desired accuracy when both the relative amplitudes and the number of those modes not included in the modal calculation were sufficiently small so as to yield errors in the mode amplitude and phase due to only measurement inaccuracies. The required accuracy of experimental measurements to ensure a desired accuracy in the modal coefficients is demonstrated to be a function of the relative amplitude, axial wave number, and circumferential order of the modes.

Monthly technical reports were completed and submitted as stipulated by the program schedule for the purpose of reporting work conducted under Contract NAS3-20047. In addition, this final report and accompanying user's manual for operation of the computer programs document the analytical analysis, experimental evaluation, and computational algorithms that lead to the accomplishment of the overall program objectives.

3.2 APPROACH FOR MEASURING COHERENT MODAL STRUCTURES

3.2.1 Background

The basic work upon which fan spinning mode theory is based was initially presented in 1961 by Tyler and Sofrin (ref. 1) following extensive analytical and experimental studies. Extending this work to include effects of axial flow, Sofrin and McCann (ref. 2) showed that the general form of any coherent acoustic wave (such as those generated by rotor-stator interactions) in an infinitely long cylindrical duct can be written as the real part of

$$p(r,\theta,x;\omega) = \sum_{m}\sum_{\mu} A_{m\mu}\, e^{i[k_x x + m\theta - \omega t + \phi_{m\mu}]}\, F_{m\mu}(k_{m\mu} r) \qquad (3.2\text{-}1)$$

$$\text{where} \qquad k_x = \frac{M_x \frac{\omega}{c} \pm \sqrt{\left(\frac{\omega}{c}\right)^2 - (1-M_x^2)\, k_{m\mu}^2}}{1-M_x^2}$$

and where notation has been chosen so as to be consistent with reference 2. The notation description is also tabulated in Appendix A. In reference 2, it was shown that the number of modes that can propagate at a given frequency is bounded by the condition that k_x must be real. If k_x becomes imaginary, it can readily be seen that as x increases, the term e^{ikxX} produces a term that decays exponentially.

In fan inlets and fan ducts typical of current turbofan engines, the assumptions underlying the acoustic theory of reference 1 are only partially met. In general, the duct geometry varies with axial distance, and the ducts are finite in length. For typical engine inlet geometries, however, these effects are probably small, because the variation in geometry with axial length and the finite length effect is only significant for duct modes near cutoff.

In spite of these difficulties, the analytical consideration of rotor-stator interaction tone noise, in terms of the general duct pressure, equation (3.2-1) has proven extremely successful. Each term in the summation is considered as a separate acoustic mode with amplitude, $A_{m\mu}$, and phase, $\phi_{m\mu}$; and it has been shown that rotor-stator interaction tone noise generates a finite set of these modes. The advantage of considering noise fields in terms of acoustic duct modes is that the generation, propagation, and radiation to the far field can be considered separately for each mode. The overall pressure at any desired location can then be determined by summing the individual mode contributions. The prime coherent noise fields that are (or can be) conveniently considered in terms of duct modes are rotor-stator interaction, rotor-steady inflow distortion interaction, and multiple pure tone noise at that location in the duct where the shock waves are sufficiently weak so as to be practically considered as linear acoustic waves.

The mathematical concept of duct modes described above, has motivated a number of experimental studies to measure modal structures and to verify theoretical results. Measurement of the amplitude and phase for low circumferential lobe numbers (m) were made by Tyler and Sofrin using a rotating microphone on a probe mounted axially in the inlet of a 10-inch diameter model fan rig. These measurements were made by essentially cross-correlating the output acoustic pressure signal with a once-per-blade passing trigger signal obtained from a proximity pickup over the blade tips. Subsequently, other investigators (ref. 2 & 3) measured low m-lobe number modes by cross-correlating while others (ref. 4, 5, 6) used cross-spectra techniques on signals from pairs of microphones in the duct.

A very thorough investigation by Plumblee et al. (ref. 7) on sound propagation in acoustically lined ducts with flow required the generation of low m-lobe number acoustic duct modes with an array of speakers and the accurate detection of the amplitudes and phases of these modes with in-duct microphones. In a set of well controlled experiments, they circumferentially traversed a duct probe in discrete steps and cross correlated the acoustic signal output with a reference microphone in the duct. Specific duct modes were thus generated and measured with a high degree of accuracy. This experimental method was then used in the verification of an analytical model that predicts the acoustic decay due to specified acoustic treatment designs on a modal basis.

The previously cited works dealt with modal structures generated by laboratory equipment under carefully controlled conditions. More recently, Kraft and Posey (ref. 8) measured the relative amplitudes of sound energy in circumferential modes in a duct upstream of a model fan stage under conditions representative of an actual jet engine (i.e., large axial flows, large numbers of generated acoustic modes - some with large lobe numbers (m), etc). They used cross-spectral techniques on the outputs from two microphones, one on a fixed probe – used as a reference – and the other on a circumferentially traversing probe. In all tests reported, they kept the pair of microphones at the same fixed radial location. Only the relative distributions of sound energy in the circumferential modes were obtained, and so the accuracy of their measurements could not be evaluated (e.g., by predicting sound field at another duct location). Also, they were not able to relate all the measured modes to the expected modal distribution that would be predicted by application of the Tyler-Sofrin theory to the fan design used for the test.

The approach for determining coherent fan sound mode structures, adopted by Pratt & Whitney Aircraft, differs from the previous approaches described above in two principle ways. First, the resultant amplitudes and phases of the coherent sound field in the duct is obtained by signal averaging the outputs from a number of fixed microphones in the duct. From an assumption of the set of duct modes considered to contain the bulk of the acoustic energy propagating out of the duct, it is possible to form a set of simultaneous complex equations relating the measured resultant amplitudes and phases to the amplitudes and phases of the duct modes. The modal amplitudes and phases then are calculated by matrix inversion, assuming that the number of microphones available is equal to the number of modes propagating significant acoustic energy.

The second difference is that microphones are not located arbitrarily in the duct (often equidistant in one axial plane). Microphones are, in fact, placed at specific duct locations to ensure that the data provided by the microphones can be suitably processed to yield the component modal amplitudes and phases.

The method for determining coherent fan sound modal structures is presented under three headings. In the first, Method of Mode Structure Determination, the theoretical analysis underlying the method will be discussed including a brief description of the computer program for calculating the mode structures. Under the second heading, Selection of Microphone Locations, a procedure is presented for selecting microphone locations in the duct which ensures the stability of the mode calculating procedure. Finally, under the heading Sensitivity of Method an analysis will be presented in the calculation of sensitivity coefficients that can be used to determine the errors in calculated modal amplitude and phase caused by errors in acoustic measurements and microphone placement. Section 3.2 is concluded by a brief description of the User's Manuals for the two computer programs discussed in this section.

3.2.2 Method of Coherent Mode Structure Determination

Objective

To establish, program, and check out an analytical method and to establish test procedures for the determination of coherent fan sound mode structures.

Approach

Any attempt at measuring amplitudes and phases of coherent modes at tone-frequencies generated by a fan (or turbine) in an annular duct must address two major problem areas. First, during typical static fan tests, the inflow contains considerable turbulence and quasi-steady distortions so that any coherent acoustic modes are generated in the presence of a multiplicity of randomly generated acoustic modes. A method must thus be found to separate the purely coherent sound field from the total sound field. Second, the number of modes that a duct can support increases rapidly with frequency. For frequencies typical of most fan designs, there can be many hundreds of modes, both coherent and incoherent, propagating at BPF at typical approach or takeoff operation and, of course, many more for harmonics of BPF.

In considering the first problem, it will be recalled that previous mode tracking methods (ref. 1 to 6) used cross-correlation or cross-spectral techniques on the output signals of pairs of microphones to suppress the contribution of randomly generated modes. An alternate method, and the one adopted by Pratt & Whitney Aircraft under this contract, is to enhance by signal averaging the purely coherent portion of the output signal from each microphone used to obtain data. This signal enhancement at a desired frequency can be achieved by filtering the signal with a phase preserving filter at the frequency of interest (such as at BPF) and then averaging the signal over a period corresponding to that frequency. A once-per-blade reference signal obtained by a proximity sensor over the blade tips can be used to separate the pressure signal into time blocks of one period, and a commercially available signal averager can sum and average the pressure signal over that period. The once-per-blade reference signal is also required to establish a time base from which relative phases at all microphone locations can be obtained.

In addition to signal enhancement, the contribution of randomly generated modes to the overall signal can be reduced during static testing with a turbulence suppressing screen and/or honeycomb placed about the inlet. Unpublished results from full scale engine tests conducted at Pratt & Whitney Aircraft have shown significant reductions in both inflow turbulence and the subsequently generated distortion tone noise at BPF.

As will be discussed more fully in section 3.4, signal enhancing in conjunction with the inlet screen was found to be the most satisfactory mode of operation during the experimental portion of the contract, providing greater repeatability and accuracy of coherent acoustic pressure amplitude and phase measurements. For the remainder of this section, it will be assumed that the random modal structure is effectively suppressed by the use of signal enhancing and the inlet screen.

It remains to consider the second problem of large numbers of propagating modes. Using the general form for the coherent portion of the acoustic pressure in the duct as given by equation (3.2-1) Tyler and Sofrin showed that, at a given frequency, the duct can support only a finite number of propagating modes. If, in addition to this set, the slowly decaying modes that may have an impact on the fan sound field in the duct are added, the double sum of equation (3.2-1) can formally be replaced by a sum over that finite set of modes. This set of modes, however, will, in most practical cases, be very large and a large number of microphone measurements would be required to provide input to a modal calculation procedure.

If information were available that identifies the modes likely to contain the bulk of the acoustic energy, the number of microphones required for obtaining data to provide input to a modal calculation procedure could be significantly reduced. One method of reducing the number of required microphones is to review the fan design (blade and vane numbers) and determine from the kinematical Tyler-Sofrin theory (ref. 1) those acoustic modes likely to control the inlet and aft radiated sound fields. Based on this information, locate microphones in the duct to determine the structure of just those modes. As shown by Kraft and Posey (ref. 8), such a determination, however, does not always identify all of the dominant modes.

Based on the above discussion, it will be assumed that there are a finite and experimentally manageable number of coherent propagating modes (or, in exceptional cases, slowly decaying modes), including the possibility of reflected waves that make up the pressure, which can be expressed for a given frequency ω in the form

$$P(r,\theta,x;\omega) = \sum_{\substack{\text{Finite Set} \\ \text{of Modes}}} A_{m\mu}\, e^{i[k_x x + m\theta - \omega t + \phi_{m\mu}]}\, E_{m\mu}(k^{\sigma}_{m\mu} r) \qquad (3.2\text{-}2)$$

$$\text{where} \quad k_x = \frac{M_x \frac{\omega}{c} \pm \sqrt{\left(\frac{\omega}{c}\right)^2 - (1-M_x^2)\, k^{\sigma 2}_{m\mu}}}{1-M_x^2}$$

and where the plus and minus sign accounts respectively for incident and reflected waves.

If the amplitude and phase of the purely coherent portion of the pressure signal is measured at a number of duct locations (either at the duct wall or at any location in the duct) and inserted into equation (3.2-2) a set of equations will be generated with unknown mode amplitudes ($A_{m\mu}$) and phases ($\phi_{m\mu}$). It should be noted that the only reason the radial orders associated with a particular circumferential mode can be determined using only wall-mounted pressure transducers is that the axial wave number, k_x, in equation (3.2-2) is a function of $k_{m\mu}$. The value of $k_{m\mu}$ is different for each duct mode. This difference gives rise to different spiral angles at the duct wall as each mode propagates in the duct. In some practical cases, for example: high radial orders of a particular circumferential order, these differences in spiral angles are sufficient to allow for the discrimination of the radial modal structure using only wall-mounted microphones.

The equation system can be written in matrix form where the matrix coefficients will be functions of the particular modes comprising the sound field and the microphone locations. If the number of microphone measurements is chosen equal to the number of modes comprising the sound field, then in principle, the equation system can be solved for the mode amplitudes and phases by standard matrix inversion methods.

Mathematics of the Method

To illustrate the method of fan sound mode structure determination, the case will be considered of a sound field consisting of ℓ coherent modes at blade passing frequency (BPF) in combination with contribution due to an incoherent source. If the incoherent portion of the sound field at BPF is given by $f(r, \theta, x, t; \omega)$, the pressure signal from a microphone at a duct location (r, θ, x) and filtered at BPF, can be written as

$$p(r,\theta,x;\omega) = \sum_{\ell \text{ modes}} A_{m\mu}\, e^{i\left[k_x^{(m,\mu)} x + m\theta - \omega t + \phi_{m\mu}\right]} E_{m\mu}\left(k_{m\mu}^{\sigma} r\right) + f(r,\theta,x,t;\omega)$$

In this equation k_x has been written as $k_x^{(m,\mu)}$ to denote that the axial wave number is a function of modal order, and it can be considered to be representative of incident and reflected waves as well as a decaying wave if $k_x^{(m,\mu)}$ is complex.

From a knowledge of the fan design (blade and vane numbers, axial flow, etc.), k_x, m, μ, $k_{m\mu}$, and $E_{m\mu}$ can be calculated. $A_{m\mu}$ and $\phi_{m\mu}$, the modal amplitude and phase, respectively, represent the unknowns. If the period associated with BPF is τ and the pressure signal is averaged over N revolutions, the signal enhanced pressure defined in the time interval $(0, \tau)$ becomes

$$\langle p(r,\theta,x,t;\omega)\rangle = \frac{1}{BN}\sum_{n=0}^{BN-1}\sum_{\ell \text{ modes}} A_{m\mu}\, e^{i\left[k_x^{(m,\mu)} x + m\theta - \omega(t+n\tau) + \phi_{m\mu}\right]} E_{m\mu}\left(k_{m\mu}^{\sigma} r\right) + \frac{1}{BN}\sum_{n=0}^{BN-1} f(r,\theta,x,t;\omega) \qquad \text{for } 0 < t < \tau$$

and B is the number of rotor blades.

Now, since $\omega\tau = 2\pi$

$$\langle p(r,\theta,x,t;\omega)\rangle = \sum_{\ell\,\text{modes}} A_{m\mu}\, e^{i[k_x^{(m,\mu)}x + m\theta - \omega t + \phi_{m\mu}]} E_{m\mu}(k_{m\mu}^{\sim} r) + \frac{1}{BN}\sum_{n=0}^{BN-1} f\left(r,\theta,x,t+\frac{2\pi n}{\omega};\omega\right) \quad (3.2\text{-}3)$$

If f is correlated over time scales less than some value τ_0, say, and if N is chosen large enough so that $N \gg \tau_0/\tau$, then contributions from the second term in equation (3.2-3) can be neglected to a good approximation. The signal enhanced, measured output $\langle p(r, \theta, x, t;\omega)\rangle$ is a sinusoidal function yielding an amplitude and a phase relative to a fixed once-per-blade signal that is used to "trigger" the signal averager. The filtered and signal averaged pressure from a microphone at a duct location (x_n, r_n, θ_n) can then be written in the form:

$$\langle p(r_n,\theta_n,x_n,t;\omega)\rangle = B_n\, e^{i(\psi_n - \omega t)} \quad (3.2\text{-}4)$$

It can be seen that at each measurement location, two parameters (B_n and ψ_n) can be obtained. If measurements are made at N locations in the duct, the following set of equations can be obtained from combining equations (3.2-3) and (3.2-4) for the unknown $A_{m\mu}$'s and $\phi_{m\mu}$'s:

$$B_n e^{i\psi_n} = \sum_{\ell\,\text{modes}} A_{m\mu}\, e^{i[k_x^{(m,\mu)}x_n + m\theta_n + \phi_{m,\mu}]} E(k_{m\mu}^{\sim} r_n) \quad (3.2\text{-}5)$$

where n = 1,2,3, . . . N.

The equation system (3.2-5) forms the basis for the calculation of the coherent fan sound modal structure. Since N was chosen to equal the number of propagating modes, a set of 2N equations (for both the real and imaginary parts) is obtained from which, in principle, the 2N unknowns ($A_{m\mu}$ and $\phi_{m\mu}$ for set of N modes) can be found. The solution for this system of equations was programmed and is now discussed.

Computer Program

The calculation procedure to solve the system of equations (3.2-5) was programmed in Fortran IV code to be run on a high speed digital computer. The code and logic which are described in a User's Manual (ref. 9), were checked out using ten analytical test cases comprising a variety of fan designs and modal structures. The test cases used are shown in Table 3.2-1. It can be seen that the modal calculation procedure was checked out for cases that included up to 15 propagating modes.

TABLE 3.2-1

MODE STRUCTURES FOR TEST CASES

Total Number Modes	(m,μ) Modes Used	Input Modal Amplitudes (dynes/cm^2) and Modal Phase (degrees)	Engine/Rig Application	Blade/Vane Number	Frequency (Hz)	
2	(-2,0) (-2,1)	(-2,0): $1725\ e^{i0^\circ}$ (-2,1): $345\ e^{i0^\circ}$	P&WA Rig	32/34	BPF	2987
2	(2,0) (-3,0)	(2,0): $690\ e^{i0^\circ}$ (-3.0): $10.0 \times 10^{-3}\ e^{i0}$	P&WA Rig	32/5	BPF	2133
3	(-4,0) (-4,1) (-4,2)	Analytical Prediction	P&WA Rig	32/34	2 BPF	6000
3	(-1,0) (-1,1) (4,0)	Analytical Prediction	P&WA Rig	32/5	2BPF	3200
3	(-4,0) (-1,0) (2,0)	Analytical Prediction	P&WA Rig	32/3	BPF	2667
5	(5,0) (5,1) (5,2) (5,3) (20,0)	NASA Suggestion	NASA Rig	15/25	2BPF	4470
7	(3,0) (2,0) (1,0) (0,0) (-1,0) (-2,0) (-3,0)	All: $345\ e^{i0^\circ}$	P&WA Rig	32/1	BPF	2133
7	(-4,0) (-4,1) (-4,2) (-4,3) (-4,4) (-4,5) (-4,6)	Analytical Prediction	P&WA Turbo-fan Simulator	18/40	2BPF	27,600
7	(11,0) (11,1) (11,2) (11,3) (-12,0) (-12,1) (-12,2)	Analytical Prediction	JT8D Refan	34/23	BPF	2210
15	(-16,0) thru (-16,14)	Analytical Prediction	JT9D-7	46/108	2BPF	3220

The Modal Calculation Program (MCP) was checked out as follows: The amplitudes and phases of the modes in given case were assigned either arbitrary values or values from an analytical deck. The resultant sound field was then calculated by the MCP from the given modal structure at specific locations in the duct. For this checkout study, the locations were specified by the Microphone Location Program (MLP) that will be discussed in section 3.2.3. The amplitudes and phases at these locations were then used as input to the MCP so that the constituent modal structure could be calculated. The computer program was checked out by making sure that the input and calculated modal structures were identical within values that could be attributed to computer roundoff errors. In fact, all the analytical test cases considered reproduced the input modal structure to at least three significant figures in amplitude and phase.

3.2.3 Selection of Microphone Locations

Objective

To establish and check out a method for determining microphone locations that will provide data input to the Modal Calculation Program so that the numerical stability of the calculation procedure will be assured.

Criteria to Ensure Method Stability

It was shown in the last section (3.2.2) that the fan sound modal structure is determined by solving for the $A_{m\mu}$'s and $\phi_{m\mu}$'s from the equation system given by equation (3.2-5). It can be seen readily that the solution requires a matrix inversion algorithm and, thus in order to get a numerically stable solution, the matrix of the equation system needs to be well conditioned in a mathematical sense. Since the matrix coefficients are functions of microphone locations, it is possible (for a sound field consisting of a distinct set of modes) to select microphone locations so that the resulting matrix leads to a numerically stable solution.

In order to establish a procedure for the selection of suitable microphone locations to determine a mode structure comprising ℓ modes, it is necessary to consider the following criteria:

1. Microphone locations must be chosen so as to yield independent complex equations.

2. For large number of modes, microphone locations must be chosen so that experimental and round-off errors do not accumulate significantly in the Modal Calculation procedure.

3. Some mode combinations will require that acoustic measurements be made in a fan inlet with microphones on radial or axial probes in addition to those located on the duct wall. Viscous wakes from these probes will interact with the rotor to generate duct modes at BPF and harmonics in addition to those predicted based on the fan design.

4. Locations chosen can only be a function of the set of modes (m, μ) considered to be propagating, and not on relative amplitudes and phases ($A_{m\mu}$ and $\phi_{m\mu}$) of the modes.

5. The method for locating microphones should be sufficiently general so as to accommodate all possible types of mode structure.

Procedure

Addressing these criteria, a procedure for selection of microphone locations was devised and computerized. This method will now be described followed by a discussion on how this method addresses the above criteria.

Given that the sound field in the duct is assumed to be composed of N propagating duct modes, and given an axial region in the duct where microphones can be placed away from the influence of the direct rotor field and effects of the inlet termination, a reference microphone is located on the duct wall at an arbitrary (or convenient) azimuthal location and within the specified axial region. The N modes are then ordered so that the highest radial order for the highest m-lobe is considered first and subsequently for that m-lobe the modes are ordered in terms of decreasing radial order. This ordering is then continued for successively decreasing m-lobe numbers.

For the first two modes in the ordered sequence, a second microphone is located on the duct wall and in the specified axial region using a two parameter (x, θ) stochastic search routine. This routine searches for a microphone location that maximizes the absolute magnitude of the determinant associated with the resulting 2x2 matrix equation system corresponding to the determination of the amplitudes and phases of the first two modes in the ordered sequence. The conditioning number – defined (ref. 10) as the ratio of the magnitudes of the largest to the smallest eigen value of the determinant of the matrix – is then calculated. As discussed in reference 10, this number provides a means for estimating the maximum number of significant figures lost in the solution of the simultaneous equations associated with the matrix. If the conditioning number is less than 100 (which, according to reference 10, translates to the loss of two or less significant figures in the resulting solution), or an alternate specified value if more or less accuracy is desired, the second microphone location is fixed and a third microphone, corresponding to the third mode in the ordered sequence, is located on the duct wall and in the designated axial region. Again, the two parameter (x, θ) search routine is used. In this case, the search routine locates the third microphone so as to maximize the absolute magnitude of the determinant associated with the resulting 3x3 matrix equation system. The conditioning number for this 3x3 matrix is then calculated and if it is less than the specified value, the third microphone location is fixed.

This process is repeated until either all the modes are exhausted or until the conditioning number is greater than the specified value. If the latter event occurs, it signifies that a numerically stable solution is not possible for the set of modes under consideration using only wall mounted microphones. In this event, a microphone on a probe within the duct is necessary. Since radial probing (rather than axial) is generally more practical during both static and flight fan noise tests, the microphone is located by a two parameter (r, θ) stochastic search, assuming a radial probe at the furthest upstream location within the specified axial region. In this way, the wake from the probe interacting with the fan rotor and the subsequent tone noise generation will be minimized. The remaining microphones will then be placed on this probe (if possible), using a one parameter (r) stochastic search. At each subsequent microphone, the absolute magnitude of the determinant of the equation system is maximized, and the conditioning number is calculated.

If a location cannot be found on the radial probe that provides a conditioning number less than the specified value, then a two-parameter (r,θ) search is made for a location in the duct on another probe (also placed at the furthest axial location). In the event that a position cannot be found that yields a satisfactory conditioning number, the last location of the microphone is fixed, and the program proceeds to locate the next microphone associated with the next mode in the ordered sequence.

Having presented the procedure, we will now discuss to what extent the procedure complies with the criteria established and listed earlier for locating microphones.

1) By constraining the conditioning number to be less than 100 (or a suitably specified alternative value) for the N x N equation system, the magnitude of the determinant of the equation system is assured to be sufficiently well away from zero. Thus, this constraint makes sure that the microphones are located so that each of the N complex equations derived is independent.

2) The maximizing of the determinant for each additional microphone is compatible with generating low conditioning numbers and makes for a convenient criteria on which to base the step-by-step application of the stochastic search routine. Ideally, a search routine that maximizes the N x N determinant of the entire equation system by simultaneously selecting all microphone locations would be desirable because the determinant always appears in the denominator of the final result. In this way, the solution of the equation system would be independent of first-order errors in the matrix elements due to errors in locating microphones that will inevitably be met in practice. Such a procedure would be impractical however, since generally it would require a 3N parameter stochastic search which is not available for the range of M being considered under this contract ($M \leqslant 15$). The procedure presented relies on maintaining a fairly low conditioning number to ensure that small experimental and round-off errors do not accumulate significantly. As discussed in reference 10, a low conditioning number ensures that the number of significant figures lost in the calculation method is kept to a minimum.

3) The procedure has been set up to avoid the need of radial probing where possible, and when it is inevitable, to minimize the adverse effects associated with the introduction of radial probing.

4) The microphone locations are selected based only on the modes considered to be contributing to the sound field and not on the relative amplitudes and phases of the modes.

5) Finally, the method is quite general, being able to locate microphones for any reasonably finite set of modes. In fact, the procedure was checked out with a number of test cases including a 15 mode set (that had a conditioning number of 5.7) and a 2 mode set that was successfully compared with a closed form solution.

Analytical Illustration of Method

In order to illustrate the underlying approach for selecting microphone locations that assume the subsequent numerical stability of the modal calculation method, the relatively simple case will be presented of determining the amplitudes of two radial orders of a given circumferential mode using two wall-mounted transducers. Incorporating the value of the E-function at the wall into the $A_{m\mu}$'s, the average pressure at a duct location of (x_1, θ_1) becomes from equation (3.2-5).

$$B_1 e^{i\psi_1} = A_{m1} e^{i[k_x(k_{r1}^{\sigma})x_1 + m\theta_1 + \phi_{m1}]} + A_{m2} e^{i[k_x(k_{r2}^{\sigma})x_1 + m\theta_1 + \phi_{m2}]} \qquad (3.2\text{-}6)$$

where $o \leq t \leq \tau$

The pressure at another duct location (x_2, θ_2), given by $(x_1 + x_0, \theta_1 + \theta_0)$ where (x_0, θ_0) represents the relative displacement of the two microphones, can be written sirailarly as

$$B_2 e^{i\psi_2} = A_{M1} e^{i[k_x(k_{M1}^{\sigma})(x_1+x_0) + m(\theta_1+\theta_0) + \phi_{M1}]} + A_{M2} e^{i[k_x(k_{M2}^{\sigma})(x_1+x_0) + m(\theta_1+\theta_0) + \phi_{M2}]} \qquad (3.2\text{-}7)$$

where $o \leq t \leq \tau$

Defining

$$D_{M1} = A_{M1} e^{i[k_x(k_{M1}^{\sigma})x_1 + m\theta_1 + \phi_{M1}]}$$

$$D_{M2} = A_{M2} e^{i[k_x(k_{M2}^{\sigma})(x_1+x_0) + m(\theta_1+\theta_0) + \phi_{M2}]}$$

Equations (3.2-6) and (3.2-7) become in matrix form

$$\begin{bmatrix} B_1 e^{i\psi_1} \\ B_2 e^{i\psi_2} \end{bmatrix} = \begin{bmatrix} 1 & e^{-i[k_x(k_{M2}^{\sigma})x_0 + m\theta_0]} \\ e^{i[k_x(k_{M1}^{\sigma})x_0 + m\theta_0]} & 1 \end{bmatrix} \begin{bmatrix} D_{M1} \\ D_{M2} \end{bmatrix} \qquad (3.2\text{-}8)$$

Thus, from the measurements of the amplitude and phase of $B_1 e^{i\psi_1}$ and $B_2 e^{i\psi_2}$, the amplitudes and phases of D_{m1} and D_{m2} can be obtained since the elements of the matrix are all known and A_{m1}, A_{m2}, ϕ_{m1}, and ϕ_{m2} can be evaluated. Clearly, the values of (x_0, θ_0) must be chosen so as not to make the exponential terms in equation (3.2-8) equal to one, since this would give rise to a zero determinant for the matrix and to two dependent equations. In that case, no solution for D_{m1} and D_{m2} can be obtained. Assuming that the determination of the 2 by 2 matrix is non-zero, the matrix equation can be inverted in the usual way yielding

$$\begin{bmatrix} D_{M1} \\ D_{M2} \end{bmatrix} = \frac{\begin{bmatrix} 1 & -e^{-i[k_x(k_{M2}^{\sigma})x_0 + m\theta_0]} \\ -e^{i[k_x(k_{M1}^{\sigma})x_0 + m\theta_0]} & 1 \end{bmatrix}}{\begin{vmatrix} 1 & e^{-i[k_x(k_{M2}^{\sigma})x_0 + m\theta_0]} \\ e^{i[k_x(k_{M1}^{\sigma})x_0 + m\theta_0]} & 1 \end{vmatrix}} \begin{bmatrix} B_1 e^{i\psi_1} \\ B_2 e^{i\psi_2} \end{bmatrix} \qquad (3.2\text{-}9)$$

Notice that the value of the determinant in the denominator is

$$1 - e^{i\left[K_x(k_{M1}^{\sigma}) - K_x(k_{M2}^{\sigma}) \right] x_o} \tag{3.2-10}$$

and the only reason that the radial modes can be determined using only duct wall microphones is that the axial wave number k_x is a function of the circumferential and radial modes that are propagating. Note also that even for this relatively simple case, poor resolution due to the denominator of equation (3.2-9) approaching zero is unavoidable if the axial wave numbers (k_x) for the two modes are almost equal and x_0 is bounded by practical constaints. Such cases often are met when several radial orders are propagating for a particular m-lobe circumferential mode at high frequencies. In particular, if m is fairly high, the axial wave numbers of the first few radial orders for typical practical situations are indistinguishable. In such cases, the detailed mode structure can best be obtained by probing within the duct. Poor resolution is also experienced if the distance between microphones is chosen such that

$$e^{i\left[K_x(k_{M1}^{\sigma}) - K_x(k_{M2}^{\sigma}) \right] x_o} \approx 1$$

From inspections of the form of the determinant, equation (3.2-10), it can be seen that a maximum value of the modulus and the real part of the determinant is obtained when

$$x_o = \frac{(2n+1)\pi}{\left[K_x(k_{M1}^{\sigma}) - K_x(k_{M2}^{\sigma}) \right]} \tag{3.2-11}$$

Two criteria are satisfied by this choice of x_0: 1) both the modulus and the real part of the determinant are well away from zero, and 2) both the modulus and the real part of the determinant are at local maxima and will be insensitive to first order errors in x_0 (that is, the microphone locations). Having established the microphone location according to the form of the denominator of equation (3.2-9), the actual values of D_{m1} and D_{m2} depend on the form of the numerator and the measured amplitudes and phases of the pressure at the two microphone locations. However, as long as the matrix-vector product in the numerator is bounded, singularities and gross sensitivity to first-order errors in measurements and microphone locations can be avoided.

For this simple case, the stochastic search that maximizes the determinant for each additional microphone location in the MLP would determine one of the values of x_0 satisfying equation (3.2-11), and within the specified axial range for locating microphones. If one of the values of x_0 is not in the specified axial range, the stochastic search will find another value of x_0 that will maximize the determinant in that range. Since the eigen values of the determinant in the denominator of equation (3.2-9) are (1 + i) and (1 - i) when a value of

x_0 is chosen that satisfies equation (3.2-11), the conditioning number is readily seen to be unity. The equation system results from the choice of microphone locations given by x_0 in equation (3.2-11) is thus seen to be well conditioned.

Computer Program

The microphone location selection procedure was programmed in Fortran IV code to be run on a high-speed digital computer. The code and logic, which are described in a User's Manual (ref. 11) were checked out by locating two microphones for a case where the sound field consisted of two propagating modes. The computer output was compared with the exact analytical solution obtained by application of equation (3.2-11). Agreement to within four significant figures was obtained. As noted in section 3.2.2, the Microphone Location Program (MLP) also was run to obtain microphone locations for the ten analytical test cases that were used to check out the MCP. Finally, once the MLP was checked out, it was used to select microphone locations for the experimental portion of this program described in section 3.4.

In this section a method has been established and checked out for determining microphone locations that will provide input to the Modal Calculation Program (described in section 3.2.2) that will ensure the numerical stability of the calculation procedure. The method for determining coherent fan sound mode structures is thus complete. In the next section, the sensitivity will be considered of the modal calculation method to errors in the knowledge of the measuring locations and in the measured phase angles and pressure amplitudes.

3.2.4 Sensitivity of Method

Objective

To derive a set of influence coefficients from which the sensitivity can be determined of the calculated mode structure to errors in the knowledge of the measuring location and in the measured phase angles and pressure amplitudes.

Derivation of Influence Coefficients

The accuracy of the modal coefficients, as computed from the measured pressures, is affected by errors in these measurements, and also by the precision of the microphone locations. Specifically the amplitude and phase errors associated with a specified mode are required as functions of amplitude and phase errors in the measured pressures, and also as functions of errors (or tolerances) in the radial, axial, and circumferential coordinates of the pressure measuring locations. In this subsection, expressions will be obtained for the influence coefficients or partial derivatives of the modal amplitude and and phase with respect to pressure and location coordinates. These can be used to estimate the sensitivity of the calculated modes to first-order measurement and position errors. By multiplying a given influence coefficient by an appropriate measurement error, the corresponding error in the amplitude or phase of the mode due to that error is obtained. In addition, the standard deviations of calculated mode amplitude and phase can be obtained in terms of assumed or experimentally derived standard

deviations of the measurement and position errors. The derivation of the influence coefficients and their use in estimating the standard deviations in calculated modal amplitude and phase are discussed in the following paragraphs. This discussion is then followed by a physical interpretation of the influence functions.

The analysis is simplified and will be easier to follow if all appropriate complex variables are denoted initially by single symbols rather than expressed in rectangular or polar form, until such time as is necessary to specifically obtain separate amplitude and phase expressions. Furthermore, matrix notation is employed as the most efficient and revealing way of manipulating the large number of variables involved.

In matrix form, the relation between N measured pressures and mode coefficients (equation 3.2-5) can be expressed compactly as

$$p = Hz \tag{3.2-12}$$

where p is the column matrix of N measured complex pressures, z is the column of N desired complex mode coefficients, and H is an N x N matrix, the elements of which are functions of microphone location and modal eigenvalues and eigenfunctions (but not mode amplitude or phase). The expressions for the H matrix elements (denoted by H_{ns}) can be written from equation (3.2-2) as

$$H_{ns} = E_{m_s \mu_s}\left(K_{m_s \mu_s} r_n\right) e^{i\left[k_{x_s} x_n + m_s \theta_n\right]} \tag{3.2-13}$$

where (x_n, r_n, θ_n) denotes the nominal location of the nth microphone and s denotes the sth mode in the ordered seqt ence of modes discussed in the last sub-section and m_s, μ_s and k_{xs} are respectively the circumferential lobe, radial order and axial wave-number corresponding to the sth mode. Solving equation (3.2-12) for the modal coefficients

where
$$z = H^{-1} p \quad \text{or} \quad z = Q p \tag{3.2-14}$$
H^{-1} or Q is the inverse of the H matrix

It should be understood that although the elements of H have closed form analytical expressions given by (3.2-13) the elements of the inverse, H^{-1} cannot generally be expressed analytically because of the complicated form of the determinants involved in matrix inversion. However, in the modal calculation procedure described in sections 3.2.2. and 3.2.3, numerical values of the H matrix are obtained, and the computation procedures included in the MCP give corresponding numerical values of the inverse, $Q = H^{-1}$. Furthermore, p is known from N duct microphone measurements and the resulting computed quantities z (the amplitude and phase of each mode) are known from the output of the modal calculation procedure.

The result on the calculated modal coefficients of errors in the measurement of p and errors in microphone location, which are manifest as errors in H, may be seen by replacing p, H, and z in equation (3.2-12) with $p + \Delta p$, $H + \Delta H$, and $z + \Delta z$. Substituting, and subtracting $p = Hz$ from each side gives

$$\Delta p = H \Delta z + \Delta H \cdot z + \Delta H \Delta z \qquad (3.2\text{-}15)$$

If the errors are small, the second-order term $\Delta H \Delta z$ can be ignored, and to denote this approximation, dp, dH, and dz will be employed in the usual sense of differentials, giving

$$dp = H\,dz + dH \cdot z \qquad (3.2\text{-}16)$$

Using standard matrix algebra the error in the mode coefficient can be expressed in terms of pressure measurement and microphone placement errors as

$$dz = H^{-1} dp - H^{-1} dH \cdot z$$

$$\text{or} \quad dz = Q\,dp - Q\,dH \cdot z \qquad (3.2\text{-}17)$$

Since Q can be numerically calculated from the known matrix H, and the z are calculated using the modal calculation procedure, it can be seen that the errors in the amplitudes and phases of all the modes dz can be expressed in terms of the known elements of Q, the calculated mode structure z, and the errors in pressure measurement, dp, and the microphone placement errors, that give rise to errors, dH in the elements of the matrix H.

In particular, from equations (3.2-17) and the form of the expression for the elements of H given by equation (3.2-13).

$$dz = Q\,dp - Q \sum_{n=1}^{N} \left(\frac{\partial H}{\partial x_n} dx_n + \frac{\partial H}{\partial r_n} dr_n + \frac{\partial H}{\partial \theta_n} d\theta_n \right) z$$

where, since H is a function only of microphone location, dH has been replaced by

$$dH = \sum_{n=1}^{N} \left(\frac{\partial H}{\partial x_n} dx_n + \frac{\partial H}{\partial r_n} dr_n + \frac{\partial H}{\partial \theta_n} d\theta_n \right)$$

From this equation, the independent effect of each error type in pressure and location coordinate can be evaluated. For example, the error in the modal coefficient Z_M, due to an error only in x, say, is given by:

$$dz_M = -Q \frac{\partial H}{\partial x_i} dx_i \cdot z$$

Multiplying out the last two terms as is shown in equation B13 of Appendix B,

$$dz_M = -Q \sum_{s=1}^{\ell} \frac{\partial H_{ns}}{\partial x_i} z_s\, dx_i$$

where H_{ns} is the element in the n^{th} row and s^{th} column of the matrix H, and z_s is the sth modal coefficient as ordered in the modal calculation method.
The expression

$$- Q \sum_{s=1}^{\ell} \frac{\partial H_{ns}}{\partial X_i} z_s$$

is defined as an influence coefficient and is simplified still further, along with all the other influence coefficients, in Appendix B. If the measured amplitude and phase of the coherent sound field at the n^{th} microphone at location (x_n, r_n, θ_n) is given by B_n and ψ_n, then the influence coefficients can be presented in terms of amplitude and phase and are equivalent to partial deviations of the modal amplitude and phase with respect to acoustic pressure and microphone location coordinates. As shown in Appendix B, these partial derivatives are as follows

$$\frac{\partial A_M}{\partial B_n} = q_{Mn} \cos \xi_{Mn} \qquad \frac{\partial \phi_M}{\partial B_n} = \frac{1}{A_M} q_{Mn} \sin \xi_{Mn}$$

$$\frac{\partial A_M}{\partial \psi_n} = - B_n q_{Mn} \sin \xi_{Mn} \qquad \frac{\partial \phi_M}{\partial \psi_n} = \frac{B_n}{A_M} q_{Mn} \cos \xi_{Mn} \qquad (3.2\text{-}18)$$

$$\frac{\partial A_M}{\partial x_n} = q_{Mn} \sum_{s=1}^{N} k_{xs} h_{ns} A_s \sin \eta_{Mns} \qquad \frac{\partial \phi_M}{\partial x_n} = - \frac{1}{A_M} q_{Mn} \sum_{s=1}^{N} K_{xs} h_{ns} A_s \cos \eta_{Mns}$$

$$\frac{\partial A_M}{\partial r_n} = - q_{Mn} \sum_{s=1}^{N} \bar{K}_{ns} h_{ns} A_s \cos \eta_{Mns} \qquad \frac{\partial \phi_M}{\partial r_n} = - \frac{1}{A_M} q_{Mn} \sum_{s=1}^{N} \bar{K}_{ns} h_{ns} A_s \sin \eta_{Mns}$$

$$\frac{\partial A_M}{\partial \theta_n} = q_{Mn} \sum_{s=1}^{N} m_s h_{ns} A_s \sin \eta_{Mns} \qquad \frac{\partial \phi_M}{\partial \theta_n} = - \frac{1}{A_M} q_{Mn} \sum_{s=1}^{N} m_s h_{ns} A_s \cos \eta_{Mns}$$

where A_m and ϕ_n are the amplitude and phases of the M^{th} mode

and $\xi_{Mn} = \beta_{Mn} + \psi_n - \phi_M$ and $\eta_{Mns} = \beta_{Mn} + \alpha_{ns} + \phi_s - \phi_M$

The remainder of the notation is fully described in Appendix A.

It should be noticed from these partial derivatives that, in general, the influence coefficients are functions of the microphone location (x_n, r_n, θ_n) and the acoustic pressure measurements (B_n and ψ_n), and also depend on the calculated modal amplitudes and phases (A_M and ϕ_m). Thus the influence coefficients are different for each modal structure that is determined.

Expressions for the standard deviations of A_M and ϕ_M can now be obtained in terms of the standard deviations in pressure measurement and microphone location errors. Since the resulting amplitude and phase errors of the Mth modal coefficients dA_M and $d\phi_M$ are linear functions of the input errors, they can be written as

$$d A_M = \sum_{n=1}^{N} \left(\frac{\partial A_M}{\partial B_n} d B_n + \frac{\partial A_M}{\partial \psi_n} d \psi_n + \frac{\partial A_M}{\partial r_n} d r_n + \frac{\partial A_M}{\partial x_n} d x_n + \frac{\partial A_M}{\partial \theta_n} d \theta_n \right)$$

$$d \phi_M = \sum_{n=1}^{N} \left(\frac{\partial \phi_M}{\partial B_n} d B_n + \frac{\partial \phi_M}{\partial \psi_n} d \psi_n + \frac{\partial \phi_M}{\partial r_n} d r_n + \frac{\partial \phi_M}{\partial x_n} d x_n + \frac{\partial \phi_M}{\partial \theta_n} d \theta_n \right)$$

Then, if it is assumed that the pressure and position errors (d_B, d_ψ, d_X, d_r, and d_θ) are independent variables having Gaussian distribution functions that are independent of n and if these standard deviations are characterized by zero mean and standard deviations σ_B, σ_ψ, σ_X, σ_r, and σ_θ, the resulting standard deviations of the computed mode amplitudes and phases are simply

$$\sigma_{A_M} = \left\{ \sum_{n=1}^{N} \left[\left(\frac{\partial A_M}{\partial B_n} \right)^2 \sigma_B^2 + \left(\frac{\partial A_M}{\partial \psi_n} \right)^2 \sigma_\psi^2 + \left(\frac{\partial A_M}{\partial r_n} \right)^2 \sigma_r^2 + \left(\frac{\partial A_M}{\partial x_n} \right)^2 \sigma_x^2 + \left(\frac{\partial A_M}{\partial \theta_n} \right)^2 \sigma_\theta^2 \right] \right\}^{1/2} \quad (3.2\text{-}19)$$

$$\sigma_{\phi_M} = \left\{ \sum_{n=1}^{N} \left[\left(\frac{\partial \phi_M}{\partial B_n} \right)^2 \sigma_B^2 + \left(\frac{\partial \phi_M}{\partial \psi_n} \right)^2 \sigma_\psi^2 + \left(\frac{\partial \phi_M}{\partial r_n} \right)^2 \sigma_r^2 + \left(\frac{\partial \phi_M}{\partial x_n} \right)^2 \sigma_x^2 + \left(\frac{\partial \phi_M}{\partial \theta_n} \right)^2 \sigma_\theta^2 \right] \right\}^{1/2}$$

Both influence coefficients (equations 3.2-18) and standard deviations σA_M and $\sigma \theta_M$ are calculated as standard procedure when the MCP calculates the amplitudes and phases of the acoustic duct modes. Thus, a significant feature of the modal calculation method is that the sensitivity of the method to errors in measurement and microphone location can be assessed for every modal structure that is calculated. The basis for this assessment is made by inputting to the MCP estimates of the standard deviations of the errors in pressure measurement and microphone location. Estimates of the errors in the amplitudes and phases of each of the calculated modes are obtained as an output of the MCP. For the remainder of this section, the form of the influence coefficients will be discussed and a physical interpretation will be presented for those cases where it is reasonably clear.

Physical Interpretation of Influence Coefficients

It is not seen readily from the expressions given in equation (3.2-18) for the influence coefficients, how errors in calculated modal amplitude and phase are influenced by acoustic measurement and microphone placement errors. It is apparent, however, that a significant term in all the influence coefficients is q_{Mn}. The q_{Mn} in turn are complicated functions of the particular mode set that is being determined, along with the microphone locations used to obtain data for input to the MCP.

In detail, the influence coefficients exhibit different characteristics depending on whether they are associated with microphone location errors or acoustic pressure measurement errors. The influence coefficient characteristics will thus be considered separately under these headings.

Microphone Location Errors

If the mode amplitude and phase sensitivities to angular or θ errors $\partial A_m / \partial \theta_n$ and $\partial \phi_m / \partial \theta_n$ are considered first, it can be seen from the equation (3.2-18) that they depend directly on the values m_s which are the set of integers giving the number of circumferential cycles of the sth spinning mode pattern. If all or most of the m_s are large, the sensitivity is high compared with cases where all the m_s are relatively small numbers. A high value of m is

associated with small circumferential wavelength, and it is to be expected that a given circumferential error $d\theta_n$ would impact determination of the phase of the pressures and modes to a greater extent when $d\theta_n/(2\pi/m)$ is large – that is when m is large – than when m is low. It is not intuitively obvious, but $\partial A_m/\partial\theta_n$ shows that the amplitude error as well as the phase error increases as the value of m increases.

In an exactly analogeous manner, large values of the axial wavenumbers (corresponding to short axial wavelength) increase the sensitivities of both A_m and ϕ_m to errors in axial location, dx_n.

The physical interpretation of sensitivities to errors in radial position, $\partial A_m/\partial r_n$ and $\partial\phi_m/\partial r_n$, is a little more obscure, and may be found by examining the expression for $k_{ns}h_{ns} = k_s E'(k_s r_n)$. This equation shows that the sensitivity depends on radial location, r_n, which is very different from the x and θ sensitivities which are independent of these coordinates. At either the inner or outer walls of the annular duct the slope of radial distribution function, $E(k_s r_n)$, vanishes. Therefore, pressure measurements at or near the duct walls are very insensitive to errors in radial location. Apart from these wall locations there are no other radial locations that will provide equivalent insensitivity in practice. If for example, the (m,0), (m,1) and (m,2) modes were present, a location in the neighborhood of the mean radius (for high hub-tip ratio) would be near the antinode of the (m,2) mode, and would thus give a very small value for $E'_{m,2}$. However, this location would be very near to the node of the (m,1) mode yielding a large value of $E'_{m,1}$. The resulting sensitivity would depend on the relative amplitudes of the (m,1) and (m,2) modes.

The eigenvalue, k_s also enters the sensitivity as a factor, and does play a similar role to the previously discussed axial and circumferential wave numbers, k_{xs} and m_s. That is, large k_s produces higher error sensitivity than low values of k_s. This relation is intuitively clear, for increasing k_s implies an increasing number of nodes and rapid changes of pressure in traversing from wall to wall. A given radial error is, therefore, reflected in relatively large pressure changes compared to cases where the radial pressure variation is more gradual, as is the case for low order radial modes (i.e., low values of k_s).

Pressure Measurement Errors

The expressions, equations (3.2-18), for the influence coefficients giving the effects of errors in measured pressure amplitude and phase upon the amplitude and phase of the resulting modal coefficients are somewhat complicated. This complication is a consequence solely of the fact that the quantities involved are complex variables. If, hypothetically, the quantities were all real, equations (3.2-14) for the modes in terms of measured pressures could be expressed as

$$\{A_m\} = [q_{mn}]\{B_n\}$$

Where A_m and B_n are amplitudes of the m^{th} mode and measured pressures at the n^{th} location respectively, and the q_{mn} are the magnitudes of the matrix Q_{mn} elements. Then, the error in a typical resultant can be obtained from the differential as:

$$dA_M = q_{M1}\, dB_1 + q_{M2}\, dB_2 + \cdots q_{MN}\, dB_N \qquad (3.2\text{-}20)$$

The influence coefficients, $\partial A_m/\partial B_n$ are seen to be simply q_{mn}, or just the elements of the Q matrix.

In the actual case, equations (3.2-14) are seen to contain q_{mn} as in the above hypothetical, real variable case, but they also include other factors, including harmonic functions of an angle that is a combination of the phases of the measured and calculated pressures and the phase of Q_{mn}. (It should be noticed, however, that the influence coefficients in this section are not functions of the calculated modal amplitudes).

To get a general appreciation for the nature of this complication, consider the case of two complex modes and two complex pressures, for illustration equation (3.2-14) becomes

$$\begin{aligned} Z_1 &= Q_{11}\, P_1 + Q_{12}\, P_2 \\ Z_2 &= Q_{21}\, P_1 + Q_{22}\, P_2 \end{aligned} \qquad (3.2\text{-}21)$$

The (complex) error relations again can be found from the differential:

$$\begin{aligned} dZ_1 &= Q_{11}\, dP_1 + Q_{12}\, dP_2 \\ dZ_2 &= Q_{21}\, dP_1 + Q_{22}\, dP_2 \end{aligned} \qquad (3.2\text{-}22)$$

Now these expressions are just as simple structurally as the hypothetical real variable case given by equation (3.2-20). It is only when we obtain the separate effects on modal amplitude and phase of both measured pressure amplitude and measured pressure phase that the extra factors (apart from q, the amplitude of Q) in the influence coefficient expressions appear.

To suggest the nature of this complication, let us examine Z_1 and dZ_1, in the above equations (3.2-21) and (3.2-22). For simplicity

$$\begin{aligned} Z_1 &= Q_{11}\, P_1 + Q_{12}\, P_2 \\ Z_1 &= U_1 + U_2 \end{aligned}$$

Then the complex error in Z_1 due to errors in the complex components, $U_1 = Q_{11}P_1$, and $U_2 = Q_{12}P_2$ can be expressed as the differential:

$$dZ_1 = dU_1 + dU_2$$

Figure 3.2-1 shows Z_1 as the resultant of U_1 and U_2. Each complex error dU_1 and dU_2 is shown resolved into two components:

1. A component colinear with the appropriate U vector. This component is the differential of the amplitude of U or the error in the U amplitude.

2. A component perpendicular to U which is equal to the error in the angle of U multiplied by the magnitude of U.

Figure 3.2-1 shows the projections of these two different components of the errors dU_1 and dU_2 upon the resultant factor Z_1. The sum of these errors may be seen to give the error dA_1 in the amplitude of the resultant Z_1. The trigonometry involved in describing this projection process mathematically can be shown to account for the factors for $\partial A_m/\partial B_n$ and $\partial A_m/\partial \psi_n$ in equations (3.2-18).

A similar process (not illustrated) may be used to find the error in the phase of the resultant Z_1. This time the same four U-component errors are projected on an axis perpendicular to Z_1. The sum of these perpendicular components is equivalent to the error in the phase of Z_1 multiplied by A_1, the magnitude of Z_1. On dividing by A_1, the phase error of the resultant is obtained. This procedure may be shown to give the mathematical expressions for the pair of influence coefficients $\partial \phi_m/\partial B_n$ and $\partial \phi_m/\partial \psi_n$ in equations (3.2-18).

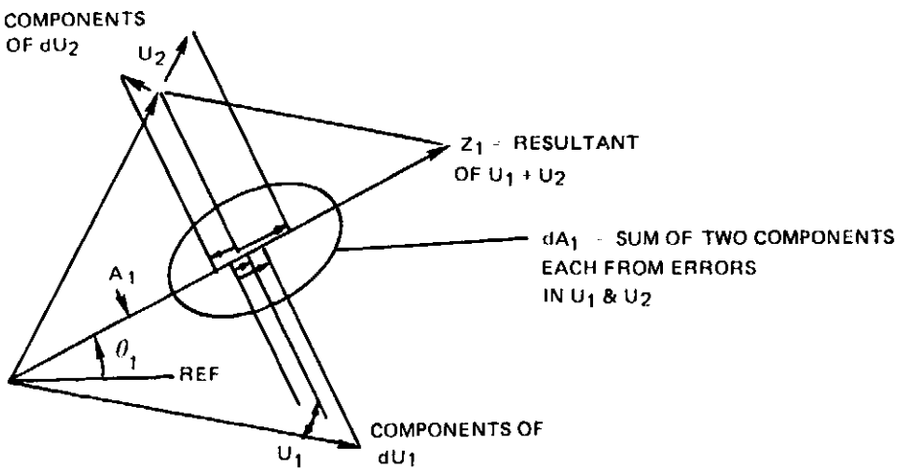

Figure 3.2-1 Error in Amplitude of $Z_1 = U_1 + U_2$

The main conclusions from the above description of the physical characteristics of the influence coefficients for both microphone location errors and acoustic pressure measurement errors are as follows:

For microphone location errors:

i) Influence coefficients are functions of the calculated modal amplitude and phase as well as of microphone location.

ii) Calculated modes with large circumferential, axial or radial wave numbers are sensitive to errors in locating microphones.

For pressure measurement errors:

i) The influence coefficients are functions of measurement position and the calculated modal phase angle only.

3.2.5 User's Manual for Computer Programs

A separate User's Manual has been written for the MCP and the MLP that were developed and checked out in section 3.2.2 and 3.2.3, respectively. They are both presented in a self contained report in references 9 and 11.

3.3 APPROACH FOR MEASURING RANDOM SOUND FIELDS

3.3.1 Introduction

In addition to coherent discrete frequency noise resulting from rotor-stator interaction, fan noise contains significant random or broadband content - produced by rotor-turbulence interaction, for example. The objectives of the analytical investigation conducted in this part of the program were to derive a means for specifying the essential properties of a random noise field in a cylindrical duct, and then to evolve instrumentation and data reduction techniques that permit experimental determination of these properties.

To simplify the problem, which is more complicated than the analysis of coherent, discrete frequency fields, attention is focused on thin annular ducts, where radial variations in the sound pressure are negligible. The content is divided into these parts:

Section 3.3.2, "Field Structure of Random Noise in Thin Annular Ducts", formulates the concept of the modal power spectral density function, its expression in terms of cross property functions of local pressures, and interpretations of the function including spinning modes. The elements of data acquisition and processing systems for experimental determination of the field structure are discussed.

Section 3.3.3 describes a special system for measuring random fields in thin annular ducts an array of circumferentially spaced detectors, incorporating progressive linear delay times. The function of the array is to provide a direct measure of the set of mode-frequency pairs having common cutoff ratios. Array performance characteristics are derived for both random and coherent, discrete-frequency sound fields.

3.3.2 Field Structure of Random Noise in Thin Annular Ducts

Background

In order to appreciate the objectives and approach of this analytical study, it is helpful to mention certain features of the current theory for ducted coherent sound fields.

The theory of coherent, discrete wave propagation in cylindrical ducts has been established for some time and has been validated by a number of experimental investigations. A central item in both formulation of this theory and also in determining the type of measurements required to acquire meaningful experimental results is the appropriate specification of the pressure distribution in a transverse plane perpendicular to the duct axis. The radial structure of this distribution is expressible in terms of sums of Bessel functions of order corresponding to the cycles of circumferential pressure variation. Thus, the transverse pressure structure depends crucially on a very clear understanding of the characteristics of the circumferential pressure variation at a fixed radial location, typically along the circumference of the duct wall. The features of this circumferential behavior are embodied in the case of a very thin annular duct having, at any instant, a constant pressure across its very narrow annulus.

By focusing on this simpler case it is possible to work with relations that are unencumbered by Bessel functions and other complications that tend to obscure certain basic features. In this way it has been possible to recognize clearly that so-called spinning modes are a useful and convenient way of describing the coherent pressure field of a rotor and the fields generated by rotor-stator interactions. In particular, simple interpretations of propagation direction, cutoff, and other properties follow from this thin annulus approach and are used to guide and interpret the results of studies of the more general cases where the duct annulus is of finite size. In the current study of random noise, the approach of formulating the problem for the case of a thin annular duct has been retained.

An analysis of random fields in cylindrical ducts (ref. 4 and 6) has been done previously by postulating the existence of a spinning mode amplitude spectral density function. However, to extend the coherent spinning mode formulations to describe random pressure fields requires that the concepts of "amplitude" and "phase" of such a mode be modified to accommodate random time variations. Providing an a priori physical basis for such a modification is difficult, and it was therefore decided in the present study to adopt a formally different model for the space-time description of a random pressure field — one that did not embody spinning modes as its starting point. This model specifies the field by products of pairs of functions — functions of space only that are strictly periodic, and functions of time alone that satisfy only the usual requirements for random time series.

After description of the space-time pressure field in terms of this mathematical model the modal power spectral density function, which specifies the pressure field in terms of mode-frequency space, is introduced. To evaluate the modal psd, expressions are first obtained for the cross correlation function of the pressure field by using the space-time model. Then the modal psd is found as the (double) Fourier transform of the cross correlation function.

Finally, the modal psd function is resolved into two component functions, each of which has mathematical properties paralleling those associated respectively with forward and reverse spinning modes in the coherent, discrete field case. Because of this correspondence, these components of the modal psd function are designated as the spinning mode components of the random field modal psd. Furthermore, it is subsequently shown (in another section of this report, section 3.3.3) that these random field spinning modes "exist" in the operationally definable and measurable sense.

Mathematical Model of Random Pressure Field

A coherent discrete pressure field in a thin annular duct may be specified by the superposition of spinning modes in the usual way by:

$$p(\theta,t) = \sum_{m=-\infty}^{\infty} \sum_{n=1}^{\infty} C_{mn} \cos(m\theta - n\omega t + \varphi_{mn}) \qquad (3.3\text{-}1)$$

This form cannot conveniently be modified to describe a random field because C_{mn} and Q_{mn} must incorporate time dependence, and a continuous frequency variation must be provided.

Instead, the following form will be taken as the mathematical model of a random field in a thin annular duct:

$$p(\theta,t) = \sum_{m=0}^{\infty} \left[a_m(t) \cos(m\theta) + b_m(t) \sin(m\theta) \right] \qquad (3.3\text{-}2)$$

where $a_m(t)$ and $b_m(t)$ are random time functions characterized only by their cross and direct correlation and power spectral functions.

Equation 3.3-2 is seen to satisfy the following requirements for a model of the pressure field:

1. Time dependence at all positions, θ, that is arbitrarily random in the conventional sense of the term as used in the context of time series (ref. 12).

2. Spatial variation at any instant of time that is strictly periodic in θ, with period 2π.

Power Spectral Density of Pressure Field

The objective is to derive a suitable function, starting with p (θ,t) given by equation (3.3-1), that will specify the distribution of acoustic pressure as a function of mode number, m, and frequency, ω. Means for obtaining this function in terms of experimental data are also required. This function is called the modal power spectral density, $S(m, \omega)$. Two basic steps are used to obtain an expression for $S(m, \omega)$. First, the cross-correlation function corresponding to equation (3.3-2) for p (θ,t) is formulated. Secondly, by virtue of the relation that power spectral density aad correlation functions are Fourier transform pairs, an immediate statement of the function $S(m, \omega)$ is obtained.

The correlation function of a function that is periodic with respect to θ and random with respect to time can be written as:

$$R(\sigma, \tau) = \lim_{T\to\infty} \frac{1}{2\pi T} \int_0^{2\pi} \int_{-T/2}^{T/2} p(\theta,t) \cdot p(\theta+\sigma, t+\tau)\, dt\, d\theta \qquad (3.3\text{-}3)$$

It will be useful to define the partial correlation function, $R_\theta(\theta;\sigma,\tau)$ by means of:

$$R_\theta(\theta;\sigma,\tau) = \lim_{T\to\infty} \frac{1}{T} \int_{-\frac{T}{2}}^{T/2} p(\theta,t) \cdot p(\theta+\sigma, t+\tau)\, dt \qquad (3.3\text{-}4)$$

$$= \overline{p \cdot p(\sigma, \tau)}$$

so that equation (3.3-3) can be expressed:

$$R(\sigma,\tau) = \frac{1}{2\pi} \int_0^{2\pi} R_\theta(\theta;\sigma\tau)\, d\theta \qquad (3.3\text{-}5)$$

The integral $R_\theta(\theta;\sigma,\tau)$ is simply the time-correlation of the pair of pressure signals at θ and $\theta + \sigma$.

The resulting modal power spectral density, $S(m, \omega)$ is the (double) Fourier transform of $R(\sigma, \tau)$, which because of theσ - periodicity (σ is the difference in θ coordinates) becomes:

$$S(m,\omega) = \frac{1}{4\pi^2} \int_{-\pi}^{\pi} \int_{-\infty}^{\infty} R(\sigma,\tau)\, e^{-i\omega\tau} e^{-im\sigma}\, d\tau\, d\sigma \quad (-\infty < m, \omega < \infty) \qquad (3.3\text{-}6)$$

On eliminating $R(\sigma, \tau)$ between equations (3.3-4) and (3.3-6), a general expression for the modal power spectral is obtained:

$$S(m,\omega) = \lim_{T\to\infty} \frac{1}{8\pi^3 T} \int_{-\pi}^{\pi}\int_{-\infty}^{\infty}\int_{0}^{2\pi}\int_{-\frac{T}{2}}^{\frac{T}{2}} p(\theta,t)\cdot p(\theta+\sigma, t+\tau)\, e^{-i(\omega\tau+m\sigma)}\, dt\, d\theta\, d\tau\, d\sigma \qquad (3.3\text{-}7)$$

This expression for $S(m, \omega)$ will be evaluated in terms of the specific model for $p(\theta,t)$ given by equation (3.3-2) by executing the following sequence of steps:

1. The explicit form for $p(\theta,t)$ given by equation (3.3-2) is substituted in equation (3.3-4) to obtain the partial correlation function $R_\theta(\theta;\sigma,\tau)$.
2. The Fourier time transform $\frac{1}{2\pi}\int_{-\infty}^{\infty} R_\theta(\theta;\sigma,\tau) e^{-i\omega\tau}\, d\tau$ is applied to $R_\theta(\theta;\sigma,\tau)$ to obtain a local cross spectral function expression in terms of modal spectral functions.
3. A space-averaging operation, $\frac{1}{2\pi}\int_0^{2\pi} d\theta$: is applied to the result of step 2. The result will be a spectral function in the form of a Fourier series with argument σ.
4. By applying the Fourier transform for $\sigma \to m$ in equations (3.3-6) or (3.3-7), the coefficients of this series are obtained. These coefficients are the desired modal power spectral density functions, and the set of these functions is $S(m, \omega)$.

Thus, the four integrations involved in obtaining $S(m, \omega)$ by equation (3.3-7) are executed in the order: t, τ, θ, σ.

Step 1 Substituting equation (3.3-2) for $p(\theta,t)$ in equation (3.3-4) for the partial correlation coefficient, R_θ, and using indices p and q for m in the double summation gives:

$$R_\theta(\theta;\sigma,\tau) = \lim_{T\to\infty}\frac{1}{T}\int_{-\frac{T}{2}}^{\frac{T}{2}} dt : \left\{\sum_{p=0}^{\infty}\left[a_p(t)\cos p\theta + b_p(t)\sin p\theta\right]\right\}\cdot$$
$$\cdot\left\{\sum_{q=0}^{\infty}\left[a_q(t+\tau)\cos q(\theta+\sigma) + b_q(t+\tau)\sin q(\theta+\sigma)\right]\right\}$$

$$= \sum_m \left\{\tfrac{1}{2}\left[\overline{a_m a_m(\tau)} + \overline{b_m b_m(\tau)}\right]\cos m\sigma + \tfrac{1}{2}\left[\overline{a_m b_m(\tau)} - \overline{b_m a_m(\tau)}\right]\sin m\sigma\right\} \qquad (3.3\text{-}8)$$

$$+ \sum_m \left\{\tfrac{1}{2}\left[\overline{a_m a_m(\tau)} - \overline{b_m b_m(\tau)}\right]\cos m(2\theta+\sigma) + \tfrac{1}{2}\left[\overline{a_m b_m(\tau)} + \overline{b_m a_m(\tau)}\right]\sin m(2\theta+\sigma)\right\}$$

$$+ \sum_{p\neq q} F_{pq}$$

where the F_{pq} terms have the general structure

$$F_{pq} = \left\{ \begin{matrix} \overline{a_p a_q(\tau)} \\ \overline{b_p b_q(\tau)} \\ \overline{a_p b_q(\tau)} \end{matrix} \right\} \cdot \left\{ \begin{matrix} \sin \\ \cos \end{matrix} \left[(p \pm q)\theta + \sigma \right] \right\}$$

Step 2 Applying the Fourier time transform to equation 3.3-8):

$$\mathcal{F}_\tau \{R_\theta(\theta;\sigma,\tau)\} = \frac{1}{2\pi}\int_{-\infty}^{\infty} R_\theta(\theta;\sigma,\tau)\, e^{-i\omega\tau}\, d\tau \qquad (3.3\text{-}9)$$

$$= \sum_m \left\{ \tfrac{1}{2}\left[\Phi_m^a(\omega) + \Phi_m^b(\omega)\right]\cos m\sigma + \tfrac{1}{2}\left[\Psi_m^{ab}(\omega) - \Psi_m^{ba}(\omega)\right]\sin m\sigma \right\}$$

$$+ \sum_m \left\{ \tfrac{1}{2}\left[\Phi_m^a(\omega) - \Phi_m^b(\omega)\right]\cos m(2\theta+\sigma) + \tfrac{1}{2}\left[\Psi_m^{ab}(\omega) + \Psi_m^{ba}(\omega)\right]\sin m(2\theta+\sigma) \right\}$$

plus sum of Fourier transforms of the F_{pq} terms in equation (8).

The following listing defines the notation for the Fourier transform pairs in equations (8) and (3.3-9):

CORRELATION FUNCTION	⟷	SPECTRAL FUNCTION
$\overline{a_m a_m(\tau)}$		$\Phi_m^a(\omega)$
$\overline{b_m b_m(\tau)}$		$\Phi_m^b(\omega)$
$\overline{a_m b_m(\tau)}$		$\Psi_m^{ab}(\omega)$
$\overline{b_m a_m(\tau)}$		$\Psi_m^{ba}(\omega)$

In equation (3.3-9) only the terms in the first line are independent of position θ, and depend only on the m-spectral functions and the separation σ of pairs of signal detectors. All other terms, including those resulting from the transforms of the $p \neq q$ terms in equation (3.3-8) involve θ-dependence.

Step 3 Apply the θ-averaging operation required by equation (3.3-8) to equation (3.3-9):

The left hand side of equation (3.3-9) becomes the space average of the cross-spectral function between detector pairs separated by σ. It is a quantity directly calculable from cross-spectral measurements and will appear in further analytical and experimental connections. Because of its importance it is represented by the symbol $S_\sigma(\sigma;\omega)$ where

$$S_\sigma(\sigma;\omega) = \frac{1}{2\pi}\int_0^{2\pi} \mathcal{F}_\theta\{R_\sigma(\theta;\sigma,\tau)\}\,d\theta \qquad (3.3\text{-}10)$$

Application of the operation $\frac{1}{2\pi}\int_0^{2\pi} d\sigma;$ to the right side of equation (3.3-9) makes all terms having harmonic θ-dependence vanish, leaving only the following simple sum from the first line of equation (3.3-9)

$$S_\sigma(\sigma;\omega) = \sum_{m=0}^{\infty}\left\{\frac{1}{2}\left[\varphi_m^a(\omega) + \varphi_m^b(\omega)\right]\cos m\sigma + \frac{1}{2}\left[\psi_m(\omega) - \psi_m^*(\omega)\right]\sin m\sigma\right\} \qquad (3.3\text{-}11)$$

(The symbols $\psi_m(\omega)$ and its conjugate $\psi_m^*(\omega)$ have replaced $\psi_m^{ab}(\omega)$ and $\psi_m^{ba}(\omega)$.

Since $b_m a_m(\tau) = \overline{a_m b_m(\tau)}$ the Fourier transforms ψ_m^{ab} and ψ_m^{ba} can readily be shown to be conjugate.

Introducing the definition:

$$\begin{aligned} \Phi_m(\omega) &= \left[\varphi_m^a(\omega) + \varphi_m^b(\omega)\right] \qquad (\text{REAL}) \\ \Psi_m(\omega) &= \left[\psi_m(\omega) - \psi_m^*(\omega)\right] \qquad (\text{IMAGINARY}) \end{aligned} \qquad (3.3\text{-}12)$$

Equation (3.3-11) becomes:

$$S_\sigma(\sigma;\omega) = \sum_{m=0}^{\infty}\left\{\frac{1}{2}\Phi_m(\omega)\cos m\sigma + \frac{1}{2}\Psi_m(\omega)\sin m\sigma\right\} \qquad (3.3\text{-}13)$$

Step 4 Fourier transforming equation (3.3-13) with respect to σ completes the process for obtaining the modal power spectral density, $S(m,\omega)$:

$$\begin{aligned} S(m,\omega) &= \frac{1}{2\pi}\int_{-\pi}^{\pi} S_\sigma(\sigma;\omega)\, e^{-im\sigma}\,d\sigma \\ &= \sum_{n=0}^{\infty}\frac{1}{2\pi}\int_{-\pi}^{\pi}\left\{\frac{1}{2}\Phi_n(\omega)\cos n\sigma + \frac{1}{2}\Psi_n(\omega)\sin n\sigma\right\} e^{-im\sigma}\,d\sigma \qquad (3.3\text{-}14) \\ &= \sum_{n=0}^{\infty}\left\{\frac{1}{4}\Phi_n(\omega)\left[\delta(m-n)+\delta(m+n)\right] + i\frac{1}{4}\Psi_n(\omega)\left[-\delta(m-n)+\delta(m+n)\right]\right\} \end{aligned}$$

The dummy index η has replaced m as the index of summation in equation (3.3-13) in keeping with conventional practice. The δ - functions required in the Fourier transformation of harmonic functions are defined to unity operators when their argument is zero and otherwise are annhilating operators. Collecting terms with $\delta(m-n)$ and $\delta(m+n)$ factors, and replacing the pure imaginary $\Psi_n(\omega)$ by $i\Psi_n'(\omega)$, $S(m,\omega)$ can be expressed in terms of real functions:

$$S(m,\omega) = \sum_{n=0}^{\infty} \left\{ \frac{1}{4}\left[\Phi_n(\omega) + \Psi'_n(\omega) \right] \delta(m-n) + \frac{1}{4}\left[\Phi_n(\omega) - \Psi'(\omega) \right] \delta(m+n) \right\} \qquad (3.3\text{-}15)$$

Letting

$$U_n(\omega) = \Phi_n(\omega) + \Psi'_n(\omega) \qquad (3.3\text{-}16a)$$

$$V_n(\omega) = \Phi_n(\omega) - \Psi'_n(\omega) \qquad (3.3\text{-}16b)$$

the modal power spectral density becomes:

$$S(m,\omega) = \sum_{n=0}^{\infty} \left\{ \frac{1}{4} U_n(\omega)\, \delta(m-n) + \frac{1}{4} V_n(\omega)\, \delta(m+n) \right\} \qquad (3.3\text{-}17)$$

This equation indicates that $S(m, \omega)$ is defined over both positive and negative values of m and ω. The U and V functions, being combinations of functions resulting from Fourier transforms are perforce defined over the entire ω domain. Also the function $\delta(m+n)$ directs $\frac{1}{4}V_n(\omega)$ to fill the negative m-domain of $S(m, \omega)$ just as $\delta(m-n)$ fills its positive domain with $\frac{1}{4} U_n(\omega)$.

Now by combining these characteristics with the symmetry properties of the constituent $\Phi_n(\omega)$ and $\Psi'_n(\omega)$ functions, $S(m, \omega)$ can be simplified. For this purpose it should be noted that since $\Phi_n(\omega)$ results from Fourier transforming the auto correlation functions of the $a_n(t)$ and $b_n(t)$ series it is an even function of ω. Similarly the combination of cross spectral functions of these series that comprises $\Psi'_n(\omega)$ (see eq. 3.3-12) results in $\Psi'_n(\omega)$ being an odd function of ω. (This can be shown by recognizing that $(\overline{a_m b_m(\tau)} - \overline{b_m a_m(\tau)})$ is an odd function of τ. Then converting the factor $\exp(-i\omega\tau)$ to rectangular form when writing the Fourier transform to obtain Ψ_m it will become evident that Ψ_m is pure imaginary and an odd function of ω.)

The following important relations are consequence of the above properties:

$$U_n(-\omega) = V_n(\omega) \qquad (3.3\text{-}18)$$

or

$$V_n(-\omega) = U_n(\omega)$$

and $$S(m,-\omega) = S(-m,\omega) \qquad (3.3\text{-}19)$$

or $$S(-m,-\omega) = S(m,\omega)$$

Equations (3.3-19) indicate that if the (m,ω) plane is divided into 4 quadrants in the usual way, as shown in Figure 3.3-1(a), quadrants I and III where m and ω have the same sign present equal information about $S(m,\omega)$, and similarly, the specification of $S(m,\omega)$ in both quadrants II and IV where m and ω have opposite signs is redundant. $S(m,\omega)$ may accordingly be specified in quadrant I by adding its (equal) values in quadrants I and III. Similarly, the quandrant II values may be added to that of quadrant IV to allow representation only in quadrant IV of $S(m,\omega)$ for values of m and ω having opposite signs.

Figure 3.3-1(b) shows a sample point of this representation of $S(m,\omega)$, where only positive values of ω are used. Values corresponding to positive m in $S(m,\omega)$ are denoted by the symbol $S_m^-(|\omega|)$ and $S_m^+(|\omega|)$ denotes the component functions for negative values of m in $S(m,\omega)$. Absolute value signs are used with the ω to ensure against the possibility of evaluating the functions for negative ω. Use of m (or n) as a subscript in $S_m^+(|\omega|)$ and $S_m^-(|\omega|)$ is restricted to positive values only, in conformity with all prior usage, starting with the time series $a_n(t)$, $b_n(t)$, and the spectral functions $\Phi_m(\omega)$ and $\Psi_m(\omega)$. The + and - superscripts are used to indicate opposite and similar pairings, respectively, of the signs of m and ω in the corresponding modal psd, S(m,ω).

The signed superscripts used with $S_m^+(|\omega|)$ and $S_m^-(|\omega|)$ have been selected to help convey this information: $S_m^+(|\omega|)$ and $S_m^-(|\omega|)$ may be interpreted as the random field counterparts of forward and reverse spinning modes in coherent discrete frequency fields. In the coherent case, $P(\theta,t) \propto \exp i[m\theta - \omega t]$, where m and ω appear with opposite signs, represents a forward spinning wave since the pressure at $\theta \& t$ is received at $(\theta+\Delta\theta)$ $\Delta t = (m/\omega)\,\Delta\theta$ seconds later. The spin rate of this mode is therefore $\Omega = \Delta\theta/\Delta t = \omega/m$. Similarly, a reverse spinning mode, in which m and ω take the same sign, has argument $[m\theta+\omega t]$ indicating that pressure at $\Delta\theta$ distant from θ was received earlier or $\Delta t = -\frac{m}{\omega}\Delta\theta$. In each case, the magnitude of the spin velocity is $|\Omega| = |m/\omega|$. These coherent case facts suggest a corresponding interpretation for the modal power spectral density function. In Figure 3.3-1(b), radial lines of slope $|\Omega| = |m/\omega|$ may be considered to represent the common average spin rate magnitude of the forward and reverse spinning mode components comprising the random field modal psd, S (m, ω) at the illustrated point values.

Figure 3.3-2 illustrates a representation of these spinning mode components of the modal power spectral density function. Clearly, S (m, ω) and the components $S_m^+(|\omega|)$ and $S_m^-(|\omega|)$ are defined over a continuous set of values of ω, but exist only for integer values of the variable, m. This property, which is a consequence of the θ — periodic boundary condition on $P(\theta,t)$, will be shown to have major significance in the operation of the delayed circular array system for duct field measurements described in section 3.3.3.

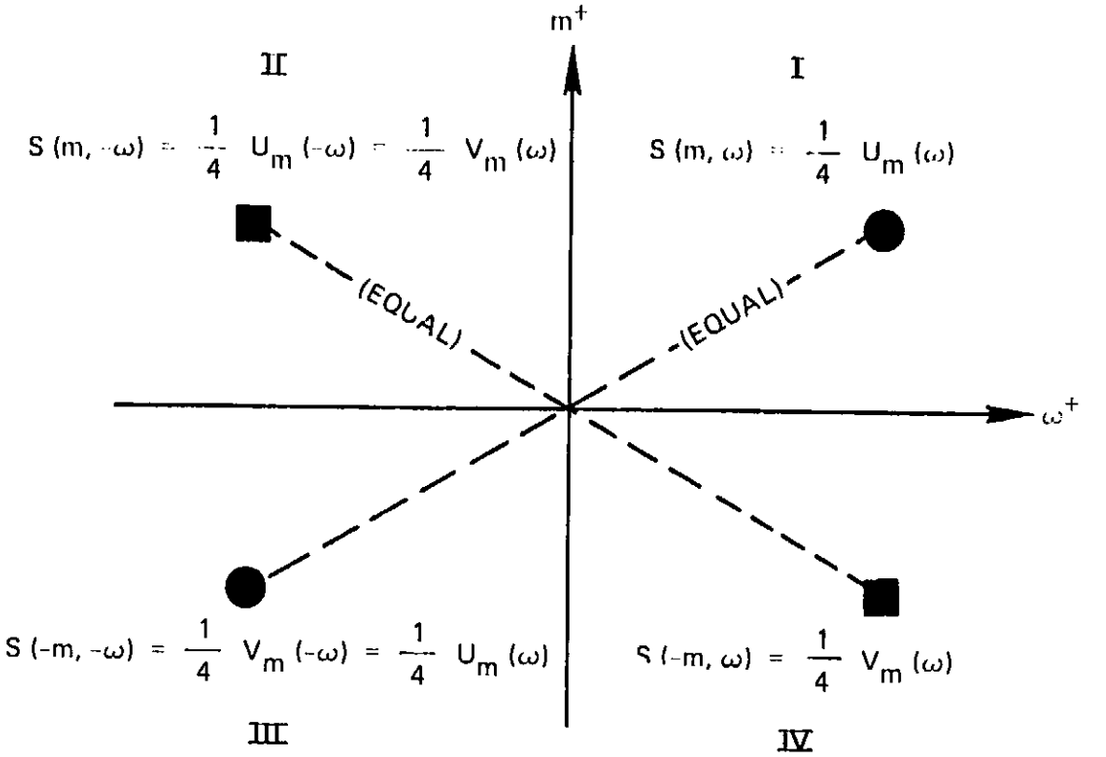

Figure 3.3-1a Modal Power Spectral Density, S (m, ω) Point Values

(m as a subscript is always positive)

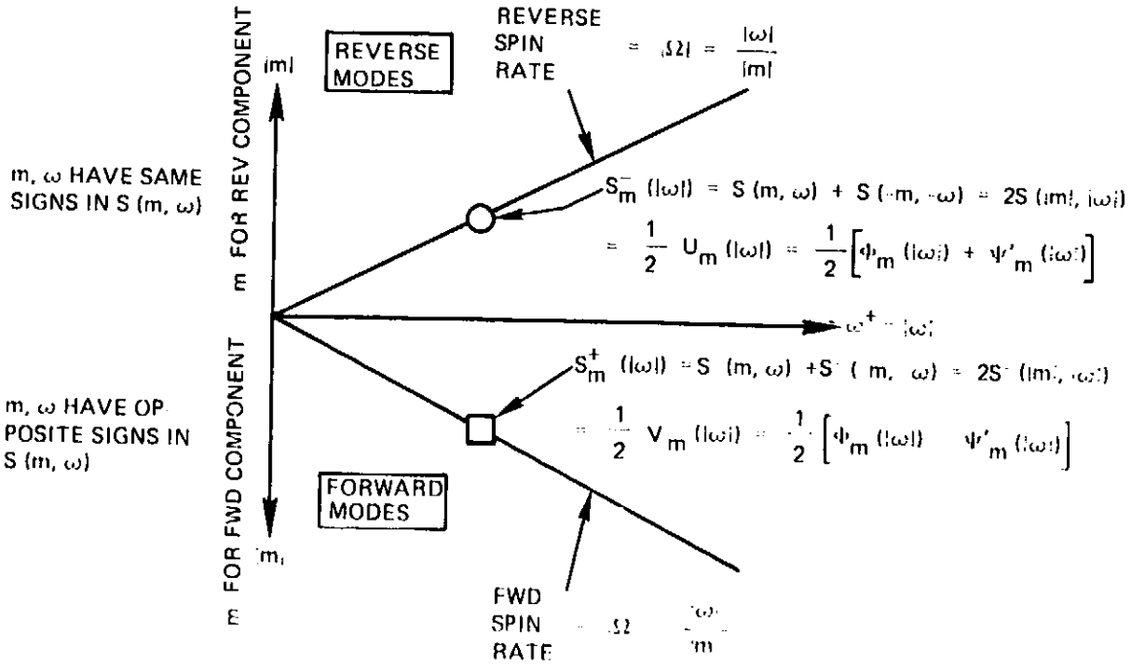

Figure 3.3-1b Point Values of $S^{-}_{m}(|\omega|)$ and $S^{+}_{m}(|\omega|)$ Components of S (m, ω)

(m as a subscript is always positive)

A more formal development of the correspondence between random and discrete field cases may be obtained by starting with a single discrete mode $C_m e^{i[m\theta - \omega t]}$, and computing the appropriate correlation functions and their Fourier transforms corresponding to those defined previously in the development of $S(m,\omega)$ for the random case. The result is found to be a single pair of δ- functions, each of effective strength $\frac{1}{4} C_m C_m^*$, one located at $(-m, \omega)$ and the other at $(m,-\omega)$. Their sum, $S_m^+(|\omega|) = S(-m,\omega) + S(m,-\omega)$ $= \frac{1}{2} C_m C_m^*$, is of course the well-known expression for the "power" or mean-square pressure of this forward mode.

Despite the similarities described above in these random and discrete case functions, the appelations of "forward" and "reverse" to the modal components $S_m^+(|\omega|) \notin S_m^-(|\omega|)$ remain to be justified more fully. In section 3.3.3, "Delayed Circular Array System" will be found a physical or operational basis for use of these terms. In concluding this subsection, it should be again mentioned that the construction of a spinning mode was completely absent in the mathematical model of the random pressure field used here as the basis for deriving the modal power spectral density. Rather, it emerged as a component of the modal psd function that satisfied certain mathematical properties held in common with coherent, discrete frequency field spinning modes. But furthermore, as will be shown in section 3.3.3, random field spinning modes turn out also to have a very close physical resemblance (defined in terms of measurable attributes) to their coherent pressure field counterparts.

The following equations summarize the expressions for the spinning mode components, $S_m^+(|\omega|)$ and $S_m^-(|\omega|)$, of the modal power spectral density function, $S(m,\omega)$.

$S(m,\omega)$
Forward spin component.
$m \notin \omega$ have opposite
sign in $S(m,\omega)$:

$$\begin{aligned} S_m^+(|\omega|) &= S(m,-\omega) + S(-m,\omega) \\ &= 2\,S(-|m|,|\omega|) \\ &= \tfrac{1}{2} V_m(|\omega|) \quad (= \tfrac{1}{2} U_m(-|\omega|)) \\ &= \tfrac{1}{2}\left[\Phi_m(|\omega|) - \Psi_m'(|\omega|)\right] \end{aligned}$$

$S(m,\omega)$
Reverse spin component.
$m \notin \omega$ have same
sign in $S(m,\omega)$:

$$\begin{aligned} S_m^-(|\omega|) &= S(m,\omega) + S(-m,-\omega) \\ &= 2\,S(|m|,|\omega|) \\ &= \tfrac{1}{2} U_m(|\omega|) \quad (= \tfrac{1}{2} V_m(-|\omega|)) \\ &= \tfrac{1}{2}\left[\Phi_m(|\omega|) + \Psi_m'(|\omega|)\right] \end{aligned}$$

(note: m as a subscript is always a positive integer)

Measurement of Modal Power Spectral Density in Terms of Cross Spectral Functions

Procedural Alternatives

There are a number of ways that can be followed to determine experimentally the modal psd of the pressure field in a thin annular duct. Choice of method depends on several factors, including the use to be made of the final result and the availability of data acquisition and processing equipment. Two procedures are described in this report. This section gives a method that is essentially patterned after the analytical procedure that was used to derive an expression for the modal psd in terms of cross spectral functions.

Section 3.3.3 presents a different method, using a circumferential array of detectors incorporating progressive time delays. In a thin annular duct, the array system maps the set of modes having a common cutoff ratio and eliminates the requirement for obtaining cross spectral properties. Additionally, the cross spectral method will provide a basis for comparison with the delayed array measurement system described in Section 3.3.3.

Before proceding to this major topic, a brief description of the use of the cross properties method in measuring random pressure fields is first presented below.

Modal psd From Cross Spectral Measurements

Since cross-properties are involved in this procedure, simultaneous information from pairs of microphones must be processed. If the field is stationary, these signals may be obtained from a reference detector, and a second detector, separated $\Delta\theta = \sigma$ from the reference, with the understanding that the θ-location of both microphones must assume a succession of values. Alternatively, signals from N detectors spaced $\Delta\theta = 2\pi/N$ apart may be selected for processing. This procedure is required if the field characteristics are not stationary.

Equation (3.3-15) gives explicit instructions for computing $S(m,\omega)$ in terms of $\Phi_m(\omega)$ and $\Psi'_m(\omega)$, and equations (3.3-20) specify clearly how the modal components $S^+_m(|\omega|)$ and $S^-_m(|\omega|)$ are to be computed in terms of the same $\Phi_m(\omega)$ and $\Psi'_m(\omega)$ functions. Therefore, it is sufficient to describe a procedure for obtaining Φ_m and Ψ'_m in terms of measured data:

First, the θ-averaged cross spectral density $S_\sigma(\sigma;\omega)$ is obtained. For equispaced detector locations obtain

$$S_\sigma(\sigma_i;\omega) = \frac{1}{N}\sum_{j=0}^{N-1} S(\theta_j, \theta_j + \sigma_i; \omega)$$

where $S(\theta_j, \theta_j + \sigma_i; \omega)$ is the measured cross spectral density between detectors at θ_j and $\theta_j + \sigma_i$. $S_\sigma(\sigma_i; \omega)$ is evaluated for $\sigma_1 = 0$, $\sigma_2 = 2\pi/N$, etc. to define $S_\sigma(\sigma; \omega)$ as a set of N functions of ω. Values of $S(\theta_j, \theta_j + \sigma_i; \omega)$ and thus $S_\sigma(\sigma_i, \omega)$, may be found for a set of frequencies, ω, in the range of interest.

Typically for such a frequency, say ω_o, the known value of $S_\sigma(\sigma; \omega_o)$ determined by the above procedure has been expressed by means of equation (3.3-13) in terms of the desired modal functions $\Phi_m(\omega_o)$ and $\Psi_m(\omega_o)$ $(= i\,\Psi'_m(\omega_o))$ i.e.

$$S_\sigma(\sigma_i; \omega_o) = \sum_{m=0}^{\infty} \left\{ \tfrac{1}{2} \Phi_m(\omega_o) \cos m\sigma_i + \tfrac{1}{2} \Psi_m(\omega_o) \sin m\sigma_i \right\} \qquad (3.3\text{-}22)$$

The right hand side of equation (3.3-22) is just a Fourier series representation of the known lefthand side function having (numerical) coefficients
These coefficients are then found by standard algorithms for N-point Fourier analysis:

$$\tfrac{1}{2}\Phi_m(\omega_o) = \frac{2}{N} \sum_{i=0}^{N-1} S_\sigma(\sigma_i; \omega_o) \cos m\sigma_i \qquad (m \neq 0)$$

and

$$\tfrac{1}{2}\Psi(\omega_o) = \frac{2}{N} \sum_{i=0}^{N-1} S_\sigma(\sigma_i; \omega_o) \sin m\sigma_i$$

In practice since $S_\sigma(\sigma; \omega_o)$ is a complex number Φ_m is real, and Ψ_m is pure imaginary, it follows that Φ_m can be obtained by processing only the real part of S in the cosine algorithm and Ψ'_m (the magnitude of Ψ_m) can be obtained by using only the imaginary part of S in the second formula above. If the complex quantities, S, are used in the algorithm, vanishing of the alternate parts of the two results will serve as a check on the computations.)

Summary of Steps

1. Before taking data decide on highest frequency, ω_{max} at which modal psd information is needed.

2. Calculate m^+, the circumferential mode number at or slightly above cutoff for ω_{max}.

3. Select N_1 the number of microphones or microphone locations, such that $N > 2M^+$ to avoid aliasing.

4. Obtain data in the form of N^2 cross spectral density functions between microphones pairs separated by θ_i $(i = 0, 1, \cdots N-1)$, that is obtain $S(\theta_j, \theta_j + \theta_i; \omega)$.

Note: Only N autospectra and one-half of the $(N^2 - N)$ cross spectra need be measured- the remaining cross spectra corresponding to values of $\sigma > \pi$ are obtainable as complex conjugates of the former since $S(\theta_j, \theta_i, \omega) = S^*(\theta_i, \theta_j; \omega)$

5. Average these functions over θ by formula (3.3-21) to get $S_\sigma(\sigma_i; \omega)$.

6. Select frequencies $\omega = \omega_0, \omega_1, \cdots \omega_{max}$, and process the results of step 5 at each of these ω by equations (3.3-23) to obtain the functions

$$\tfrac{1}{2}\,\Phi_m(\omega) \qquad \text{and} \qquad \tfrac{1}{2}\,\Psi'_m(\omega)$$

7. Compute the $S_m^+(|\omega|)$ and $S_m^-(|\omega|)$ components of the modal psd, $S(m, \omega)$, from the sum and difference of $\frac{1}{2}\,\Phi_m$ and $\frac{1}{2}\,\Psi'_m$ obtained in step 6 by the simple formula (3.3-20).

3.3.3 Delayed Circular Array Systems for Measurement of Discrete Frequency and Random Pressure Fields

Introduction

A prime objective of the background material presented in section 3.3.2, "Field Structure of Random Noise in Thin Annular Ducts – Background" has been to define the modal power spectral density function, its properties, and a method for its measurement. This information will be needed now to establish the operating characteristics of the delayed circular array for pressure field measurements in a thin annular duct – the subject of this main subsection. The background matter has formulated the concept of modal power spectral density, S (m, ω), and its components $S_m^+(|\omega|)$ and $S_m^-(|\omega|)$. This function, shown in Figure 3.3-2 for an illustrative random field, gives the distribution over circumferential mode number, m, and frequency, ω, of the mean-square pressure. Only integer values of m apply because of the requirement for circumferential pressure periodicity. Associated with each value of m is a continuous distribution over frequency. Parenthetically, a coherent, discrete frequency field may be characterized by a corresponding modal psd – in this case, the frequency distribution for any mode is not a continuous function but rather consists of one or more "spikes" or (effective) δ-functions.

The methods used to evolve the analytical formulation of the modal psd, S (m, ω), in terms of the mathematical model for the pressure field, p (θ, t) involved cross correlation and Fourier transform operations. The resulting expressions for S (m, ω) and its components, $S_m^+(|\omega|)$ and $S_m^-(|\omega|)$, equations (3.3-17), were given explicitly in terms of cross spectral functions. In concluding this background, section 3.3.2, details of one procedure for calculating S (m, ω) from measured values of cross spectral functions of data obtained experimentally were specified. In essence, S (m, ω) was mapped as a function of the coordinate pairs m and ω, using cross spectral functions of pairs of microphone signals.

Now, in the (m, ω) plane over which the modal psd is defined, lines of constant slope, ω/m, correspond to a common value of cutoff ratio, or equivalently, circumferential spin velocity, Ω, for wave spiral angular direction, as illustrated in Figures 3.3-1(b) and 3.3-2. It should be possible to evolve an alternative method for mapping S (m, ω), using a

variety of non-orthogonal coordinates such as m and Ω, m and η, or ω and η, where $\eta = \frac{1}{\Omega}$, defines the direction of a radial line in the (m, ω) plane and corresponds to a fixed value of cutoff ratio, mode spin rate, or wave spiral direction — quantities that are uniquely related in a thin annular duct.

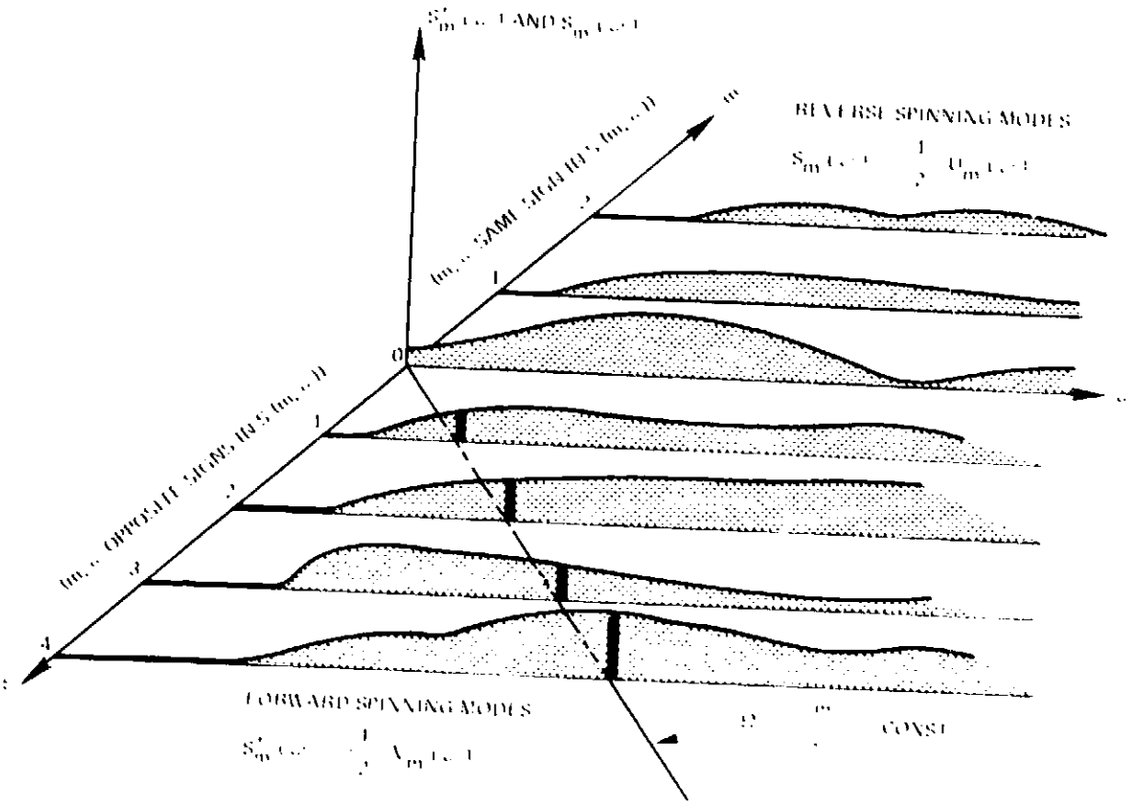

Figure 3.3.2 $S'_{m}(\omega)$ and $S_{m}(\omega)$, Spinning Mode Components of $S(m, \omega)$

The search for such a method is not motivated by interest in novelty. Rather, there are certain practical problems in fan noise control where it is important to obtain a measure of the total acoustic power and its spectral distribution associated with the set of all modes propagating at a common cutoff ratio. Examples of these problem areas include determination of peak radiation directivity, and the specification of sound absorbing liner requirements.

A circumferential array of microphones, incorporating a selectable, progressive time delay between elements provides just such a measurement system. By adjusting the time delay rate, the array is tuned effectively to follow all waves having a common circumferential velocity or spin rate. Thus the array acts as a filter in mode-frequency space to enhance the set of waves having the common properties of the selected spin rate, spiral direction, or cutoff ratio.

An outstanding feature of this array system is the complete elimination of the need to execute any cross-properties signal processing operations -- for each array rate setting a single, ordinary frequency spectrum is used to obtain values of the modal psd spinning mode components at the selected spin rate and the overall power of the set of these modes. Another desirable feature of the method is that it applies equally well to the mapping of discrete frequency pressure fields.

As a guideline to the array analysis that follows, the material is organized as follows:

Section	Features
(1) The Array Response Function	Using a single spinning mode discrete frequency field for convenience, the main features of the array response are determined. This case is preliminary to analysis of array response in random fields.
(2) Array Application to Discrete Frequency Field Measurements	An example of array use in mapping discrete frequency fields is given before proceeding to random fields.
(3) Array Response to Random Fields	The power spectral density of the (single) array signal is expressed as the Fourier transform of the signal autocorrelation function. This result is a combination of the pressure field characteristics and the array response function. Using only the simpliest property of the response function, a method is given for determining the modal psd of the delayed array system. A basis is found for the existence of random spinning modes as a physically meaningful concept. Further properties of array response and its use in random fields are deferred to the subsection "Details of Array Function".
(4) Application to Distortion Tone Measurement, and (5) Application to Broadband Noise Measurements	These two subsections, "Application to Distortion Tone Measurement" and "Application to Broadband Noise Measurements" present essentials of how the array method may be used in measurement of two random field cases.

(6)	Details of Array Response Function	A more comprehensive examination of the response function is given in order to allow evaluation of the sources of error in array measurements. Possible means for sharpening the response are mentioned.
(7)	Extentions to General Cylindrical Ducts	Mention is made of the possible uses of arrays in general cylindrical rather than narrow annular ducts

The Array Response Function

In this section are presented the basic features of the performance characteristics of the delayed circular array when deployed in a narrow annular duct and subjected to the pressure field of a single spinning mode. This simple discrete frequency single mode input is used to determine what amounts to the filter characteristics in (m, ω) space of the array, and corresponds to the practice of analyzing ordinary (ω) filters under harmonic excitation. This procedure is a helpful preliminary to considering array detection of a plurality of coherent modes and the detection of random fields – the main objective of the investigation. After finding some of the key properties of the array response, a more complete presentation of its features is deferred until section "Details of Array Response Function".

Two purposes are served by this break: 1. use of the array in measuring a discrete frequency, coherent field containing a plurality of modes and frequencies is illustrated in the section "Array Application to Describe Frequency Field Measurement". Then the next section gives the derivation of the array response to random fields, followed by illustrated applications in the next two sections. The material in these sections, "Application to Distortion Tone" and "Application to Broadband Noise Measurements", requires minimal information about the response function and is, therefore, presented immediately after such information is obtained. This procedure should help to convey the essential concepts better than if more details of the response function were given here.

After the basic principles and usage of the array method have thus been presented, a more detailed examination of the array response function is resumed in section "Details of Array Response Function".

The basic features of the system may be perceived by reference to Figure 3.3-3, which shows an array of N detectors equi-spaced $\Delta\theta = 2\pi/N$ around the circumference of a narrow annular duct. An incident wavefront traveling in a general direction, α, is shown, together with its phase velocity $V_\theta = \Omega$ in the θ-direction. Note that, since the concept of wavelength is not even presented in Figure 3.3-3, all wave trains, regardless of frequency, that spiral in the direction α have the same circumferential phase velocity or spin rate, Ω. Further, at any or all frequencies it can be seen that there is a one-to-one correspondence between direction and spin rate. In addition, cutoff ratio of a wave train is also uniquely related to α or Ω since it equals the tangential Mach number, $\frac{1}{\sin\alpha} = \Omega r/C$.

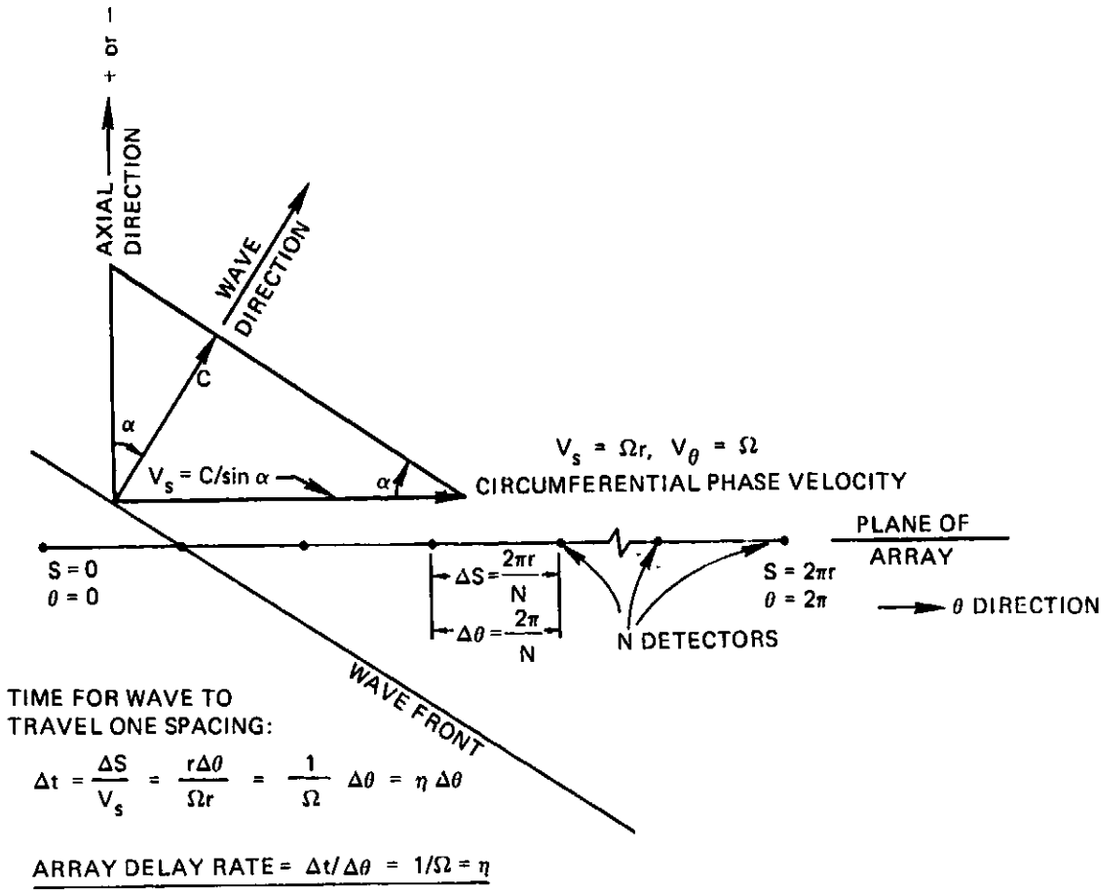

Figure 3.3-3 Delayed Circular Array – Developed View

Independently of the pressure field existing in the duct, the array system is designed to incorporate a progressive time delay for detection of a signal by successive microphones. (This time delay is usually best provided in the data reduction phase of the array system operation). The array delay characteristic is adjustable and is conveniently specified by a parameter, η, called the array delay rate. The selectable delay rate is given by $\eta = \Delta t/\Delta\theta$ seconds per radian. Thus, for a selected value of η, signals received simultaneously by all detectors are delayed in processing by time increments: $0,\ \eta\Delta\theta,\ 2\eta\Delta\theta \cdots$ $\cdots (N-1)\,\eta\,\Delta\theta$ corresponding to the microphones at $\theta = 0,\ (2\pi/N)$ $2(2\pi/N), \cdots$ These progressively delayed signals are added to form the array signal.

Returning now to Figure 3.3-3 and in particular to the illustrated wavefront traveling in the θ-direction at Ω radians/sec, it is easily seen that if the array delay rate, η sec/radian, is selected according to the expression $\eta = 1/\Omega$, the delayed array detectors effectively sense the wave simultaneously instead of progressively as would be the case for zero delay. Thus the array is adjusted by means of η to "follow" the wavefront. The array signal, being the sum of such progressively delayed detector signals will, therefore, enhance all waves traveling in the direction α (and hence having a common spin rate, Ω) compared with

other waves traveling in different directions or with spin rates different from Ω . Notice that this enhancement applies to the set of all wave trains (independently of frequency) having the spin rate $\Omega = 1/\eta$, in a complicated pressure field structure.

It should therefore be anticipated that in a complex pressure field (regardless of periodic or random time dependence and independently of the degree of modal coherence) that the ideal array signal overall mean-square value is proportional to the total acoustic power of all waves traveling in the direction corresponding to $\Omega = 1/\eta$. Further, it may be expected that an ordinary narrowband analysis of the array signal will give the spectral distribution of the acoustic power propagating in this direction.

These expectations are indeed realized, as will be seen in the following material. At this point, it should also be made clear that use of the delayed circular array completely eliminates the need for employing cross-correlations or cross-spectral signal processing operations. Thus the need for executing a large number of relatively complicated cross properties operations required by the method previously described in section 3.3-2, "Field Structure of Random Noise in Thin Annular Ducts", is completely eliminated in the determination of the modal psd function of complicated pressure fields.

The remainder of the report on this subject establishes the validity of the above-mentioned array properties. The key questions to be resolved are: How well does the array enhance the desired set of modes or wave trains having a common spin rate, $\Omega = 1/\eta$? Also, how well does the array suppress contamination of the signal by waves traveling in directions differing from the "target" direction, α ?

Answers to these questions (which are really two aspects of the same question) are provided by deriving the array response to a single, coherent, discrete-frequency spinning mode. Such a mode plays the counterpart role of the pure harmonic signal used to define the transfer or window function of an ordinary (time-series) filter. For, as will be seen, the time-delayed circular array is in essence a filter in the (θ, t) or (m, ω) domains.

Consider a single m -lobe pattern spinning at Ω radians per second in the θ -direction. The pressure field will have harmonic variation at frequency $\omega = m\Omega$ and can be represented in conventional notation by

$$p(\theta, t) = \mathrm{Re}\, C_m e^{i(m\theta - \omega t)} \tag{3.3-24}$$

where the complex number C_m gives the amplitude of the mode and its phase with respect to an arbitrary reference harmonic signal.

Let the array consist of N detectors spaced $\Delta\theta = 2\pi/N$. With a delay rate $\eta = \Delta t/\Delta\theta$ the pressure at the n^{th} detector located at $\theta_n = n\Delta\theta$ will be sensed at a time $\tau_n = \eta\theta_n$ later than by the detector at $\theta_0 = 0$. If the pressure at θ_n is $p_n = p(\theta_n, t)$, the delayed signal will be $p_n' = p(\theta_n, t+\tau_n)$, giving

$$\begin{aligned} p_n' = p(\theta_n, t+\tau_n) &= \mathrm{Re}\; C_m \exp i\left[m\theta_n - \omega(t+\tau_n)\right] \\ &= \mathrm{Re}\, C_m e^{-i\omega t} e^{i(m-\omega)\eta n\Delta\theta} \end{aligned} \tag{3.3-25}$$

Denote by $f_\eta(t)$, the averaged sum of the N delayed detector signals. Then:

(3.3-26)

$$f_\eta(t) = R_e C_m e^{i\omega t} Z \qquad (3.3\text{-}27)$$

where

$$Z = \frac{1}{N} \sum_{n=0}^{N-1} e^{in(m-\omega\eta)2\pi/N}$$

In linear array theory (ref. 10) Z is called the array factor. The behavior of the magnitude of Z as a function of ω and m , and of the combination $\beta = (m - \omega\eta)$ is illustrated in Figures 3.3-4 and 3.3-5 in section "Details of Array Response Function", these characterictics are derived and discussed in detail.

Clearly when $Z = 1$ the array output, $R_e C_m e^{i\omega t}$, is a harmonic signal with amplitude and phase corresponding exactly to those of the m -lobe spinning pattern. Therefore, the objective of this investigation is to determine how Z can in fact be made equal to unity, which then results in the array tracking perfectly the target wave. This is easily done:

Z is a function of the four variables, m , ω , η , and N . Two of these, m and ω depend only on the pressure field. Of the remaining two, N is fixed for a given array, and η , the delay rate, is a selectable constant. For a given array with a fixed number of detectors Z depends upon the value of the quantity $(m - \omega\eta)$. Accordingly let

(3.3-28)

$$\beta = (m - \omega\eta)$$

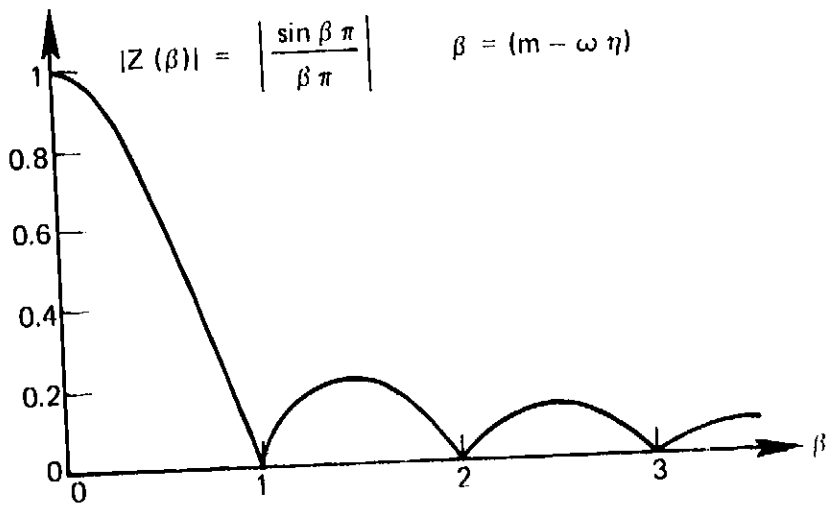

Figure 3.3-4 Array Response Function (N is large)

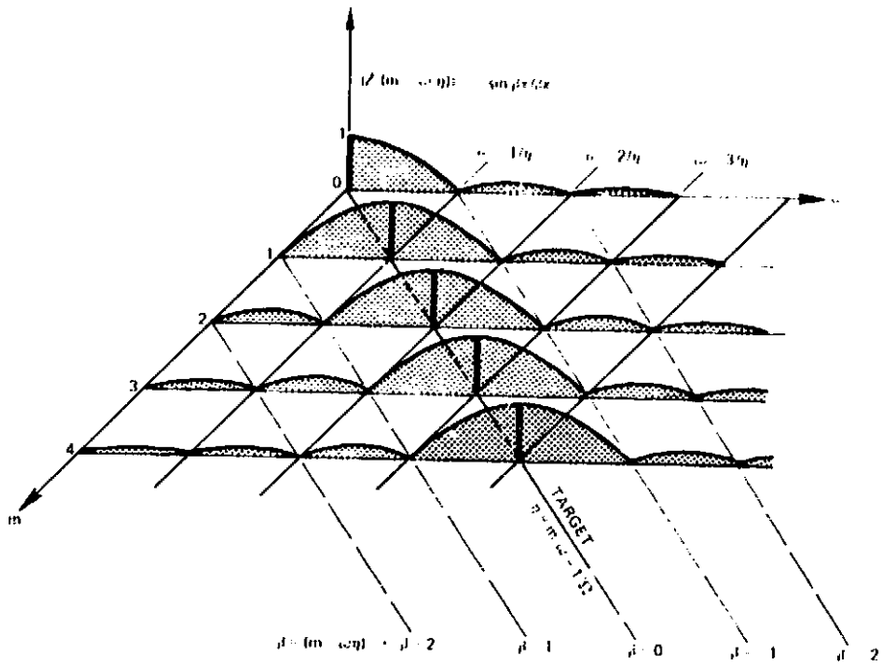

Figure 3.3-5a Array Response Function for η Fixed (N is large) $|Z(\beta)| = |Z(m - \omega\eta)| = |\sin \beta\pi/\beta\pi|$

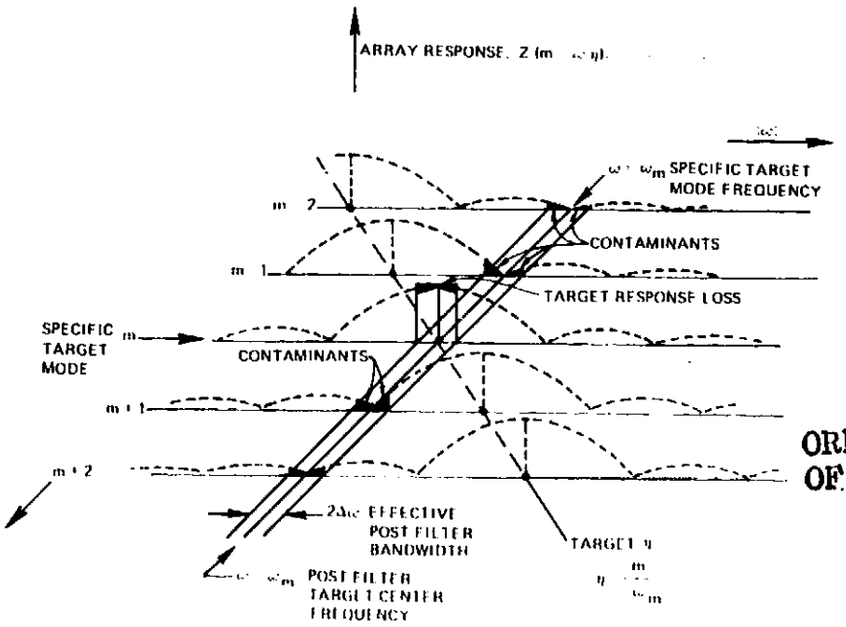

ORIGINAL PAGE IS OF POOR QUALITY

Figure 3.3-5b Array Off-Target Response and Contamination

Then the array factor Z can be expressed as

$$Z = \frac{1}{N} \sum_{n=0}^{N-1} e^{in\beta 2\pi/N} - \qquad (3.3\text{-}29)$$

Now let the array delay rate be set to the value $\eta = m/\omega \; (= 1/\Omega)$. This makes $\beta = 0$ and makes each of the (unit) complex terms $\exp[in\beta 2\pi/N]$ equation in (3.3-29) a unit real number. Their sum will be N and Z is thus exactly unity. Consequently, from equation (3.3-26), the array signal reduces to

$$f_\eta(t) = R_e \; C_m \; e^{-i\omega t}$$

Thus, as was explained previously in a qualitative way, the array signal is identical in amplitude and phase with the complex modal pressure, C_m the array is tracking perfectly.

But suppose we leave the array tracking the mode C_m undisturbed and add to the pressure field a new mode $C_M e^{i(M\theta - \omega t)}$ at the same frequency, ω . What happens to the array signal as a result of superposing the new mode? The answer turns out to be -- absolutely nothing. The array continues to track C_m perfectly as before, and its signal is completely undisturbed when the C_M mode is superposed.

This complete lack of signal contamination by a mode different from the target mode (and thus spinning at a rate different from the target rate $\Omega = \omega/m$) is exactly what had been hoped for. To see why there is zero contamination, examine equation (3.3-29) for Z .

The terms are all unit complex numbers with successive angular orientations in the complex plane differing by $\beta 2\pi/N$ radians or β/N revolutions. Now η was set to make $\omega\eta = m$ of the target mode. So β for the new M mode will be $(M-m)$. If M is one more than m or one less than m , it is clear that the terms in equation (3.3-29) consist of N complex numbers in a symmetrical "wheel spoke" arrangement.

The sum of this arrangement is obviously null and the average, which is the array factor, is therefore zero. Hence the array signal response to the added M -lobe pattern is null, and its response to the original target m -mode remains unaltered and uncontaminated. For other values of M , it is shown in section "Details of Array Response Function" that the terms comprising Z also make symmetrical, null-sum spoke patterns, provided that N, the number of microphones in the array, is "sufficiently" large.

This elementary analysis explains the previous statement that the array enhances the response to the target mode. If the acoustic pressure field consisted only of the target m -mode, the array signal (before averaging) would be N times the output of a single microphone. Consequently, local contaminating pressure fluctuations, due for example to hydrodynamic pressure fluctuations of airflow over the detectors ("noise"), are very poorly correlated. It is easily shown that the signal-to-noise ratio of the array is also enhanced in this case by a factor of $\sqrt{N}$.

It is worth mentioning that, for the case where several modes exist, all at the same frequency, the ability of the circular array to reject totally all modes except the target mode depends critically on the fact that the wave number m in the quantity $\beta = (m - \omega\eta)$ is restricted by physical considerations to integer values. In conventional linear array theory there is no corresponding requirement that the number of cycles of signal variation along the array at any instant be an exact integer. Consequently, the equivalent wave number can vary continuously, and waves arriving from other than the target direction cannot be completely prevented from contaminating the array signal.

Thus the success of the delayed circumferential array system depends both upon the system design per se and also upon its use in a field having inherent pressure periodicity in the array direction. While this result has been obtained for the coherent modes at a given frequency, it will be shown in section "Array Response to Random Fields" that the same integer restriction on m implied by θ-periodicity is an important element in the use of the array in measuring random pressure fields having such periodicity.

The next feature to examine is the ability of the array to track not only single or multiple modes at a given frequency, but also an entire set of modes having a common spin rate Ω. To do this, the array delay rate η is made equal to $1/\Omega$. When the array signal is spectrally analyzed, the spectrum levels at frequencies $\Omega, 2\Omega, 3\Omega, \ldots$ correspond exactly to the amplitudes of the successive modes $m = 1, 2, 3 \ldots$. This case is examined in more detail in section "Array Application to Descrete Frequency Field Measurement."

The last matter to be examined in this section is the problem of mistuning. That is, suppose the pressure field consists of the pair of modes characterized by m and M at a common frequency ω, as before. The delay rate η remains set to track the m-mode, and the array signal is exactly $C_m e^{-i\omega t}$. Now suppose that the frequency is changed by an amount $\Delta\omega$. Two effects result:

1. The array response to the target m mode is slightly reduced by the drop in the value of the array factor for the target mode, $Z(\beta) = Z(m - [\omega + \Delta\omega]\eta)$

2. Secondly, a slight amount of contaminating signal is introduced into the array signal from the off-target M mode. This contamination results because the array factor for the M-mode, $Z(\beta) = Z(M - [\omega + \Delta\omega]\eta)$, is not exactly zero unless $\Delta\omega = 0$. The amount of contamination depends not only on the magnitude of $\Delta\omega$, but also on the proximity of M to the target mode number m.

These effects are disclosed by the graphs in Figures 3.3-4 and 3.3-5 which present the magnitude $|Z|$ of the (complex) array factor. $|Z|$ is called here the array response function. Figure 3.3-4 gives $|Z|$ versus $\beta (= m - \omega\eta)$. When $\beta = 0$ (on target), $|Z|$ is 1, and Figure 3.3-4 shows that for $\Delta\omega \to \Delta\theta << 1$, $|Z|$ differs trivially from unity.

The M-mode contamination is harder to understand. Figures 3.3-5(a) and 3.3-5(b) show $|Z|$ as a function of the separate parameters m and ω for a fixed value of η. In particular, Figure 3.3-5(b) shows what happens to $|Z|$ when the target mode frequency

changes by a small amount, $\Delta\omega$. Careful examination of this figure shows the contaminating contributions from modes in the neighborhood of the target mode, m. For $\omega = \omega_m + \Delta\omega$, the largest contamination results from mode m+1, with successively lesser amounts from modes m+2, m+3,. . ., and m − 1, m − 2, . . . when $\omega = \omega_m - \Delta\omega$, the greatest contamination is produced by the m − 1 mode, with progressively smaller contributions from more distant modes.

The properties of the array response function, $|R|$, revealed in these figures are derived in section "Details of Array Response Function". Before taking up this detailed subject, the array response to a random field will be given in section "Application to Broadband". However, in section "Application to Distortion Tone", an application of the array system for mapping coherent, discrete frequency field is given first.

Array Application to Discrete Frequency Field Measurement

The delayed array system can be used to map the complex modal coefficients, of the pressure field of the fundamental and harmonics of fan blade frequency noise, e.g.

$$P(\theta,t) = Re \sum_{n=1}^{3} \sum_{m=-m^*}^{m^*} C_{mn} e^{i(m\theta - n\omega_0 t)}$$

where ω_0 is fundamental blade-passage circular frequency, $n = 3$ is the highest harmonic index of interest and $|m^*|$ is the greatest propagating wavenumber at this harmonic. Values of $m = m^*$ for $n = 1$ and $n = 2$ will be decaying modes, but such modes can be detected if their amplitudes are sufficient. Also note that negative m-subscripts are now used and identify reverse modes since $\omega = -n\omega_0$ is taken with a negative sign. (This usage is consistent with conventional spinning mode formulations.)

A typical modal amplitude (not power) spectrum is shown in Figure 3.3-6. Also shown is the first target delay rate setting, $\eta = \frac{m}{\omega} = 1/\omega_0$. This rate targets the modes: $m = 1$ for $\omega = \omega_0$ $m = 2$ for $\omega = 2\omega_0$ and $m = 3$ for $\omega = 3\omega_0$:

As has been mentioned several times, the number of microphones, N, in the array is selected such that $N > 2m^*$ at $\omega = 3\omega_0$ to avoid aliasing. Then the following steps are followed:

1. Set $\eta = \frac{1}{\Omega} = \frac{m}{\omega} = \frac{1}{\omega_0}$

2. a. Filter $f_\eta(t)$ the array signal at ω_0 giving $|C_{11}|$
   b. Filter $f_\eta(t)$ the array signal at $2\omega_0$ giving $|C_{22}|$
   c. Filter $f_\eta(t)$ the array signal at $3\omega_0$ giving $|C_{33}|$

3. Set $\eta = 2/\omega_0$ to target $m = 2$ for $\omega = \omega_0$, $m = 4$ for $2\omega_0$, $m = 6$ for $3\omega_0$

4. a. Filter array signal at ω_0 giving $|C_{21}|$
   b. Filter array signal at $2\omega_0$ giving $|C_{42}|$
   c. Filter array signal at $3\omega_0$ giving $|C_{63}|$

5. Repeat the process for other delay rate settings, including negative rates for reverse modes to completely map the (m,ω) field. Figure 3.3-6 can be used to see what values of $\eta = m/\omega$ are required.

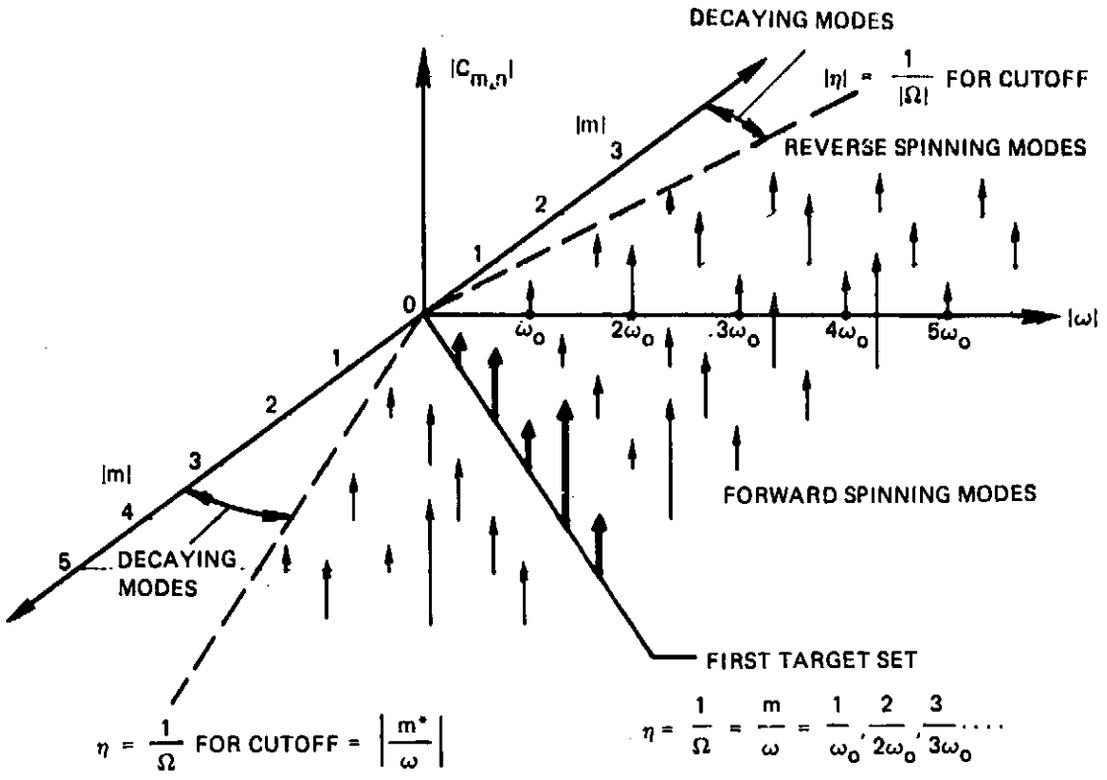

Figure 3.3-6 Sample Mode Amplitude Spectrum of Fan and First Target Set of Array

Notes:

a. If the random broadband noise spectral density is "low", the effective post-array filter bandwidth need be only narrow enough to resolve components one octave apart.

b. If the random broadband noise levels are high, the post filter bandwidth must, of course, be reduced.

c. If the array signal is low-passed so that frequency information beyond $\omega = 3\omega_o$ is suppressed, the signal total mean square value is the "power" of the set of modes traveling at $\eta = 1/\eta$. For example, for the target set illustrated in Figure 3.3-6 the array signal mean square reading equals $\frac{1}{2}[C_{11} \cdot C_{11}^* + C_{22} \cdot C_{22}^* + C_{33} C_{33}^*]$

d. The relative "phases" of the modes at any one harmonic, $\omega_o, 2\omega_o$ OR $3\omega_o$ can be found if reference signals $e_1 = \cos\omega_o$, $e_2 = \cos 2\omega_o$, and $e_3 = \cos 3\omega_o$ are provided and if the field is perfectly coherent (frequency, amplitude, and phase of each mode are substantially constant over the analysis time). This is accomplished by the usual methods for phase determination, operating successively on the filtered signals at a given array setting corresponding to the modes $m\cdot\omega_o\eta$, $2\omega_o\eta$, $3\omega_o\eta$. The fact that the complex array factor (2) is exactly real and unity at these (m, ω) combinations makes possible this phase detection, or equivalently, determination of the complex modal coefficients, C_{mn} as well as simply amplitudes $|C_{mn}|$

e. If there is some signal jitter ($\omega_0 = const + \Delta\omega_0(t)$) where $\Delta\omega_0(t)$ is a "small", randomly varying component, the array may be used in at least two ways. This signal jitter may be due to fan speed fluctuations, or it may result from cutting of upstream wakes that have some degree of unsteadiness.

e1. First: If the amplitudes (C_{mn}) alone are wanted, there is no problem the post filtered array will detect components having frequency bandwidth small compared with both the array (frequency) bandwidth at a particular γ and to the post filter effective bandwidth. Figure 3.3-5(b) shows how small frequency shifts result in only slight loss of array response and small contamination from neighboring modes. Section "Details of Array Response Function" explains this "off-target" response in terms of detailed properties of the array response function, $|\varepsilon|$.

e2. Second: If the fan speed is constant, but signal jitter occurs, phase as such has no meaning and only the amplitudes $|C_{mn}|$ can be found. However, if frequency changes result from deviations in fan speed, the portion of the field that is coherent with respect to the rotor may be determined by synchronous detection techniques. Here the reference signals $e_n = \cos n[\omega_0 + \Delta\omega_0(t)]t$ are generated by a rotor shaft transducer that follows shaft speed or fundamental blade frequency, $\omega_0 + \Delta\omega_0(t)$ By sampling the array signal $f_\eta(t)$ at time intervals controlled by the instantaneous value of $(\omega_0 + \Delta\omega_0)$ the coherent portion of the array signal is enhanced. Processing of this synchronously detected signal component by the methods described above will give mean values of both coherent modal coefficient amplitude and phase, again assuming that the range of $\Delta\omega_0$ is not too large. (A more sophisticated procedure would involve using a variable delay rate $\eta(t) = \int_0^t \dot{\chi}(\epsilon)$ for the target mode set.)

Array Response to Random Fields

This topic is the major item of concern in the investigation reported here. It will be shown that the delayed circular array provides a relatively simple and effective system for mapping the modal power spectral density function, $S(m,\omega)$ which was established in section 3.3-2, "Field Structure of Random Noise in Thin Annular Ducts", as an appropriate function to specify the characteristics of random fields.

Although the final result of this study a method for use of the array system is simple, the derivation of the array response when deployed in a random field is somewhat complicated. These complexities are just a consequence of having to employ cross properties analytical techniques (not measurements) and of having to use some of the fairly intricate results of the background material in section 3.3-2.

Despite the complexities of executing the required algebra, the analytical method can be specified in one sentence. the analytical model of the pressure field given by equation (3.3-2), $P(\theta,t) = \sum_{n=0}^{\infty} [a_n(t)\cos n\theta + b_n(t)\sin n\theta]$ is used to obtain the array signal, after which the modal power spectral density of the signal is obtained by Fourier transforming the signal auto-correlation function. The following material results from completing these instructions.

As in the previously analyzed discrete frequency case, the array signal is given by

$$f_\eta(t) = \frac{1}{N} \sum_{n=0}^{N-1} P(\theta_n, t + \tau_n) \qquad (3.3\text{-}30)$$

where $\tau_n = \eta \theta_n$ and η is the array delay rate.

The corresponding auto-correlation function is

$$R(\tau) = \lim_{T \to \infty} \frac{1}{T} \int_{-T/2}^{T/2} f_\eta(t) \cdot f_\eta(t+\tau)\, dt$$

$$R(\tau) = \frac{1}{N^2} \sum_{j=0}^{N-1} \sum_{K=0}^{N-1} \lim \frac{1}{T} \int_{-T/2}^{T/2} P(\theta_j, t + \tau_j) \cdot P(\theta_K, t + \tau_K + \tau)\, dt \qquad (3.3\text{-}31)$$

This can be reduced to

$$R(\tau) = \frac{1}{N^2} \sum_{j=0}^{N-1} \sum_{K=0}^{N-1} R_{jK}(\tau + [K-j]\eta\, 2\pi/N) \qquad (3.3\text{-}32)$$

where $R_{jK}(\tau)$ is the ordinary cross correlation between the undelayed pressures at θ_j and θ_K :

$$R_{jK}(\tau) = \lim_{T \to \infty} \frac{1}{T} \int_{-T/2}^{T/2} P(\theta_j, t) \cdot P(\theta_K, t + \tau)\, dt \qquad (3.3\text{-}33)$$

The power spectral density of $f_\eta(t)$, $S_\eta(\omega)$, is the Fourier transform of equation (3.3-33). It is known that if the transform of a function of τ is given by $\phi(\omega)$, then the transform of the function with argument $\tau + C$ is $e^{i\omega C}\phi(\omega)$. Thus with $C = [K-J]\eta\, 2\pi/N$,

$$S_\eta(\omega) = \frac{1}{2\pi} \int_{-\infty}^{\infty} R(\tau) e^{-i\omega\tau}\, d\tau$$

$$= \frac{1}{N^2} \sum_{j=0}^{N-1} \sum_{K=0}^{N-1} e^{i(K-j)\omega\eta\, 2\pi/N} S_{jK}(\omega) \qquad (3.3\text{-}34)$$

where $S_{jk}(\omega)$, the cross spectral density between the undelayed signals at θ_j and θ_k is the Fourier transform of $\rho_{jk}(\tau)$. Equation (3.3-34) shows that the single output psd of the array $S_\eta(\omega)$ automatically "performs" the operations of measuring N^2 separate cross spectral densities, $S_{jk}(\omega)$ and adding them after appropriate phase shifting by the factors $\exp(ks\omega\eta 2\pi/N)$.

Let the N^2 terms in equation (3.3-34) be collected into groups for which the combination $k-j$ is constant and is denoted by the index, s. Also, for $S_{jk}(\omega)$ the cross spectral density between detectors at θ_j and θ_k put $S(\theta_j, \theta_k)$, suppressing the ω-dependence for simplicity. Then θ_k can be written as $\theta_j + s2\pi/N$ and $S(\theta_j, \theta_k) = S(\theta_j, \theta_j + s2\pi/N)$. $S_\eta(\omega)$ will be:

$$S_\eta(\omega) = \frac{1}{N^2} \sum_{j=0}^{N-1} \sum_{s=-j}^{N-1-j} e^{is\omega\eta 2\pi/N} S(\theta_j, \theta_j + s2\pi/N)$$

Collecting terms for which s is constant, and distinguishing between those with positive and negative exponentials, the N^2 terms can be arranged as follows:

$$S_\eta(\omega) = \frac{1}{N} \sum_{s=0}^{N-1} \left\{ \frac{1}{N} e^{is\omega\eta\frac{2\pi}{N}} \sum_{j=0}^{N-1-s} S(\theta_j, \theta_j + s2\pi/N) + \frac{1}{N} e^{i(s-N)\omega\eta 2\pi/N} \sum_{j=N-s}^{N-1} S(\theta_j, \theta_j + s2\pi/N) \right\} \qquad (3.3\text{-}35)$$

This rather complicated expression is a mixture of spectral functions of the pressure field and components of the array factor Z. One reason for the complexity is that it involves a double summation which in turn is a consequence of representing a power spectral density rather than an amplitude spectral density.

The form of equation (3.3-35) contains fragments of (finite) Fourier transforms on the two j-sums of the field cross spectral functions. If the two exponential weighting factors happened to be numerically identical, the expression would be greatly simplified. This simplification can in fact be achieved if attention is restricted to integer values of the quantity $\omega\eta$. Invoking this restriction will be shown not to impair use of the array method in measuring the modal psd.

Operationally this restriction means that for a given array delay rate setting, η the array signal psd $S_\eta(\omega)$ will be evaluated or used only at the successive values of ω: $1/\eta, 2/\eta \ldots N/\eta$. It is important to recognize that this procedure ensures that the array factor Z is exactly unity or zero since $\beta = m - \omega\eta$ is zero for $m - \omega\eta = m$ and $\beta =$ a non-zero integer for $m \neq \omega$. The use of $S_\eta(\omega)$ in evaluating $S(m, \omega)$ at intermediate frequencies will not be discussed at this time (see section "Details of Array Response Function"). For the present consideration will be limited to obtaining $S(m, \omega)$ from $S_\eta(\omega)$ for this specific value of ω. Accordingly let $\omega = M$ an integer.

Then the second exponential in equation (3.3-35) becomes

$$e^{-i(s-N)M2\pi/N} = e^{-isM2\pi/N} e^{+iNM2\pi/N} = e^{-isM2\pi/N}$$

which is just the factor of the first set of terms in equation 3.3-45. Accordingly

$$S_\eta(\omega) = \frac{1}{N} \sum_{s=0}^{N-1} e^{-iMs2\pi/N} \left\{ \frac{1}{N} \sum_{j=0}^{N-1} S(\theta_j, \theta_j + s2\pi/N) \right\} \quad (3.3\text{-}36)$$

The quantity in braces is simply the (finite-element) space average of the cross spectral density of detector pairs spaced $\sigma = s2\pi/N$ apart. This quantity was denoted in section 3.3.2, equation (3.3-10) as $S_\sigma(\sigma_s; \omega)$. Hence

$$S_\eta(\omega) = \frac{1}{N} \sum_{s=0}^{N-1} S_\sigma(\sigma_s; \omega) e^{-iM\sigma_s} \quad (3.3\text{-}37)$$

Replacing the above s-sum average by the exact equivalent integral representation (ref. 12) gives:

$$S_\eta(\omega) = \frac{1}{2\pi} \int_{-\pi}^{\pi} S_\sigma(\sigma; \omega) e^{-iM\sigma} d\sigma \quad (3.3\text{-}38)$$

In this form, $S_\eta(\omega)$ can be recognized as the Fourier transform of $S_\sigma(\sigma; \omega)$ with the transform variable $-M = -\omega\eta$ replacing m. Since the transform of $S_\sigma(\sigma; \omega)$ was found to be the modal power spectral density of the random pressure field, the link between $S_\eta(\omega)$ and $S(m, \omega)$ has been made.

$S_\eta(\omega)$ is obtained in terms of $S(m,\omega)$ by replacing m with $-M$ in the previously obtained expression for $S(m,\omega)$ equation (3.3-17) giving

$$S_\eta(\omega) = \sum_{n=0}^{\infty} \left\{ \frac{1}{4} U_n(\omega) \delta(-M-n) + \frac{1}{4} V_n(\omega) \delta(-M+n) \right\} \quad (3.3\text{-}39)$$

Evaluating equation (3.3-39) for the positive and negative values of M, namely $M = \omega/\eta$ and $M = -\omega/\eta$, contributions will result from U_n and V_n only for $\omega = \pm n/\eta$ resulting in

$$S_\eta(\omega) = \sum_{n=0}^{\infty} \left\{ \frac{1}{4} U_n(-n/\eta) + \frac{1}{4} V_n(n/\eta) \right\}$$

Finally, since by equations (3.3-20) the forward η -lobe mode power spectral density component $S_n^+(|\omega|)$ is given by $\frac{1}{2} W_n(-|\omega|)$ or $\frac{1}{2} V_n(|\omega|)$, there follows:

$$S_\eta(\omega) = \sum_{n=0}^{\infty} \left\{ \frac{1}{2} S_n^+(|n/\eta|) + \frac{1}{2} S_n^+(|n/\eta|) \right\}$$
$$= \sum_{n=0}^{\infty} S_n^+(|\omega| = |n/\eta|) \qquad (3.3\text{-}40)$$

Now $S_n^+(|\omega|)$ was seen in section 3.2.2 to be the component of the modal psd, $S(n, \omega)$, associated with values of n and ω having opposite signs. It was described there that the choice of notation, involving + and - superscripts was based on a formal correspondence of forward and reverse spinning modes between the random and coherent field mathematical results, and that it also anticipated information that would be (and has just been) obtained in this section. $S_n^+(|\omega|)$ from equation (3.3-40) is a term in the expression for the array signal psd. The array delay rate η has been positive throughout this entire derivation and it was seen in the previous section on arrays in discrete frequency fields that this selection will cause the array to track coherent forward spinning modes. We have just found out that with positive delay rate the array in a random field tracks only the portions of $S(n,\omega)$ with opposite n and ω signs, which were called the forward spinning modal components, $S_n^+(|\omega|)$. Because the same array in a coherent field with positive tracks only forward discrete frequency spinning waves, it emerges that the array in a random field recognizes values of $S_n^+(|\omega|)$ in exactly the same way as it identifies coherent forward spinning modes.

$S_n^+(|\omega|)$ is the power spectral density of the forward spinning mode with circumferential wave number n, and $S_n^-(|\omega|)$ is the random field counterpart of the modal power of the reverse spin n-lobe pattern in the coherent field case. Therefore, it can now be stated that spinning modes do "exist" for the random field case in the sense that the array provides an operationally definable way of obtaining their power spectral densities which comprise the field modal psd, $S(n, \omega)$.

Returning to equation (3.3-40), the array signal psd, $S_\eta(\omega)$, is the set of the numerical values of successive forward-spinning modal components $S_n^+(\omega)$, each evaluated at a specific frequency $|\omega| = |n/\eta|$. This is the equivalent of the class of forward modes having a common spin rate $\Omega = \omega/n = 1/\eta$. Values of the array psd at other frequencies are undefined, since the derivation of equation (3.3-10) specifically restricted the results to integer values of $\omega\eta$. (By similar means it can be shown that if the delay rate is made negative, the array will track the corresponding set of reverse spinning modes, $\sum_n S_n^-(|\omega| = |n/\eta|)$.

Figure 3.3-7 shows the sample random field spinning modal distribution illustrated in "Field Structure of Random Noise in Thin Annular Ducts," section 3.3.2. In the (m, ω) plane, the line with slope $\eta = m/\omega$ represents the target setting of the array. At the intersections of this line with the lines $m = 1, 2, 3 \ldots$, ordinates of the component modal psds, $S_1^+(|\omega| = |2/\eta|)$, etc. are shown. The set of these ordinates is the meaningful part of the array signal psd, as given by equation (3.3-40).

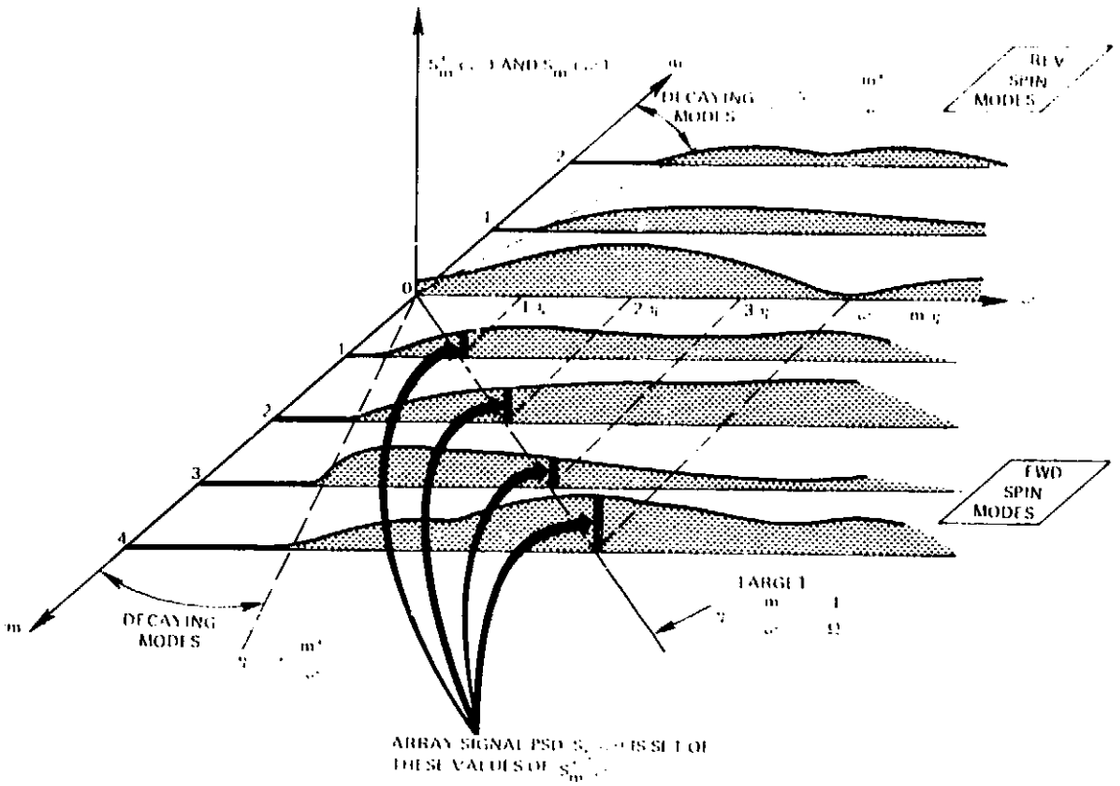

Figure 3.3-7 Circumferential Array Target Set PSD in Random Field

In practice, the values of the array psd $S_\eta(\omega)$ at the specific frequencies $\omega = 1/\pi$, $2/\pi$, etc. are obtained simply by computing or measuring the signal psd at these frequencies only, ignoring intermediate frequency information. As will be seen in section "Details of Array Response Function", the intermediate frequency information is contaminated by array signal contributions from neighboring, off-target modes as was seen to be the case when measuring coherent fields. This contamination is a consequence of the incomplete vanishing of the array factor Z for bordering modes at frequencies in the neighborhoods of the target frequencies.)

In the subsections immediately below, two examples are given of the use of the delayed circular array system in mapping the S_{+m} and S_{-m} spinning mode components of the modal psd for random fields.

Application to Distortion Tone Measurement

The term distortion tone denotes narrowband energy in the neighborhood of rotor blade passage frequency for example, due to fan cutting of unsteady inflow disturbances. Let $|\omega_0|$ be a circular frequency in the neighborhood of blade passage frequency, but not exactly coincident with BPF. The array system can be used to measure the modal composition of the field at $|\omega_0|$ in the following way:

Values of the power spectral densities of all propagating forward and reverse spinning modes contributing to the signal at frequency $|\omega_o|$ are required. Let the array signal be filtered (digitally or electronically) with a narrowband filter centered at $|\omega_o|$. It will be convenient to suppose the filter effective bandwidth to be unity; if some other bandwidth is used, division of the filtered signal power reading by the actual bandwidth will give the power spectral density at $|\omega_o|$.

(In this and the following subsection, the same remarks concerning selection of a sufficient number of microphones in the array to satisfy the Nyquist requirements apply as well to the random field cases as were made in connection with the discrete frequency fields discussed in section, "Array Application to Discrete Frequency Field Measurement".)

Since equation (3.3-40) for the array signal psd applies only when $\omega\eta$ is an integer, the delay rate, η, must be selected to correspond to successive mode number n. That is, to determine the power spectral density at $|\omega_o|$ of the forward mode, $S_n^+(|\omega_o|)$, $|\omega_o|\eta = n$ requires $\eta = n/|\omega_o|$. Reverse modes are detected by setting corresponding negative delay rates. The following tabulation indicates the delay rate settings and the resulting output of the filtered array signal:

Frequency $|\omega_o|$ (Array signal filtered at $|\omega_o|$)

Forward mode	n :	1	2	3	...	n
Delay rate	η :	$1/\|\omega_o\|$	$2/\|\omega_o\|$	$3/\|\omega_o\|$		$n/\|\omega_o\|$
Array output	$S_\eta(\omega)$:	$S_1^+(\|\omega_o\|)$	$S_2^+(\|\omega_o\|)$	$S_3^+(\|\omega_o\|)$		$S_n^+(\|\omega_o\|)$
Modal psd	$S(m,\omega)$:	$S(-1,\omega_o)$	$S(-2,\omega_o)$	$S(-3,\omega_o)$		$S(-n,\omega_o)$
Reverse mode	n :	1	2	3	...	n
Delay rate	η :	$-1/\|\omega_o\|$	$-2/\|\omega_o\|$	$-3/\|\omega_o\|$		$-n/\|\omega_o\|$
Array output	$S_\eta(\omega)$:	$S_1^-(\|\omega_o\|)$	$S_2^-(\|\omega_o\|)$	$S_3^-(\|\omega_o\|)$		$S_n^-(\|\omega_o\|)$
Modal psd	$S(m,\omega)$:	$S(1,\omega_o)$	$S(2,\omega_o)$	$S(3,\omega_o)$		$S(n,\omega_o)$

By repeating this process for a set of $|\omega_o|$ in the neighborhood of blade passage frequency, a map of the modal composition of distortion tone noise is obtained. In performing this data analysis it is assumed that for the ω_o nearest to BPF the filter effective bandwidth is sufficiently narrow and the rotor speed steady enough so that coherent BPF signal is excluded from the filtered array signal. If such is not the case, it may be necessary to obtain a reconstructed signal in which the periodically sampled coherent blade passage component has been eliminated from the total signal. (If a discrete frequency component is contained in the filter bandwidth, the array will of course respond to this signal as well as to the band-limited random power.)

Application to Broadband Random Noise Measurement

There are applications where knowledge of the general shape of the modal power spectral density function, $S(m, \omega)$ for a broadband random noise field is desired. An alternative to the methods based on cross spectral measurements described in section 3.3.2, "Field Structure of Random Noise in Thin Annular Ducts", is provided by the array system. This procedure once again is based on the property that the array signal provides a correct measure of the power spectral density of each mode only at those frequencies for which ω_k is an integer.

For efficient mapping of the modal power spectral density the delay rate η is set to a (small) value, say η_1. The resulting array signal, $S_{\eta_1}(|\omega|)$ is narrowband filtered or FFT transformed at the following sequence of center frequencies, giving the indicated modal power spectral densities:

Delay rate $\eta = \eta_1$ Array signal narrowband filtered over $0 < |\omega| \leq |\omega_{max}|$

Mode,	n :	1	2	...	n
Read array signal	$S_{\eta_1}(\|\omega\|)$				
at following:	$\|\omega\|$:	$1/\eta_1$	$2/\eta_1$		n/η_1
Result:	$S_n^+(\|\omega\|)$:	$S_1^+(\|\omega\| = 1/\eta_1)$	$S_2^+(\|\omega\| = 2/\eta_1)$		$S_n^+(\|\omega\| = n/\eta_1)$
Modal psd	$S(m,\omega)$:	$S(-1, 1/\eta_1)$	$S(-2, 2/\eta_1)$		$S(-n, n/\eta_1)$

This procedure is repeated for a set of $\eta_1, \eta_2, \eta_3 \ldots\ldots$ up to a value of $\eta = 1/\Omega$ corresponding to the value of Ω for which cutoff occurs. Negative values of η produce the reverse mode spectral densities.

Figure 3.3-7 illustrates the process for sample value η. It is clear that this procedure is an alternative mapping of the S_m^+ and S_m^- components of $S(m, \omega)$ where values of S are determined at the intersections of lines of constant $\eta = m/\omega$ with grid lines at integer m in the (m, ω) plane, as shown in Figure 3.3-7.

It may be noticed that the mode S_0 ($|\omega|$) has not been specified in these tabulations. If the system described above were extended to the case $n = 0$, the corresponding frequency $|\omega| = n/\eta$ would be $|\omega| = 0$. In practice, information about the spectral content of the $n = 0$ mode is obtained by setting the array rate η at zero and simply performing a narrowband frequency analysis of the basic array signal. The case of $\eta = 0$ corresponds to enhancement of all waves arriving simultaneously in the plane of the array (plane waves), independently of frequency.

Details of Array Response Functions

In this section, the detailed properties of the array factor Z and the array response function $|Z|$ are developed. The objective is to determine characteristics affecting the inherent accuracy of the array method, such as number of array detectors, aliasing, off-target modal contamination, and (m,ω) space filter bandwidth. The advantages of possible future "superenhanced" arrays are also indicated. It will first be necessary to go through some algebraic detail before an interpretation of the results can be made.

For convenience the previously obtained expression for the array factor, Z, is repeated here:

$$Z = \frac{1}{N} \sum_{n=0}^{N-1} e^{i n \beta 2\pi/N}$$

$$\text{where } \beta = (m - \omega\eta)$$

The properties of Z can be found by considering two cases:

Case A: $\beta = I$, an integer

In this case, Z is generally the sum of N unit complex numbers spaced apart by $I\,2\pi/N$. There are three subcases: $I = 0$; I is a multiple of N; and $I \neq kN$, k integer. Now for $\beta = I = 0, \pm N, \ldots \pm kN$ all such complex elements of the summation are simply real and unity. Their sum is N and Z = 1, the desired result when the array is set to track the mode C_m . The three subcases are treated separately below.

(Subcase 1) —

The first integer value I = O is especially significant. In this case, $\beta = 0 = m - \omega\eta$ results when $\eta = m/\omega$. That is, since $\omega = m\Omega$, $\eta = 1/\Omega$ and the delay rate is set to track the spin rate of this mode. In fact, for all modes having the ratio $m/\omega = 1/\Omega$ the array will respond perfectly. In a field composed of a plurality of modes and frequencies, all those having this ratio will be received perfectly by the array. All that is required is that for any mode the ratio m/ω be equal to the set delay rate η .

(Subcase 2)

To discuss the other cases where $\beta = I$ is a non-zero multiple of N, let $\beta = kN$, $(k \neq 0)$. Suppose the array is set to track a <u>specific</u> mode, say $m = M$ at frequency ω . The delay rate η is therefore set by $\eta = M/\omega$ so that $\omega\eta = M$, as described in the preceeding paragraph. Let there be other modes indicated by m , also present in the pressure field at this frequency, ω . Then when β has value kN ($k \neq 0$) there follows:

$$\beta = kN = m - \omega\eta = m - M$$

Hence $m = M + kN$ will also make the array factor $Z = 1$. This means that if there exists a mode having $m = M + kN$, its strength will contribute fully to the array signal, even though its spin rate is radically different from the value of the target mode, ω/M. In discussions of signal processing, this type of contamination is called aliasing.

To avoid aliasing, a procedure analogous to that employed in ordinary signal processing is indicated: At the highest frequency of interest, ω_{max}, let m^* be the largest mode number that can propagate. If the number of detectors is made larger than $2m^*$, then for any target M less than m^*, $|m| = |M \pm kN|$ will be larger than m^* and will correspond to a mode that cannot exist in the duct. The requirement $N > 2m^*$ may be recognized as the equivalent of the Nyquist criterion in signal processing. In this way false signals due to aliasing are eliminated from the array output.

(Subcase 3)

In the following it is now assumed that the Nyquist criterion, $N > 2m^*$, has been satisfied. When $\beta = I$, an integer that is <u>not</u> a multiple of N, the sum of the N unit complex numbers spaced apart by $I 2\pi/N$ is easily seen to vanish. Thus the array signal vanishes for all modes having integer values of $\beta = m - \omega\eta$ different from zero. Thus, if at a given frequency η is set to track the specific mode $m = M$, $\omega\eta = M$, and $\beta = m - M$. All values of m other than $m = M$ make β a non-zero integer. Therefore, with $N > 2m^*$, if a plurality of modes, m, exists at a frequency ω and the array is set to track a specific mode, M, the array signal will completely reject the contributions from all the other modes.

Case B : $\beta = (m - \omega\eta)$ a non-integer

When the array rate η is set to target a specific mode-frequency combination, it has been seen that the array signal gives the amplitude of the target mode, rejecting completely all other modes that may be present at this frequency. It remains to determine what happens to the array signal, if the delay rate is not precisely set equal to m/ω, and also how the array responds to the presence of other modes with this mistuned delay rate. This information is obtained by evaluating the array factor, Z, for noninteger values of β. In particular, it may be convenient to suppose that η is targeted to some m/ω ratio so that β is initially zero, and to then suppose that β increases as a consequence of a continuous change in the frequency, ω, of the target mode, m. This frequency change, for example, could be produced by changing fan speed, and its effect on the array output is obviously important to determine.

Z is evaluated for noninteger β by observing in equation (3.3-29) that NZ is the sum of a geometric series of N complex terms, starting with 1 for $n = 0$ and with subsequent terms having a ratio of $\exp i\beta 2\pi/N$. Using the standard expression for the sum of a geometric series, after some rearrangement, Z can be shown (ref. 13) to become

$$Z = \frac{\sin \beta\pi}{N \sin \beta\pi/N} \; e^{i\left(\frac{N-1}{N}\right)\beta\pi}$$

The magnitude of Z, |Z| (sometimes called the array pattern) is significant in determining the array response. In this report |Z| is called either the array response or the array response function. It is not likely to be confused with the (generally) complex quantity Z which is called the array factor, because of the notation used. Since the exponential factor in equation (3.3-40) is just a unit complex number, the array response function is simply:

$$|Z| = \left| \frac{\sin \beta\pi}{N \sin \beta\pi/N} \right|$$

when the array is on target $\beta = 0$ and $Z = 1$. Also it is clear that for $\beta = 1,2,3...$ $Z = 0$. When N is reasonably large (as will be the case when the Nyquist criterion for aliasing suppression is satisfied, the array response becomes essentially independent of N and equation (3.3-43) simplifies to:

$$|Z(\beta)| = \left| \frac{\sin \beta\pi}{\beta\pi} \right| \qquad (N \text{ Large})$$

By means of Figure 3.3-4, the array response, |Z|, may be seen in a simple manner. If there is but a single mode at some frequency and if η is selected by $\eta = m/\omega$ to track this target, then $\beta = 0$ and $|Z| = 1$. As the frequency, ω, is changed, the response falls gradually to zero when $\beta = 1$ and then behaves as indicated. Furthermore, the effect of other modes in addition to the target may be seen. At the target frequency other modes given by $m \neq \omega\eta$ generate values of $\beta = 1, 2$, etc. and zero response. When the frequency of other modes differs from the target the array response will be given by noting the behavior of $|Z(\beta)|$.

To illustrate the array response as a function of the discrete variable m, and the continuous frequency ω, Figure 3.3-5 may be helpful. The array is illustrated when operating with a specific delay rate η so that the entire class of modes for which $m/\omega = \eta$ are on target and the array responds fully. Mode-frequency combinations departing from the target η contribute responses as illustrated. by the shaded curves.

With array systems incorporating just a selectably constant delay rate, $\eta = \partial\tau/\partial\theta = \text{const}$ and incorporating no independent frequency filtering, it is not possible to avoid signal contamination by mode-frequency combinations that depart from the target setting $m/\omega = p$. This contamination is a result of the limited ability of such arrays to discriminate among waves having directions slightly off the target value. In linear array technology (ref. 13) methods for sharpening the array response have been developed. These include unequal detector spacings and unequal weighting of the individual detector sensitivities. It is reasonable to assume that corresponding methods may possibly be developed to sharpen the response of the circular array. The ideal response would be the δ-function: $|Z(\beta)| = \delta(\beta) = \delta(m - \omega\eta)$. For an array approaching such a response function, the output for a discrete frequency field would be a set of δ-functions of strength C_m located at frequencies $\omega = m/\eta$, and mode-frequency combinations departing from the target set would contribute trivially to the array signal. Similarly the random field signal psd would automatically be the set of modal psd's $S_m^+(i\omega)$ or $S_m^-(i\omega)$ given by equation (3.3-40) and shown in Figure 3.3-7.

In the absence of any such beam-sharpened array, the basic array can be used with frequency-filtering of the array signal to reject contaminating spectral components (either discrete or random) outside of the very near neighborhood of the set of target frequencies. This procedure has been illustrated in sections "Array Application to Discrete Frequency Field Measurement", "Application to Distortion Tone Measurement", and "Application to Broadband Noise Measurement". Figure 3.3-7, shows the (small) effects of reduced target frequency response and contamination from off-target modal components due to deviations from a particular target frequency on the target line. These effects apply to the discrete frequency case if the target tone hunts about ω_M, the specific filtered target frequency by $\pm\Delta\omega$. Similar effects for the continuous modal psd case occur. Here, if $2\Delta\omega$ is the array post filter effective bandwidth of the processing algorithm or electronic filter, the filtered array signal will be contaminated slightly (if $\Delta\omega$ is small) by the energy in the $2\Delta\omega$ bandwidth associated with the modes that are close neighbors of the target mode M. Modes $m = M + 1$ and $m = M - 1$ are seen to be the most important contaminants. Obviously, such contamination is reduced by narrowing the effective bandwidth of the frequency-filtering process applied to the array-delayed signal. Care must be taken, however, when processing spectra containing both discrete and continuous components that the effective filter bandwidth is not made so narrow as to miss detection of important discrete tones. Preliminary spectral analysis of some of the individual microphone signals is recommended to guide selection of the final array signal post-filtering effective bandwidths.

This concludes the discussion of some of the detailed features of the delayed array measurement system. Other relevant properties exist (such as array bandwidth dependence on delay rate, and array response function distinctions when applied to amplitude versus power spectral field functions (for example), but discussion of these matters is beyond the scope of this report.

Application to General Annular Ducts

For reasons fully described in the introductory subsection, this investigation (both basic modal psd background and array methods) has focussed on thin annular ducts (hub/tip ratio $\approx$ 1) supporting only constant acoustic pressure distributions across the annulus width. In general, problems with cylindrical or annular ducts (hub/tip ratio <1) are naturally more involved.

For one thing, cutoff ratio or spin rate of a mode at some cutoff ratio depends not only on m (it is independent of m in the thin annular case), but also upon the radial mode number, usually denoted by μ. A delayed circumferential array of microphones that are flush-mounted on the outer annulus wall will still enhance detection of all modes having a common tangential wall velocity or common spin rate, as in the narrow annulus duct. However, depending on the combinations of m and μ defining such modes the members of this set of enhanced detected modes may have a significant range of cutoff ratios instead of a common value. It may turn out, nevertheless, that the property of a common wall speed for a set of (m, μ) modes is a parameter that could be useful in certain applications. If this is indeed the case, the array system previously described can be used for studies involving this application without the need for modification.

As far as using arrays to map the modal psd in (m, μ, ω) space, it is obvious that more information is required than can be obtained from a circular array of microphones at a single radius in one transverse plane. It may be possible to extend the techniques that were explored in this section to provide the required information in general duct geometries. Such extensions would involve the deployment of array detector elements in either or both radial and longitudinal directions. To arrive at efficient data acquisition-processing systems to handle this problem would require further investigation.

3.3.4 Summary of Section 3.3 Results

1. A simple mathematical model was obtained for the random acoustic pressure field in a thin annular duct, $p(\theta,t)$, in the form of a sum of products of random functions of time alone with harmonic functions of space, θ, only.

2. Starting with this model, an expression was produced for the modal power spectral density, $S(m, \omega)$ – the distribution over wavenumber – frequency space of the mean square modal pressure. This function is expressed in terms of the power spectral densities of the random time series comprising the mathematical model of the pressure field.

3. From the symmetry properties of the modal psd, $S(m,\omega)$ was found to be resolvable into two unique sets of components, $S^{+}_{m}(|\omega|)$ and $S^{-}_{m}(|\omega|)$, having mathematical properties similar to those of forward and reverse spinning modes in coherent, discrete-frequency fields. Because of the formal similarity, these components are called random field spinning modes.

4. Means for experimentally determining the modal psd in terms of measurements in a transverse plane of a thin annular duct were devised. Either two separately movable (in. θ) microphones or a set of fixed microphones may be used to acquire cross power spectral density functions which are combined and harmonically analyzed (spatially) to obtain $S(m,\omega)$ and/or its spinning mode components, $S^{+}_{m}(|\omega|)$ and $S^{-}_{m}(|\omega|)$. The same techniques may be used in coherent discrete frequency field analysis or for pressure fields containing a mixture of random and periodic components.

5. A data acquisition and processing system was devised, using a circumferential array of microphones and incorporating a selectable, progressive time delay. The time delayed outputs from the microphones can be filtered at a specified frequency and added. The resulting signal from this system can then be used to determine the modal psd (random or coherent) in two-dimensional annular ducts.

6. In general annular ducts, having hub/tip ratios too small to be representable by the narrow annulus simplification, the delayed circular array system will enhance all (circumferential-radial) modes having a given frequency and a common spin rate, as it does for the thin duct case. Although there is no longer a one-to-one correspondence between mode spin rate and cutoff ratio, the common spin rate property of the enhanced mode set may have value in certain applications.

7. The ordinary power spectral density of the delayed array signal is used to map the acoustic modal power spectral density function, $S(m,\omega)$ and/or its components $S^{+}_{m}(|\omega|)$ and $S^{-}(|\omega|)$.

8. When the sound field is concentrated in integer harmonics of BPF, selective information about the total modal power associated with all modes spinning at a common speed is available from the delayed circular array signal without the need to map $S(m,\omega)$ extensively. For a thin annular duct this selection on the basis of common spin rate is equivalent to obtaining the power associated with all modes having a common cutoff ratio.

9. An especially attractive feature of the delayed array system is that it eliminates the need to execute any cross spectral data reduction procedures. Thus, the large number of relatively complicated cross-properties operations required by the basic (non-array) method for obtaining $S(m,\omega)$ are completely bypassed through use of the delayed circular array method.

3.4 EXPERIMENTAL ASSESSMENT OF METHOD ACCURACY

3.4.1 Objective

To conduct an experimental assessment of the method to determine coherent fan sound mode structures.

3.4.2 Approach

An experimental program was conducted on a small-scale, low-speed fan rig at Pratt & Whitney Aircraft. The rig was capable of generating specified modes under controlled conditions. Six fan sound mode structures were generated in the fan inlet under conditions carefully controlled to maintain constant fan tip speed and ambient temperature. For each mode structure, the MLP was run to determine suitable locations for the duct microphones. Because of the simple mode structures generated, all the microphone locations chosen by the MLP were on the outer-diameter duct wall. The microphone measurements were used to provide input to the MCP which in turn was used to calculate the amplitude and phase of each of the propagating duct modes for each of the six generated mode structures. The MCP also was used to calculate the resultant sound fields at other locations in the duct where microphone measurements were made that were not used to provide input to the MCP. Assessment of the method accuracy was based on a comparison of the predicted pressure amplitude and phase at these locations and the actual measured pressure amplitude and phase.

3.4.3 Facility Description

The Pratt & Whitney Aircraft 25.4 cm (10 in.) diameter research fan rig was used throughout the experimental portion of the program. This rig consists of a low axial flow, 32 bladed fan that has an operating speed range between 3000 and 6000 rpm. The fan tip Mach number operating range is approximately 0.12 to 0.24, and axial flows of up to 25 meters-per-second (80 ft/sec) result. The fan is cantilevered from a flaired flange 38 cm (15 in.) downstream of the fan and, in its baseline configuration has no inlet or exit guide vanes.

In order to comply with a maximum number of the assumptions used in formulating the Tyler-Sofrin analysis, a constant annular inlet duct was constructed by positioning a cylindrical centerbody concentrically in the duct. The diameter of the centerbody (or ID duct wall) was 11.2 cm (4.4 in.), and it extended 2.8 meters ahead of the rotor, with a support strut 1.8 meters ahead of the rotor. At this distance, the wake from the support strut was considered negligible.

To reduce both steady inflow distortion and unsteady inflow turbulence, a wire mesh screen was placed about the inlet at a distance sufficient for there to be negligible pressure loss across the screen. The screen was supported by 0.6 cm (0.25 in.) diameter rods. The loss factor ($k = \Delta P/q$) of the screen was calculated from a formula due to Schubauer (ref. 15) to be 2.84 for the Reynolds number range: $50 \leqslant R_e \leqslant 200$. At lower Reynolds number (typical of those through the screen when placed ahead of the fan rig), the pressure drop cannot be measured accurately, but indications from available information are that the loss factor increases at the lower Reynolds numbers. Experience from as yet unpublished work shows that screens with loss factors on the order of two to three are effective in reducing inflow distortions; thus the screen material used for the tests conducted under this program was considered suitable. A schematic of the rig is shown in Figure 3.4-1, and a photograph taken from ahead of the inlet is shown in Figure 3.4-2.

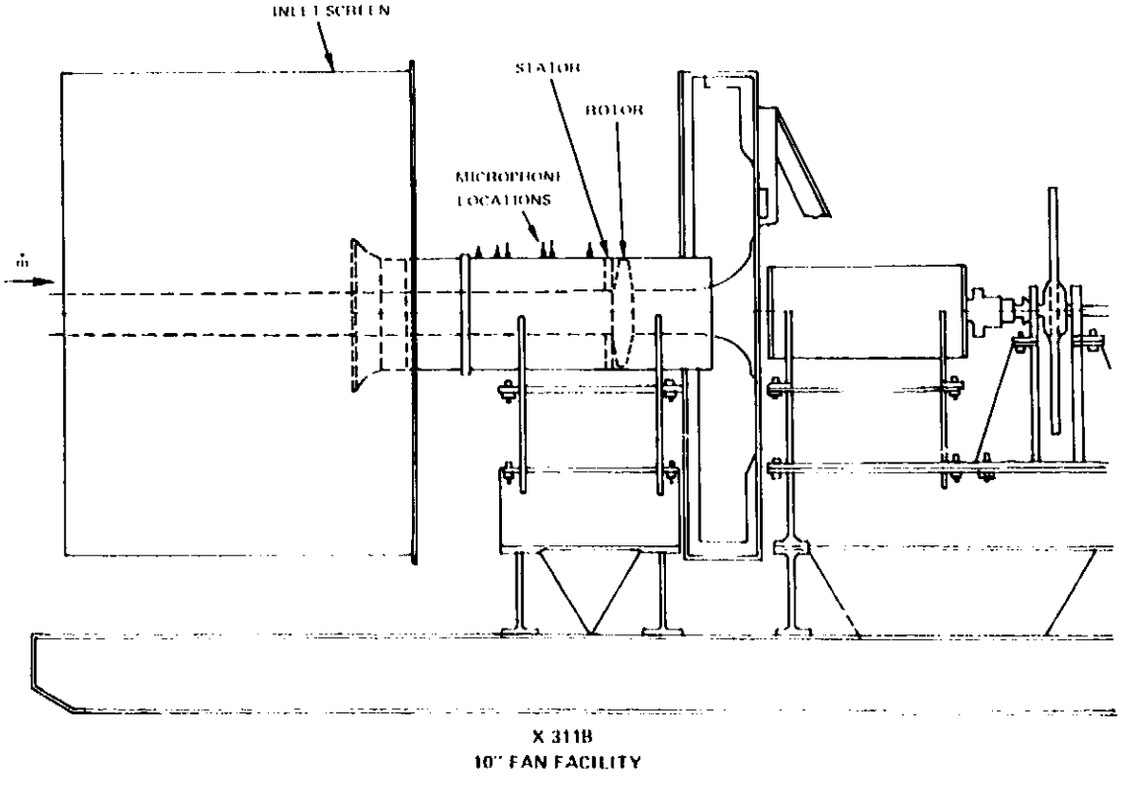

Figure 3.4-1 Schematic of 25 cm (10 in.) Acoustic Fan Rig

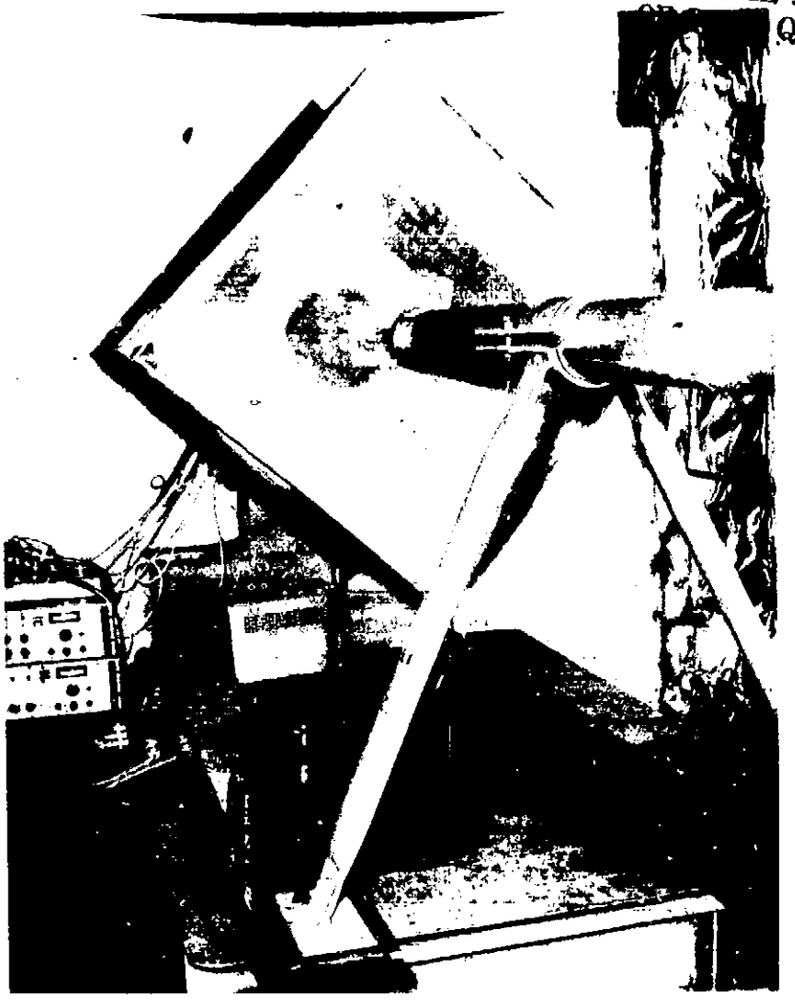

Figure 3.4-2 Photograph of 25 cm (10 in) Acoustic Fan Rig

The reason for using an inlet screen to reduce steady inflow distortions was to comply with the assumption of uniform axial flow in the Tyler-Sofrin analysis. Reducing steady inflow distortions in turn reduces the amplitude of modes generated as a direct cause of the steady inflow distortion (see Appendix C for such a generation mechanism). These modes (called extraneous modes in this text) are not predicted from a direct application of the Tyler-Sofrin analysis and, as will be seen later in section 3.4.6, cause inaccuracies in the method presented for the determination of coherent sound mode structures predicted to exist by the Tyler-Sofrin theory.

The reason for using the screen to reduce unsteady inflow turbulence was to increase test repeatability and thereby to reduce the amount of time needed for signal averaging. This objective was achieved effectively as can be seen by Figure 3.4-3. This figure shows the deviation (in decibels) of the enhanced signal amplitude generated by the wakes from 34

rods interacting with a 32 bladed rotor at 2 BPF (obtained from five sample outputs at a given microphone) as a function of the averaging time (or number of samples). A comparison of the deviations is presented for the two configurations with and without the inlet screen. It can be seen that the convergence for the configuration with the inlet screen is obtained with shorter averaging times than for the configuration without the screen. A similar result was also obtained at BPF. This improvement in repeatability and in the accuracy of measured coherent signals is achieved without significant change in the tone or broadband sound pressure levels. The two Figures, 3.4-4 and 3.4-5, show spectra obtained from a wall mounted microphone when the inlet control screen was respectively removed and installed. A comparison of the spectra indicates that the tone and broadband levels are almost identical and, thus, the predominant sound field in the duct could not be generated by rotor turbulence interaction.

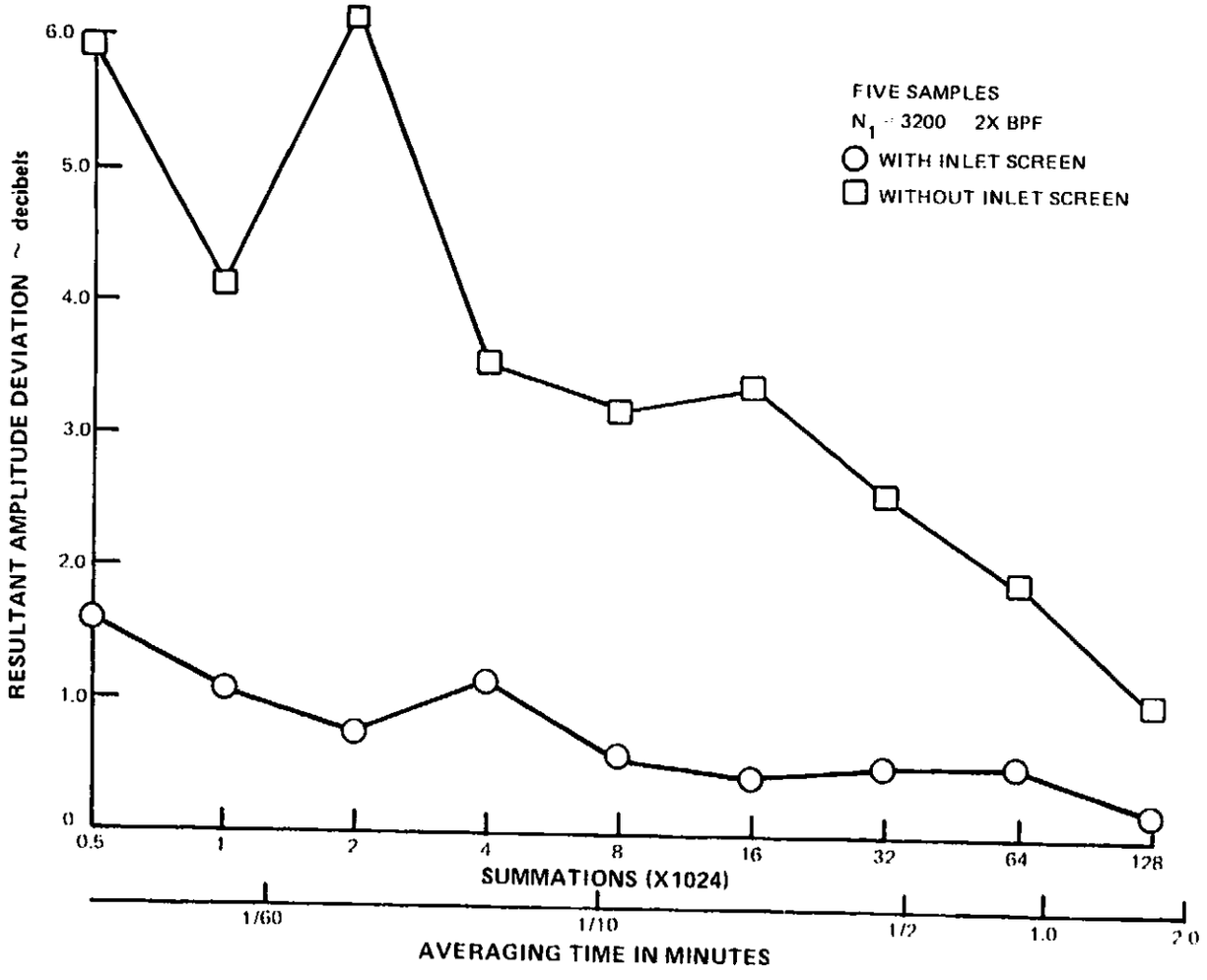

Figure 3.4-3 *Accuracy of Measured Pressure Amplitude With and Without Turbulence Suppression Screen*

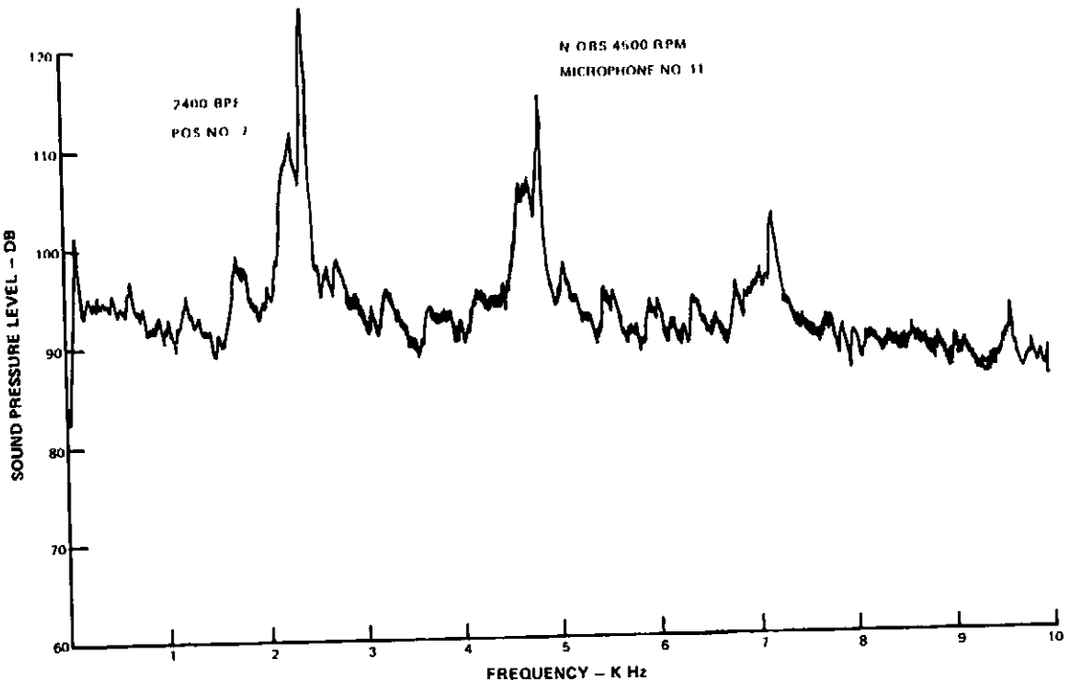

Figure 3.4-4 *Overall Spectrum Generated at 4500 rpm at Microphone Location No. 11 - Without Inflow Control Screen*

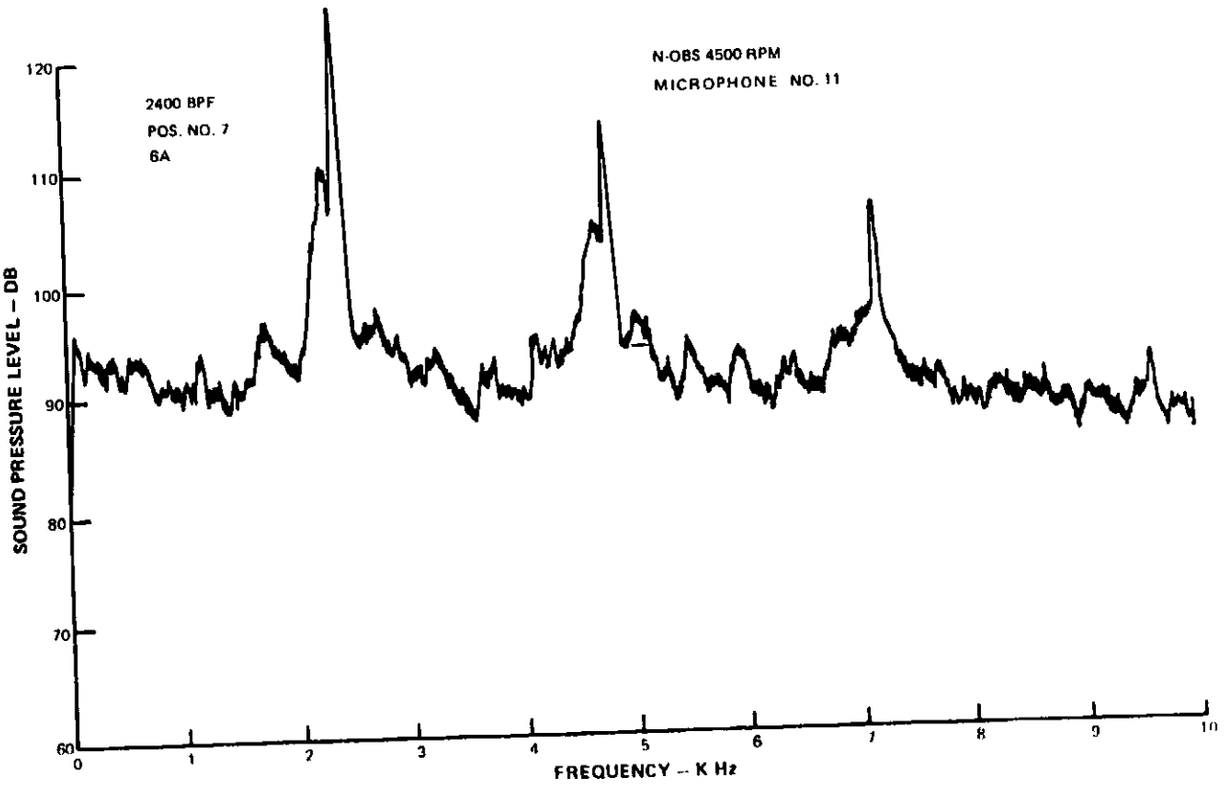

Figure 3.4-5 *Overall Spectrum Generated at 4500 rpm at Microphone No. 11 - With Inflow Control Screen*

3.4.4 Data Acquisition and Processing System

An "on-line" data processing system was developed to provide coherent pressure signals for subsequent use in the calculation procedure to determine amplitude and phase of the constituent modes. Input to the processing system is the overall signal from each microphone along with a rotor-locked time-reference signal. The overall acoustic pressure signal includes the contribution from two components: a periodic coherent signal and a random incoherent signal. The principal output of the data analysis system is the coherent amplitude and phase at each microphone location. In addition, the output includes filtered tone noise at desired frequencies (BPF and 2 X BPF for the purpose of the present test) versus fan rpm or time and spectral analysis. Analog recording capability was also provided, so that data could be stored for any subsequent analysis that may be required.

Each of these system components is discussed in detail along with an accompanying description of how they were employed during the experimental evaluation program. The components of the data analysis system include: 1) signal enhancement, 2) tone tracking, 3) spectral analysis, and 4) analog recording. First, however, a description will be presented of the instrumentation for acquiring the overall pressure signal that is input to the data analysis system.

Instrumentation for Acquiring Input Signal

For each configuration tested, ten microphone systems were used to measure the sound field at ten locations on the duct wall. These ten locations incorporated the number of microphones and locations as specified by the MLP for each configuration, and the remainder were used to provide data for checking the method accuracy. Locations for each configuration were determined prior to the test and provision for the different locations required were made by drilling 14 holes in the test section of the duct. These locations are shown for reference purposes in Figure 3.4-6. The microphones used were B&K, model 4138, 1/8-inch diameter condenser type. They were calibrated for output sensitivity before and after each test run with a B&K, model 4220, pistonphone calibrator. The microphone and pistonphone calibrator were certified acceptable by the Pratt & Whitney Aircraft standards laboratory with the pistonphone output being certified at 124.0 ± 0.2 dB. All microphone outputs were normalized at 1.0 volts equal to 124 dB.

Data Analysis System

The input to the data analysis system was processed "on-line" and also recorded on magnetic tape to be processed at a later time by the "on-line" instrumentation. The "on-line" data analysis system used throughout the test program is shown in Figure 3.4-7. It can be seen that in addition to providing signal enhanced amplitude and phase values, the "on-line" signal could be spectrum analyzed, filtered at desired frequencies, and plotted versus fan rpm or time.

In Figure 3.4-8 is a block diagram of the magnetic tape recording system. This later system was developed to document the acoustic pressure signal at each microphone location as stipulated by the experimental assessment program.

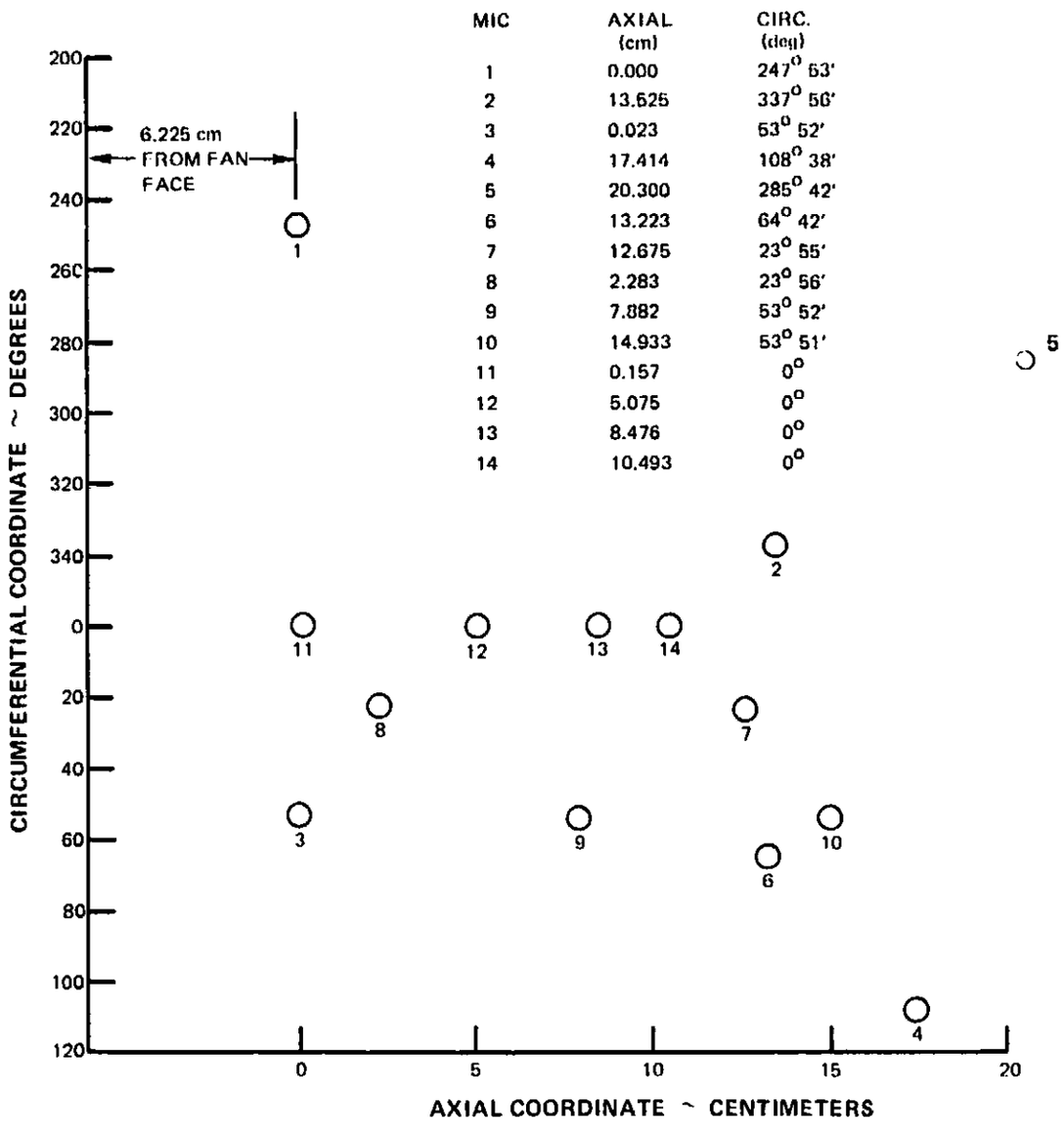

Figure 3.4-6 *Inlet Wall Microphone Positions*

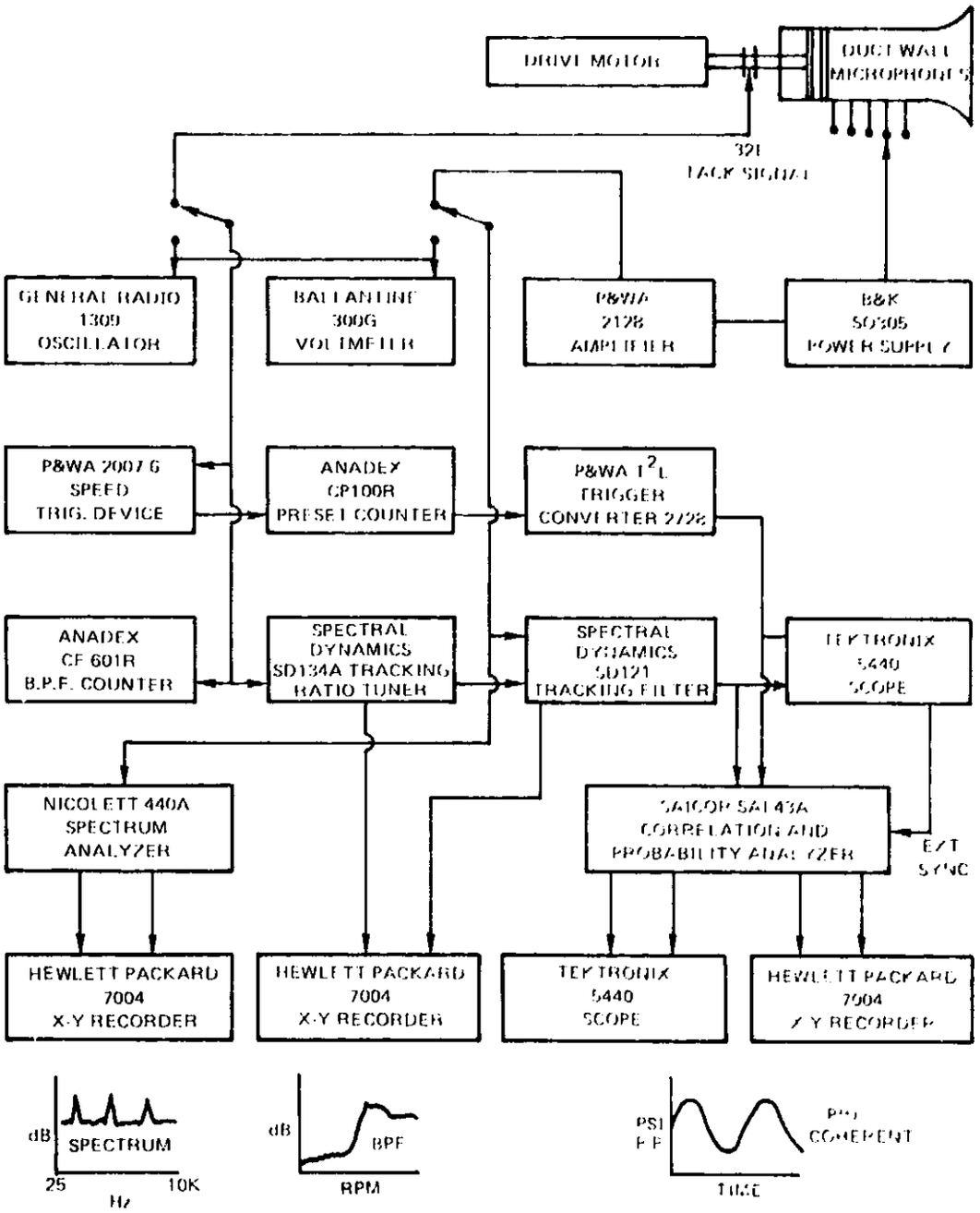

Figure 5-4: Block Diagram of On-Line Data Analysis System

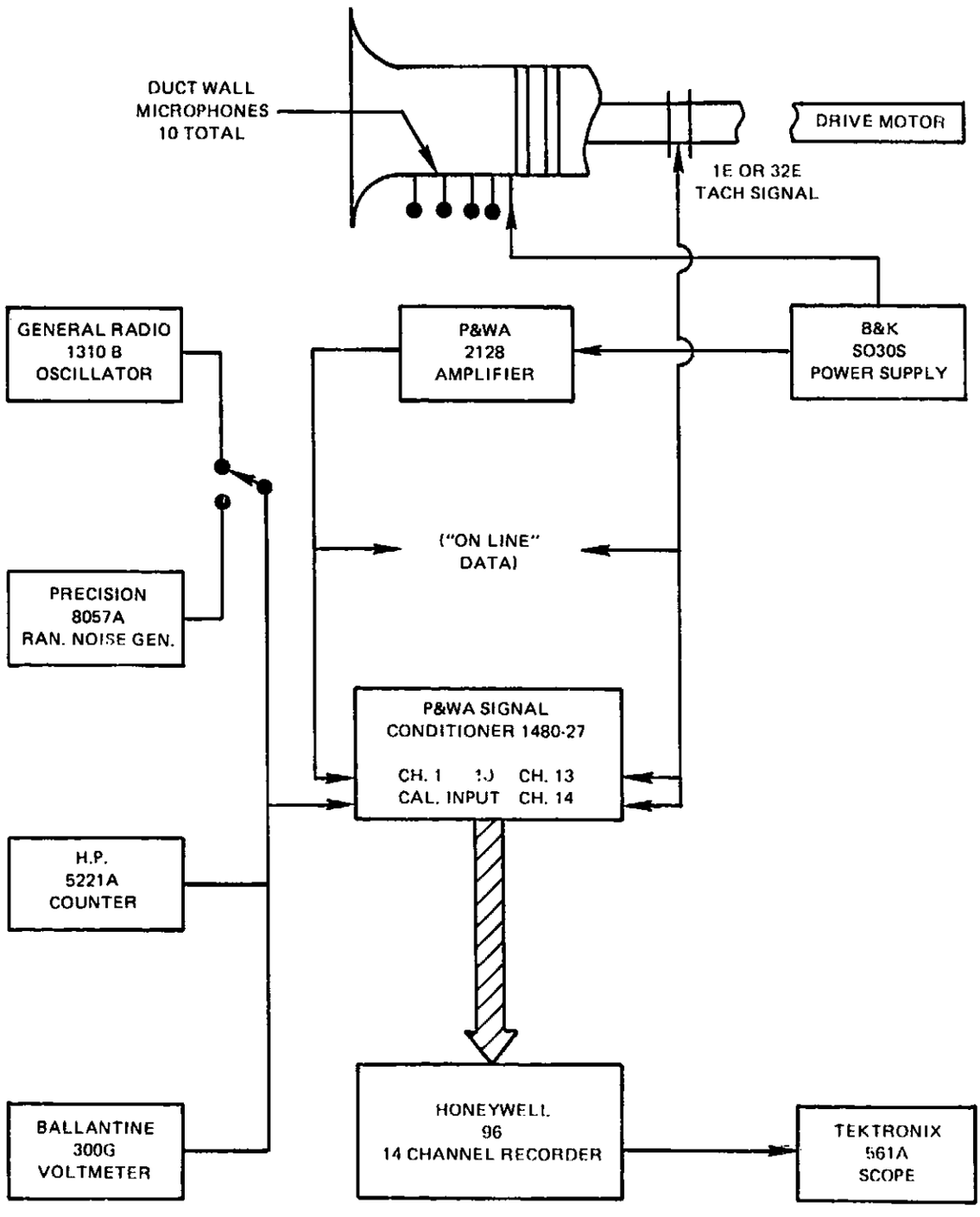

Figure 3.4-8 Block Diagram of Analog Tap Data Acquisition System

Signal Enhancement

To provide coherent acoustic pressure signals at microphone locations identified by the MLP, a rotor-locked time reference was obtained from a speed triggering system that used a trigger circuit to generate a pulse every time a rotor blade passed a point of reference. The triggering system operated on the 32-pulse per revolution speed signal and generated a pulse at the zero crossing of the signal. This zero crossing occurred at equal time increments as each blade passed. The output was a transistor-transistor logic (TTL) pulse that was time locked to the rotating fan. The TTL pulse was used in signal enhancement to determine the zero reference time and repetition rate of the enhancement.

During the test, all microphone signals were filtered at either BPF or 2 X BPF and stored by the memory of the signal enhancer. This storing was achieved by digitizing the analog input over a time period sufficient to acquire at least one full cycle of the input frequency. Subsequent cycles, triggered by the TTL pulse, were digitized and added to the memory. A total of 32,768 summations were achieved for signals at BPF, and 65,536 summations, for signals at 2 X BPF. The summations were chosen as optimum based on repeatability studies.

The enhancer output was the average of the summations, and thus the coherent portion of the microphone signals was obtained. In order to measure signals representative of more than one blade pressure pattern, the blade related TTL trigger signal was fed to a preset counter that generated a pulse on every third blade. The rotor assembly contained 32 blades, so triggering on every third blade caused the enhancer to sample all of the rotor-locked pressure patterns every three revolutions of the fan. The enhancer output, representing the coherent portion of the microphone signal, was plotted on an x-y plotter from which the averaged signal amplitude and phase could be obtained.

Tone Tracking

The overall tone sound pressure level is also an output of the data-analysis system. This output is used to demonstrate the cut-on of a specific mode by increasing the rotor speed and recording the overall microphone signal for the blade-passing tone or harmonic of interest. The tone level at a specific frequency could also be compared with the coherent amplitude to determine whether most of the sound energy is either coherent or incoherent.

To provide plots of BPF or 2 X BPF versus rpm or time and to provide a suitably filtered signal for signal enhancement, a tracking ratio tuner and a tracked filter system was required. This capability was provided as follows:

The microphone signals were filtered with a 50 hertz phase-locked bandwidth filter centered on the frequency of interest (BPF or 2X BPF). The tracking filter was continually tuned by the 32 pulse per revolution speed signal which was passed through a phase coherent tracking ratio tuner that had the capability of following any rotor speed variation and to tune the tracking filter to any multiple of the blade passing frequency. The 32 pulse per revolution signal was input to the tracking ratio tuner and was multiplied by one or two to provide the proper driving frequency to the tracking filter for BPF or 2 X BPF, respectively. For plots of tone noise versus rpm or time, the output from the tracking filter was directed to the Y axis of the x-y plotter. The "DC proportional to frequency" output from the tracking ratio tuner provided the X axis (rpm) signal for plotting during accel decels.

Spectral Analysis

To assess the spectral content of the overall microphone signal, a spectral analyzer was incorporated in the data analysis system. Spectral plots could be readily assessed to determine whether the sound pressure level of the blade-passing tone or its harmonics dominate the broadband noise component. Spectral data obtained during the test program indicate that this was always the case.

A parallel output from the microphone was connected to the high speed spectrum analyzer which allowed simultaneous spectrum analysis during signal enhancement. The analysis was made over a frequency range from 25 hertz to 10K hertz with a 25 hertz bandwidth filter. The analyzer provided digital storage and averaging of the analyzed signal. In order to obtain data sampling consistent with the enhanced data, the analyzer was set to accumulate 512 spectrum averages. Stored averaged spectra were then plotted on the x-y plotter.

Analog Recording

An analog tape recorder was employed to record the microphone output to enable analysis similar to that performed on-line. The advantage of the recorded analysis was that each microphone signal could be analyzed over the same time period; however, disadvantages included the careful calibrations required to preserve phase relationships.

Data from the ten microphones were recorded on magnetic tape simultaneously for each configuration tested. Five microphones were recorded on the odd record head; and five, on the even head. The 32 pulse per revolution speed signal was recorded simultaneously on the odd and even heads. All data were recorded on the wide band Group I recorder in the FM mode at a tape speed of 30 inches per second. Figure 3.4-8 is a sketch of the magnetic tape recording system.

Calibration signals were recorded on all the recorder channels simultaneously, including the speed channels. Signal enhancement of these calibration signals provided a measure of individual data channel amplitude sensitivity. The enhancement also provided a channel-to-channel and head-to-head relative phase correction. Data recorded on the odd head were enhanced using the speed signal recorded also on the odd head and similarly for the even head data.

3.4.5 Test Program

The matrix inversion method for determining coherent fan-sound-mode structures was assessed for six mode structures. The assessment was made with measurement input obtained from the test program described in this section. These modes structures were generated by two sets of distortion generating rods on the Pratt & Whitney Aircraft 25.4 cm (10 in.) diameter research fan rig. Four of the six mode structures were generated by one set of hardware which simulated a stator wake-rotor interaction by positioning 34 equally spaced rods of 0.23 cm (0.90 in.) in diameter, 3.71 cm (1.46 in.) from leading edge to trailing edge upstream of the rotor. For this configuration, the 32 bladed rotor was operated at both 3400 rpm and 5813

rpm. Microphone locations were determined for each of these modal structures by use of the Microphone Location Program (MLP), as discussed in section 3.4.4. At each rotor speed, data were obtain at both blade passing frequency (BPF) and twice blade passing frequency (2 X BPF). In this way, four modal structures were calculated by the Modal Calculation Program (MCP).

The other set of hardware simulated steady inflow distortion by placing a single rod assembly in front of the rotor. Two modal structures were evaluated by operating the rotor at two speeds (3400 rpm and 3740 rpm) and acquiring data at BPF. For this configuration, the MLP was used to locate microphones for the modal structure generated at the 3400 rpm rotor speed. For the higher speed, which represents a ten percent increase in rotor speed, the same set of microphone positions were used as for the lower speed. The objective of this test was to determine if a set of microphone locations as determined by the MLP for a given rotor speed and frequency, can be used successfully to obtain data at a slightly different frequency and rotor speed.

A summary of the test program is provided in Table 3.4-1. This table includes: the geometric configuration, rotor speed, frequency, the total number of propagating incident modes supported by the duct, the mode structures predicted by the Tyler-Sofrin analysis to be determined for each case, and the conditioning number associated with the microphone locations as determined by the MLP for each case.

For each of the six mode structures, the amplitude and phase of each of the modes was calculated using the MCP. Input to the MCP was obtained "on-line" from a set of microphones at duct locations determined by running the MLP, as described in section 3.2.3. Additional acoustic pressure measurements were obtained at other locations in the duct, and were used to check the method accuracy by comparing the measured sound field at various locations with the predicted sound field at those locations based on a knowledge of the calculated mode structure. Shown in Table 3.4-2, for each test configuration, are the microphone locations used to provide data for the modal calculation and the locations for the microphones used to check the accuracy of the modal calculation method.

In addition to these measurements, an evaluation of the standard deviation for the errors in measurement of acoustic pressure and microphone location was conducted for each of the six mode structures. Table 3.4-3 presents, for each test configuration, the values used as input to the MCP so that the standard deviations for each of the calculated modes could be determined.

The standard deviations of the errors in microphone location (as obtained from the P&WA Standards Laboratory) are related to the tolerance of the measurement for determining the axial and azimuthal coordinate of the microphone. Errors in the radial location of flush mounted transducers reflect the variation in the roundness of the outer duct wall and thus is seen to be small.

TABLE 3.4-1
TEST PROGRAM SUMMARY
32-BLADE ROTOR
(25.4 CM FAN RIG)

Test Designation	Stator	Speed (rpm)	Frequency	Duct Supported[a]	MODE GROUP Mode Structure to be Calculated[c]	Conditioning Number
Stator-rotor interaction	34 rod					
1		3400	BPF	7	(-3,0) (-2,0)[b] (-1,0) (0,0) (3,0) (2,0) (1,0)	2.1
2		3400	2XBPF	20	(-4,0)	-
3		5813	BPF	16	(-2,0) (-2,1)	1.3
4		5813	2XBPF	53	(-4,0) (-4,1) (-4,2)	2.0
Steady inflow distortion	1 rod					
5		3400	BPF	7	(-3,0) (-2,0) (-1,0) (0,0) (3,0) (2,0) (1,0)	2.1
6		3740	BPF	7	(-3,0) (-2,0) (-1,0) (0,0) (3,0) (2,0) (1,0)	3.1

Notes: (a) Not including reflected modes.

(b) (-2,0) is only one in the group predicted by Tyler-Sofrin Theory for a stator-rotor interaction

(c) Predicted by Tyler-Sofrin analysis for a stator-rotor interaction

TABLE 3.4-2

DESIGNATION OF INPUT OR CHECK MICROPHONES

Microphone Number (See Fig. 3.4-4 for location)	Test Designation								
	1a	1b	2a	2b	3a	3b	4	5	6
1	I	I	C	I	C	I	C	I	I
2	I	C	I	I	C	I	C	I	I
3	I	I	C	I	C	C	I	I	I
4	I	C	C	I	C	I	C	I	I
5	I	C	C	I	C	I	C	I	I
6	I	C	C	I	C	I	C	I	I
7	I	C	C	C	I	I	C	I	I
8	C	C	C	I	I	I	C	C	C
9	C	C	C	I	C	I	I	C	C
10	C	I	C	C	C	I	I	C	C
11			C*	C*	C*	C*			
12			C*	C*	C*	C*			
13			C*	C*	C*	C*			
14			C*	I*	C*	C*			

Microphone not used to obtain data

I Microphone used to obtain data for input to calculation procedure (MCP)

C Microphone used to obtain data for checking calculated modal structures

* Microphone used to obtain additional data by repeating the test.

TABLE 3.4-3
STANDARD DEVIATIONS OF MEASUREMENT ERRORS

Error Source	Error Source	Test Designation 1	2	3	4	5	6
Microphone Location Errors	Axial σ_X (Centimeters)	1.3×10^{-3}	1.3×10^{-3}	1.3×10^{-3}	1.3×10^{-3}	1.3×10^{-3}	1.3×10^{-3}
	Circumferential σ_θ (degrees)	8.5×10^{-3}	8.5×10^{-3}	8.5×10^{-3}	8.5×10^{-3}	8.5×10^{-3}	8.5×10^{-3}
	Radial σ_r (centimeters)	5.1×10^{-3}	5.1×10^{-3}	5.1×10^{-3}	5.1×10^{-3}	5.1×10^{-3}	5.1×10^{-3}
Pressure Measurement Errors	Amplitude σ_B (decibels)	0.3	0.5	0.6	1.0	1.0	1.2
	Phase σ_ψ (degrees)	1.5	2.0	1.5	3.5	2.0	2.0

The standard deviation of the inaccuracies in acoustic pressure measurement are not only due to measurement system variations, but also to the different sound fields at the different frequencies considered during the test program. The accuracy of the microphones to measure acoustic pressure amplitudes was assessed by comparing a precalibration and a postcalibration of the microphones for each test. During this test program it was experimentally manageable to adhere to careful procedures so that the standard deviation of the errors associated with transducer calibration was relatively small (about 0.2 to 0.3 dB). In addition to calibration errors, the standard error for pressure measurement includes an evaluation of measurement repeatability for each of the six mode structures. The variation in repeatability was assessed in a similar manner as the deviation shown in Figure 3.4-3. By this procedure, an enhanced signal was obtained from five sample outputs at a given microphone at the number of summations chosen as optimum based on such repeatability studies. The standard deviations of the variation in repeatability are typically larger than those attributed to transducer response. Thus, a combined standard deviation (in decibels) of both calibration errors and variations in repeatability, as presented in Table 3.4-3, yields values that are controlled by the relatively larger observed variations in the repeatability of the enhanced signal.

In light of this observation, it is expected that the magnitude of the variation in the enhanced signal will depend on whether the random contribution in the overall signal is comparable to the coherent sound pressure level. The random component of the overall sound pressure level was compared to the coherent level for the two mode structures that were generated at BPF (test configuration 1) and 2 BPF (test configuration 2) by the wakes from 34 rods interacting with a 32 bladed rotor operating at a speed of 3400 rpm.

At BPF, the variation of the enhanced signal for five sample outputs at a given microphone was 0.3 dB. However, it was found that the coherent sound pressure level at five microphone locations was from 9.1 to 11.5 dB higher than the random component. Thus, in this case the randomly phased noise structure was on an order of 10 dB below the coherent signal so the variation in amplitude and phase of the enhanced signal is assigned the smallest pressure measurement error of those given in Table 3-4-3.

At 2 BPF, a similar analysis at three microphone locations was conducted by comparing signal enhanced and overall tone level data. This analysis indicates that the coherent noise field is between 4.2 to 5.4 dB higher than the randomly phased structure. The pressure measurement error of 0.5 dB in Table 3-4-3 for test configuration 2 reflects the larger variation in pressure amplitude measurement due to the relatively higher randomly phased component.

A final comparison of the overall tone level and signal enhanced pressure amplitude was conducted for the fifth mode structure configuration. In this test configuration a single rod was placed upstream of a 32 bladed rotor operating at 3400 rpm. At several microphone locations the measured resultant pressure amplitude was small due to the cancellation of the constituent modes. Thus, a comparison of the relative amplitude of the coherent and randomly phased sound fields varied substantially from one microphone location to another. In particular, at microphone location 5 the coherent sound field was 10.6 dB higher than the amplitude of the randomly-phased component. However, at microphone 3 the measured enhanced pressure amplitude was 16.3 dB lower than the sound pressure level for the random structure. As may be expected, accurate measurement of the enhanced signal at some microphone locations was difficult so that in Table 3.4-3 a relatively larger standard deviation was assigned to the pressure amplitude error.

In the next section, 3.4.6, the amplitudes and phases and the calculated standard deviations are presented for each of the six modal structures investigated. In addition, the accuracy of the calculated mode structure is demonstrated by comparing the measured sound field at various duct locations with the predicted sound field at those locations based on the calculated mode structure. Discrepancies between predicted and measured data are discussed and related to the calculated standard deviations associated with each of the modes. A summary and an assessment of the test results are presented in section 3.4.7. Readers wishing to avoid the detailed test description may proceed directly to section 3.4.7.

3.4.6 Test Results

Results from each of the six mode structures will be presented under a separate heading. An assessment of the overall test results will be reserved until the next section, 3.4.7.

Mode Structure Configuration No. 1

The first modal structure was generated at BPF (1813 Hz) by the wakes from the 34 rods interacting with the 32 bladed rotor operating at a speed of 3400 rpm. The overall acoustic spectrum generated at this speed at microphone No. 10 is shown in Figure 3.4-9, and it can be seen that BPF is well above the background broadband noise level as determined from a 25 Hz bandwidth filter. At BPF, the fan inlet can support seven incident modes: (-3, 0), (-2, 0), (-1, 0), (0, 0), (1, 0), (2, 0), and (3, 0). Based on an application of the Tyler-Sofrin analysis, it was expected that the sound pressure level of the (-2, 0) would be much greater than the sound pressure levels generated by the remaining six incident modes. However, because of the low number of modes supported by the duct, it was decided to locate seven microphones in the duct to provide data for calculating the amplitudes and phases of all seven incident modes. It was assumed in this test that modes reflected from the inlet do not contribute significantly to the sound field. The actual locations as determined by the MLP of the seven

microphones are given in Table 3.4-2 and resulted in a conditioning number (see section 3.2.3) of 2.1. Also, data were obtained at three other microphone locations so that a check on the accuracy of the calculated mode structure would be obtained.

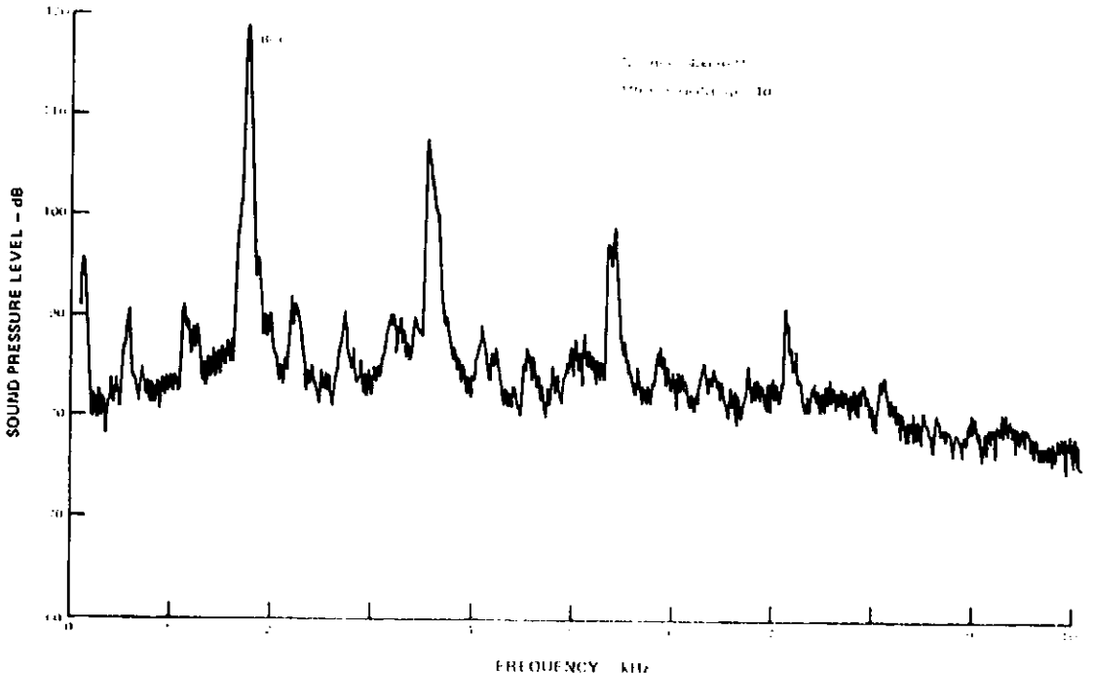

Figure 3.4-9 *Overall Spectrum Generated at 3400 RPM at Microphone Location No. 10 Mode Structure Configuration No. 1*

The coherent acoustic pressure amplitude and phase at all ten microphone locations are listed in Table 3.4-4. The first seven amplitudes and phases were used as input to the MCP, and the amplitudes and phases of the seven propagating incident modes were calculated. In addition, the standard deviations for the amplitude and phase of each mode were calculated using the standard deviations due to amplitude and phase measurement errors. These standard deviations in measurement errors were defined in Table 3.4-3. The calculated amplitudes and phases of each mode along with the corresponding standard deviations are listed in Table 3.4-5(a). The modal amplitudes and error bands given by plus and minus one standard deviation are illustrated in Figure 3.4-10.

The modal structure was used to predict the resultant sound field at three microphone locations: No. 8, No. 9, and No. 10 of Table 3.4-2. The discrepancy between predicted and measured acoustic pressure amplitude (in decibels) and phase (in degrees) is listed in Table 3.4-6. It can be seen that the phase is predicted slightly high (3.9° to 6.7°) at all three locations and that the amplitude is within -0.8 dB to 1.7 dB. Since three check locations are a statistically small population, it is difficult to assess accurately the method for this test case. To get a better estimate, advantage will be taken of the fact that the (-2, 0) mode is much greater in amplitude than the other propagating modes. If the contribution from modes other than the (-2, 0) mode is considered to be insignificant, only one microphone is required to determine the amplitude and phase of the dominant mode. The ten microphone measurements made during this test thus give ten samples from which the average amplitude and phase of the (-2, 0) mode can be determined along with the respective standard deviations.

TABLE 3.4-4
MEASURED DUCT ACOUSTIC PRESSURE
(RPM = 3400 BPF = 1813 Hz)

CONFIGURATION NO. 1

Microphone No.	(dB)	Coherent Resultant Amplitude (dynes/cm^2)	(lbf/in.^{2})	Phase (deg.)
1	121.4	235.9	3.422×10^{-3}	204.5
2	120.6	213.5	3.096×10^{-3}	237.8
3	120.1	203.0	2.945×10^{-3}	244.5
4	117.8	154.9	2.247×10^{-3}	30.2
5	120.1	202.2	2.933×10^{-3}	91.0
6	118.1	161.3	2.340×10^{-3}	57.8
7	120.1	203.0	2.945×10^{-3}	128.5
8	119.7	193.4	2.805×10^{-3}	329.3
9	119.4	187.0	2.712×10^{-3}	356.4
10	119.4	187.8	2.724×10^{-3}	99.9
Avg Resultant Amplitude B_0 =	119.7	195.5	2.8169×10^{-3}	

TABLE 3.4-5
CALCULATED MODE STRUCTURE AND ERROR

CONFIGURATION NO. 1

A. SEVEN MODE INVESTIGATION

Mode	Amplitude (dB)	Error (dB)	Phase (deg)	Error (deg)
(-3,0)	108.8	1.0	9.7	8.3
(-2,0)	125.6	0.2	243.0	0.9
(-1,0)	107.7	1.2	295.9	7.1
(0,0)	103.0	1.5	77.2	8.3
(1,0)	102.1	1.9	54.9	15.4
(2,0)	101.2	2.3	130.6	18.9
(3,0)	99.5	2.5	344.1	20.9

B. THREE MODE INVESTIGATION

(-3,0)	107.1	1.5	31.8	12.3
(-2,0)	126.5	0.2	246.0	1.0
(-1,0)	108.8	0.9	324.4	6.5

C. AMPLITUDE AND PHASE OF (-2,0) MODE BASED ON AVERAGE OF 10 MICROPHONES

(-2,0) $A_{-2,0}$	125.4	1.0	241.8	3.1

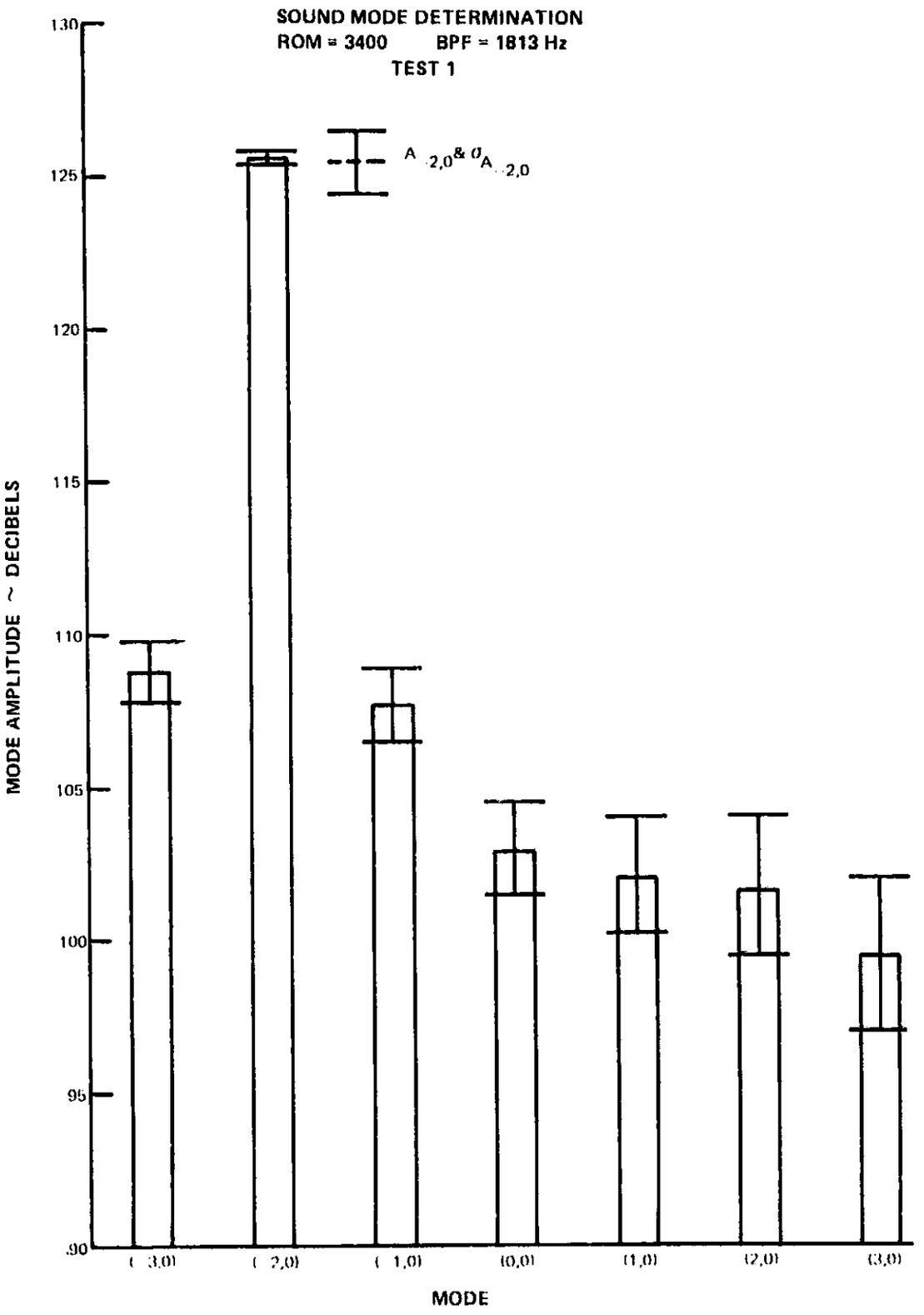

Figure 3.4-10 Sound Modal Amplitudes and Standard Deviations Mode Structure Configuration No. 1

TABLE 3.4-6

DIFFERENCE BETWEEN PREDICTED AND MEASURED DUCT
ACOUSTIC PRESSURE
(PREDICTED MINUS MEASURED)

CONFIGURATION NO. 1

Microphone No.	Amplitude Delta (dB)	Phase Delta (deg)
8	1.7	5.5
9	0.4	3.9
10	-0.8	6.7

Superimposed on Figure 3.4-10 and listed in Table 3.4-5(c) is the average amplitude and standard deviation of the (-2, 0) mode obtained from the 10 microphone measurements as described above. It can be seen that the average amplitude is only 0.2 dB below the level predicted by the matrix inversion method. The standard deviation about the average, however, is greater than that predicted from the influence coefficients and estimates of the measurement errors. The average phase of the (-2, 0) mode is 241.8° with a standard deviation of 5.4° when projected to the same reference location used for the matrix inversion method (i.e., at the rotor plane and 180° from top dead center). Again this compares well with the 243° phase predicted by the matrix inversion method; but the standard deviation is much greater than the 0.9° predicted from the influence coefficients and estimates of the measurement errors.

Thus it can be seen that the matrix inversion method predicts well the amplitude and phase of the dominant mode out of the seven possible incident propagating modes. Parenthetically, it may be noted that the results substantiate in this case the assumption that the contribution to the sound field of reflected waves is insignificant.

Finally, the modal distribution of acoustic theory is worth mentioning. Figure 3.4-10 shows that the sound pressure levels of the modes neighboring the principle (-2,0) mode are higher than the remaining modes. This feature may be explained by the presence of a small residual steady one lobe inflow distortion modulating the wakes from the 34 rods interacting with the rotor. A more precise description of this mechanism is given in Appendix C.

In light of this observation, it was decided to check the method accuracy with three microphone measurements assuming the (-2, 0) and its immediate neighbors (-1, 0) and (-3, 0) contain the bulk of the acoustic energy. Firstly, the MIP was run using its second option to select the three microphone locations out of the ten possible locations that gave the lowest conditioning number. It was found that microphone locations 1, 3, and 10 conditioned the

equation system so as to yield a conditioning number of 1.1. Data from the three selected microphones were used as input to the MCP and the resulting mode amplitudes and phases along with respective standard deviations were calculated. These values are shown in Table 3.4-5(b) for the (-3, 0), (-2, 0), and (-1, 0) modes. Comparison with the mode structure obtained using seven microphones shows a discrepancy in amplitude of 0.9 dB for the dominant (-2, 0) mode and on the order of 1.5 dB for the other two modes. Also the calculated phase of the dominant (-2, 0) mode changes from 243° to 246° – a value further removed from the estimate of 241.8° based on the average of ten microphones.

Thus it can be seen how the omission of only the four smallest modes out of the seven incident propagating modes affects the predicted amplitude of the dominant mode. In this case the differences are small, showing that a good estimate of the dominant mode amplitude and phase can be obtained without considering all seven modes. Despite the small difference, however, it is interesting to note that the omission of the four smallest modes (more than 20 dB down from the (-2, 0) mode) results in a 0.9 dB change in the calculated amplitude of the dominant (-2, 0) mode.

Mode Structure Configuration No. 2

The second modal structure considered was that generated at 2 X BPF (3627 Hz) by the wakes from the 34 rods interacting with the 32 bladed rotor operating at a speed of 3400 rpm. At this frequency, the fan inlet can support twenty incident modes although only the (-4, 0) mode is predicted by the Tyler-Sofrin analysis to contain significant acoustic energy. For this case, it was beyond the scope of the program to make a sufficient number of measurements to determine the amplitude and phase of all twenty incident modes. It was assumed, therefore, that the incident (-4, 0) mode contained the bulk of the acoustic energy in the duct sound field. With this assumption, only one microphone measurement was necessary to determine the amplitude and phase of the (-4, 0) mode and the respective standard deviations based on a multiplication of the influence coefficients and estimated measurement errors. Although the choice is arbitrary, microphone location No. 2, listed in Table 3.4-2 was selected to provide input to the MCP -principally, of course, to determine the standard deviations of the mode amplitude and phase. In order to have a large sample of check microphones, measurements were made at ten microphone locations. The measured amplitudes and phases at each microphone location are listed in Table 3.4-7.

The amplitude and phase of the (-4, 0) mode and the corresponding standard deviation as calculated from the influence coefficients and measurements from microphone No. 2 are shown in Table 3.4-8. Also shown is the amplitude and phase of the (-4, 0) mode along with the standard deviation in amplitude and phase obtained by averaging the ten microphone measurements. The main observation to be seen from this example is that, as was seen in the first test configuration, the predicted errors based on the influence functions, underestimates the actual measured variations in amplitude and phase. A comparison of the average mode amplitude and phase with that obtained from microphone No. 2 has no real significance in this example, because of the arbitrariness in the initial selection.

TABLE 3.4-7
MEASURED DUCT ACOUSTIC PRESSURE
(RPM = 3400 2 X BPF = 3627 Hz)

CONFIGURATION NO. 2

Microphone No.	(dB)	Coherent Resultant Amplitude (dynes/Cm^2)	(lbf/in.^{2})	Phase (deg.)
1	108.4	52.89	7.672×10^{-4}	233.1
2	106.3	41.47	6.015×10^{-4}	330.9
3	106.9	44.35	6.433×10^{-4}	320.6
4	107.8	49.24	7.142×10^{-4}	285.1
5	109.8	61.59	8.933×10^{-4}	38.5
6	106.6	42.88	6.219×10^{-4}	325.8
7	105.5	37.85	5.489×10^{-4}	133.2
8	108.2	51.20	7.425×10^{-4}	145.5
9	107.4	46.89	6.801×10^{-4}	195.6
10	106.9	44.09	6.394×10^{-4}	64.3
Avg. Resultant: Amplitude B_n =	107.5	47.24	6.394×10^{-4}	

TABLE 3.4-8
CALCULATED (-4,0) MODE AMPLITUDE AND PHASE
AND CORRESPONDING ERRORS
(ONE MODE INPUT TO MCP)

CONFIGURATION NO. 2

Mode	Amplitude (dB)	Error (dB)	Phase (deg)	Error (deg)
(-4,0)	114.2	0.6	317.3	2.0
Avg. (-4,0) from 10 microphones	115.3	1.2	315.5	10.4

To determine a better estimate of the sound mode structure in this case, it was decided to apply the matrix inversion method to the determination of the structure of nine modes (including the (-4, 0) mode) using nine microphone measurements as input. The nine modes selected were the zeroth and first order radial modes in the immediate vicinity of the (-4, 0) mode. The rational for this selection was based on the observation from the last test case that the larger modes grouped about the dominant mode predicted by the Tyler-Sofrin analysis.

The nine modes selected were: (-6, 0), (-5, 0), (-4, 0), (-3, 0), (-2, 0), (-3, 1), (-2, 1), (-1, 1) and (0, 1). Nine microphone locations were chosen from the set of fourteen available locations. This was done by running the MIP for various combinations of nine out of fourteen until a set with a low conditioning number of 8.4 was obtained. The chosen locations are listed in Table 3.4-2.

The calculated amplitudes and phases of the nine modes are listed in Table 3.4-9. The amplitude distribution along with the predicted amplitude standard deviations are shown in Figure 3.4-11. It can be seen that the amplitude of the dominant (-4, 0) mode is within 0.6 dB of the average of 10 microphones but that the phase is off by 10.5°.

It should be noted also that the magnitudes of the remaining calculated modes cannot be considered to have negligible effect on the overall sound field since four of the modes (-3, 0), (-3, 1), (-2, 1), and (-1, 1) are within 10 dB of the dominant (-4, 0) mode. Despite the high amplitude of these modes, however, the amplitude and phase of the dominant (-4, 0) mode is reasonably well determined.

TABLE 3.4-9

CALCULATED MODE STRUCTURE AND ERROR

(NINE MODES INPUT TO MCP)

CONFIGURATION NO. 2

Mode	Amplitude (dB)	Error (dB)	Phase (deg)	Error (deg)
(-6,0)	86.2	6.6	225.6	24.4
(-5,0)	100.8	2.6	220.2	25.8
(-4,0)	115.9	4.2	326.0	6.2
(-3,0)	106.1	2.2	175.2	25.3
(-2,0)	103.3	1.7	301.3	15.2
(-3,1)	107.7	1.7	332.1	12.3
(-2,1)	108.8	2.8	308.8	25.0
(-1,1)	106.8	2.8	89.8	22.1
(0,1)	92.0	2.8	60.0	19.9

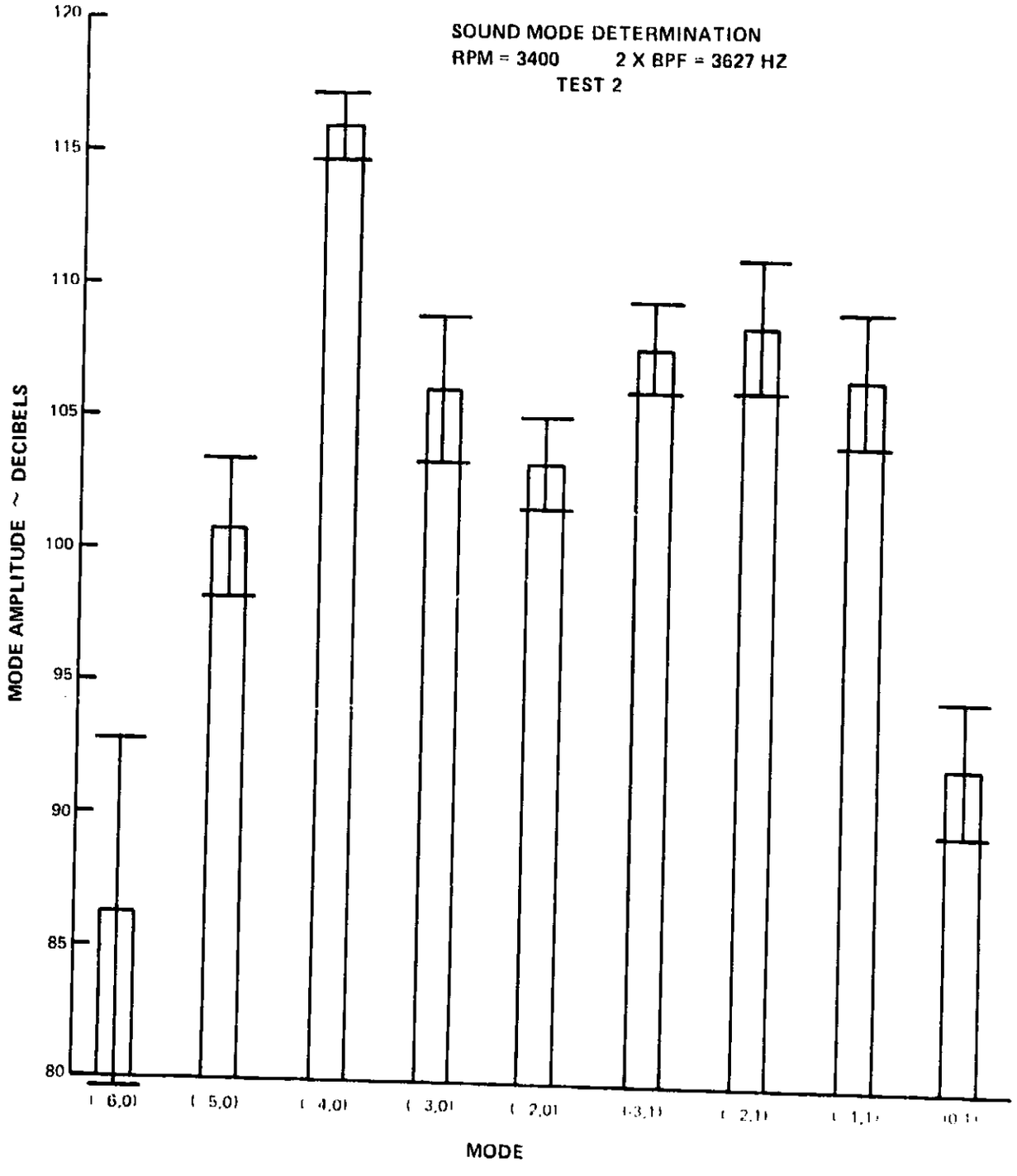

Figure 3.4-11 Sound Modal Amplitudes and Stand Deviations Mode Structure Configuration No. 2

An additional estimate of the method accuracy was obtained for this nine mode case, by repeating the test with three additional microphone locations designated No. 11, No. 12, and No. 13 in Figure 3.4-6. These three microphones together with microphones No. 7 and 10 (not used to provide input to the calculation) provided data, so that the measured sound field at these specific duct locations could be compared with the predicted sound field based on the calculated mode structure of nine modes. The difference between predicted and measured amplitude and phase are shown in Table 3.4-10. It can be seen that the predictions are generally good. The amplitude is predicted somewhat low by about 0.5 dB to 1.9 dB with a standard deviation of 1.4 dB about the mean and the phase is within +9° and -8° with a standard deviation of 8.0° about the mean. It is difficult to estimate the accuracy with which the modes other than the (-4, 0) are predicted. However, it is seen from Figure 3.4-11 that the standard deviation of modal amplitude calculated from the influence function, is larger for modes with low sound pressure levels.

Mode Structure Configuration No. 3

The third modal structure considered was that generated at BPF (3100 Hz) by the wakes from the 34 rods interacting with the rotor operating at a speed of 5813 rpm. At this frequency, the fan inlet duct can support sixteen propagating incident modes. From an application of the Tyler-Sofrin analysis, the (-2, 0), and (-2, 1) modes were predicted to contain the bulk of the acoustic sound energy in the duct. For this case, the MLP was used to select microphones No. 7 and No. 8 from those listed in Table 3.4-2, and the microphone combination had a conditioning number of 1.3. Again, measurements were made at a total of ten microphone locations (microphone No.'s 1 to 10 in Table 3.4-2) to provide eight locations to check the accuracy of the calculated mode structure. The measured amplitudes and phases from these ten microphones are listed in Table 3.4-11.

TABLE 3.4-10

DIFFERENCE BETWEEN PREDICTED AND MEASURED

DUCT ACOUSTIC PRESSURE

(PREDICTED MINUS MEASURED)

CONFIGURATION NO. 2

Microphone No.	Amplitude Delta (dB)	Phase Delta (deg)
[illegible]	1.2	[illegible].3
10	1.3	9.2
11	-0.5	-8.0
12	1.5	-5.1
13	-1.9	-5.1
	σ_B 1.1	σ_A, 8.0

TABLE 3.4-11
MEASURED DUCT ACOUSTIC PRESSURE
(RPM = 5813 BPF = 3100 Hz)

CONFIGURATION NO. 3

Microphone No.	(dB)	Coherent Resultant Amplitude (dynes/cm^2)	(lbf/in.^{2})	Phase (deg.)
1	131.2	725.4	10.521×10^{-3}	53.2
2	128.3	521.6	7.565×10^{-3}	328.9
3	128.9	555.9	8.063×10^{-3}	61.9
4	126.9	441.2	6.398×10^{-3}	205.3
5	130.8	692.0	10.036×10^{-3}	288.9
6	125.5	377.2	5.471×10^{-3}	144.4
7	126.1	405.8	5.886×10^{-3}	201.8
8	130.3	654.1	9.487×10^{-3}	197.8
9	125.7	386.2	5.601×10^{-3}	336.9
10	126.8	438.0	6.353×10^{-3}	226.1

The calculated amplitudes and phases of the (-2, 0) and (-2, 1) modes and the respective standard deviations calculated from the influence coefficients and estimated measurement errors for this case are shown in Table 3.4-12. The predicted sound field based on the amplitudes and phases of the (-2, 0) and (-2, 1) modes was compared with measured data at the eight check microphone locations and is presented in Table 3.4-13. It can be seen from this sample that the predicted amplitude is within -1.4 dB to 3.0 dB with a standard deviation of 1.5 dB, and the predicted phase between -22.1° and 11.4°, with a standard deviation of 14.5°.

In an effort to determine the amplitudes and phases of modes other than the (-2, 0) and (-2, 1) modes and, thus, improve the predicted accuracy at a set of check microphones, a larger set of microphones and modes was selected to test the method in a manner similar to that used in the last test case. Again nine modes were selected so as to be grouped about the predicted dominant (-2, 0) and (-2, 1) modes. The modes selected were: (-4, 0), (-3, 0), (-2, 0), (-1, 0), (0, 0), (-2, 1), (-2, 1) reflected, (-1, 1) and (0, 1). The reflected (-2, 1) mode was included in the selection because the incident (-2, 1) mode had a cutoff ratio near one and a significant portion of the acoustic energy was expected to be reflected.

The nine modal amplitudes and phases and the respective standard deviations are shown in Table 3.4-14. The amplitudes and amplitude standard deviations are shown graphically in Figure 3.4-12. It can be seen that the (-3, 0) mode and the (-1, 1) modes are quite comparable in amplitude to the (-2, 0) and (-2, 1) modes illustrating for this case the weakness of the assumption that the sound field is controlled only by the modes predicted by the Tyler Sofrin analysis.

TABLE 3.4-12
CALCULATED MODE STRUCTURE AND ERROR
(2 MODES INPUT TO MCP)

CONFIGURATION NO. 3

Mode	Amplitude (dB)	Error (dB)	Phase (deg)	Error (deg)
(-2,0)	134.1	0.4	341.2	1.2
(-2,1)	128.8	0.9	253.5	6.3

TABLE 3.4-13
DIFFERENCE BETWEEN PREDICTED AND MEASURED
DUCT ACOUSTIC PRESSURE
(PREDICTED MINUS MEASURED)

CONFIGURATION NO. 3

Microphone No	Amplitude Delta (dB)	Phase Delta (deg)
1	-0.4	- 8.6
2	-1.4	- 5.0
3	2.0	11.4
4	3.0	-20.9
5	0.0	-15.7
6	1.1	- 4.5
9	0.4	-22.1
10	1.4	- 7.6
	$\sigma_{\Delta B} = 1.5$	$\sigma_{\Delta\phi} = 14.5°$

TABLE 3.4-14
CALCULATED MODE STRUCTURE AND ERROR
(9 MODES INPUT TO MCP)

CONFIGURATION NO. 3

Mode	Amplitude (dB)	Error (dB)	Phase (deg)	Error (deg)
(-4,0)	111.5	4.8	267.9	64.2
(-3,0)	127.5	1.8	349.2	18.7
(-2,0)	132.5	1.3	13.8	5.2
(-1,0)	117.2	3.5	326.2	21.5
(0,0)	113.9	2.5	155.2	17.8
(-2,1)	130.4	1.5	222.3	13.7
$(-2,1)_{reflected}$	118.7	2.6	152.1	25.6
(-1,1)	126.4	2.1	286.0	28.3
(0,1)	115.2	1.7	249.5	19.4

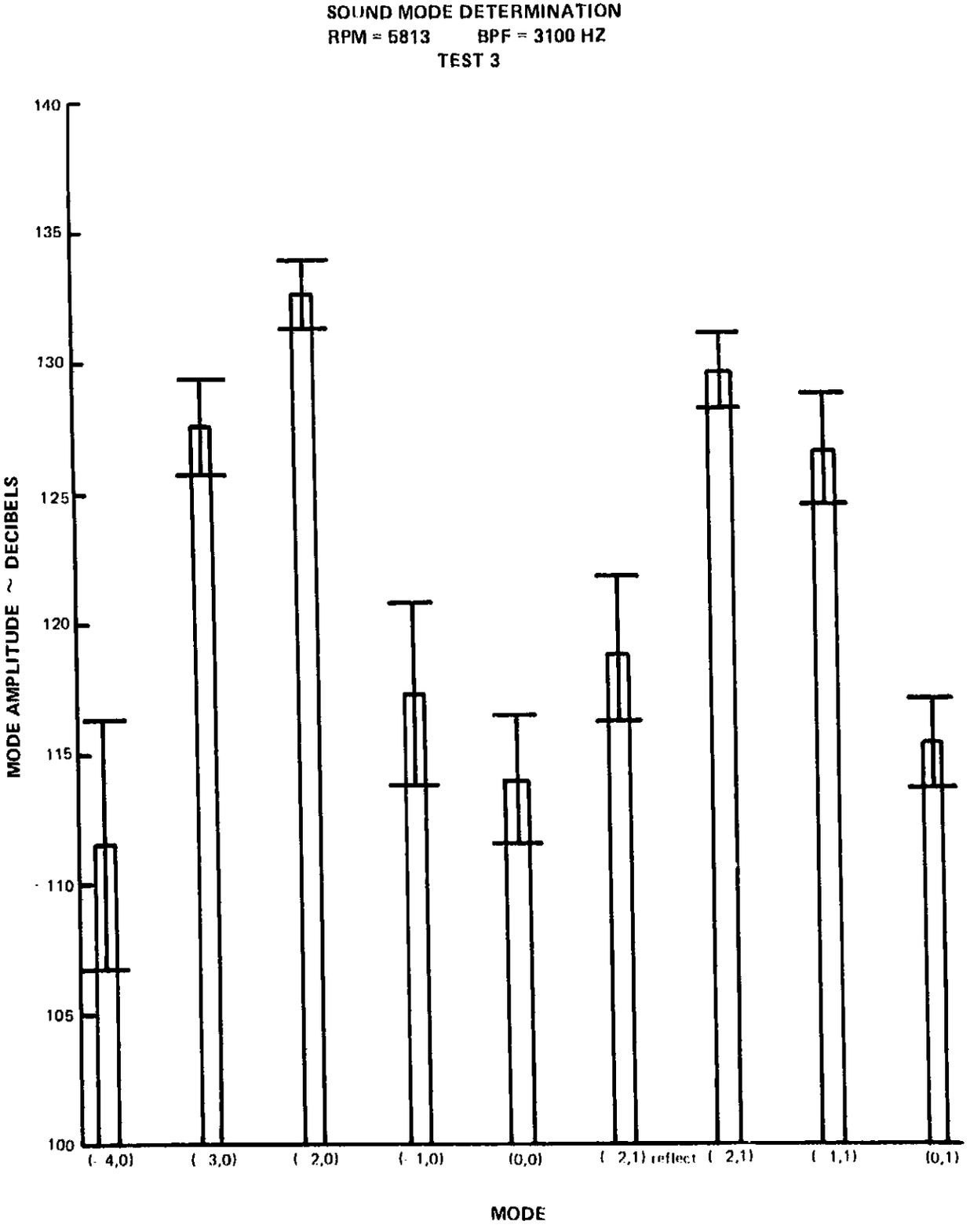

Figure 3.4-12 Sound Modal Amplitudes and Standard Deviations - Mode Structure Configuration No.3

Again, this test was repeated with check microphones at four locations different from the original ten. A comparison was made of the measured and predicted sound field based on the calculated amplitudes and phases of the nine modes at these four microphone locations and a fifth from the original test that was not used to provide data input to the MCP. This comparison is shown in Table 3.4-15 along with the standard deviations in amplitude and phase of the resultant sound field at the five microphone locations. It can be seen that the accuracy obtained using the calculated structure of nine modes is similar to that obtained using the calculated modal structure from two modes. It is possible that no improvement was obtained because one or more modes were omitted from the modal calculation that actually contribute significantly to the duct sound field.

Mode Structure Configuration No. 4

The fourth modal structure considered was that generated at 2 X BPF (6200 Hz) by the wakes from the 34 rods interacting with the rotor operating at a speed of 5813 rpm. At this frequency the fan inlet duct can support 53 propagating incident modes. From an application of the Tyler-Sofrin analysis, the (-4, 0), (-4, 1), and (-4, 2) modes are predicted to contain the bulk of the acoustic energy in the duct. For this case the MLP was used to select microphones No. 3, No. 9, and No. 10 of those listed in Table 3.4-2. Measurements were made at a total of ten microphones locations (as in previous tests), thus providing seven locations to check the accuracy of the calculated mode structure. The measured amplitudes and phases from these ten microphones are listed in Table 3.4-16.

TABLE 3.4-15

DIFFERENCE BETWEEN PREDICTED AND MEASURED DUCT ACOUSTIC PRESSURE (PREDICTED MINUS MEASURED)

CONFIGURATION NO. 3

Microphone No.	Amplitude Delta (dB)	Phase Delta (deg)
3	2.4	17.3
11	-1.7	1.7
12	1.4	11.8
13	0.2	-2.9
14	0.1	-30.2
	$\sigma_{\Delta B}$ = 1.6 dB	$\sigma_{\Delta\psi}$ = 18.4

TABLE 3.4-16
MEASURED DUCT ACOUSTIC PRESSURE
(RPM = 5813 2 X BPF = 6200 Hz)

CONFIGURATION NO. 4

Microphone No.	(dB)	Coherent Resultant Amplitude (dynes/cm^2)	(lbf/in.^{2})	Phase (deg.)
1	118.5	167.9	2.436×10^{-3}	238.8
2	117.2	144.3	2.093×10^{-3}	54.4
3	121.2	229.9	3.335×10^{-3}	329.7
4	103.3	29.31	0.4250×10^{-3}	254.0
5	118.9	175.8	2.550×10^{-3}	39.2
6	118.4	165.7	2.403×10^{-3}	80.2
7	118.4	166.8	2.419×10^{-3}	188.9
8	113.7	96.93	1.406×10^{-3}	237.0
9	116.2	129.6	1.880×10^{-3}	135.5
10	112.5	84.54	1.226×10^{-3}	252.2

The calculated amplitude and phase of the three modes predicted to be dominant and the respective standard deviations are shown in Table 3.4-17 and the amplitude components are illustrated in Figure 3.4-13. The predicted sound field, based on the calculated modal structure, at the seven check microphone locations was compared with measured amplitudes and phases and are presented in Table 3.4-18. The standard deviations are also shown of the difference between predicted and measured amplitudes and phases. It can be seen that the errors are large, 12.2 dB to -4.2 dB in amplitude resulting in a standard deviation of 3.5 dB about the mean, and between 33.6° and -32.1° in phase, resulting in a standard deviation of 25.5° about the mean.

TABLE 3.4-17
CALCULATED MODE STRUCTURE AND ERROR
(THREE MODE INPUT TO MCP)

CONFIGURATION NO. 4

Mode	Amplitude (dB)	Error (dB)	Phase (deg)	Error (deg)
(-4,0)	126.5	0.6	157.8	2.9
(-4,1)	120.8	1.2	324.9	0.8
(-4,2)	115.1	2.0	304.0	21.0

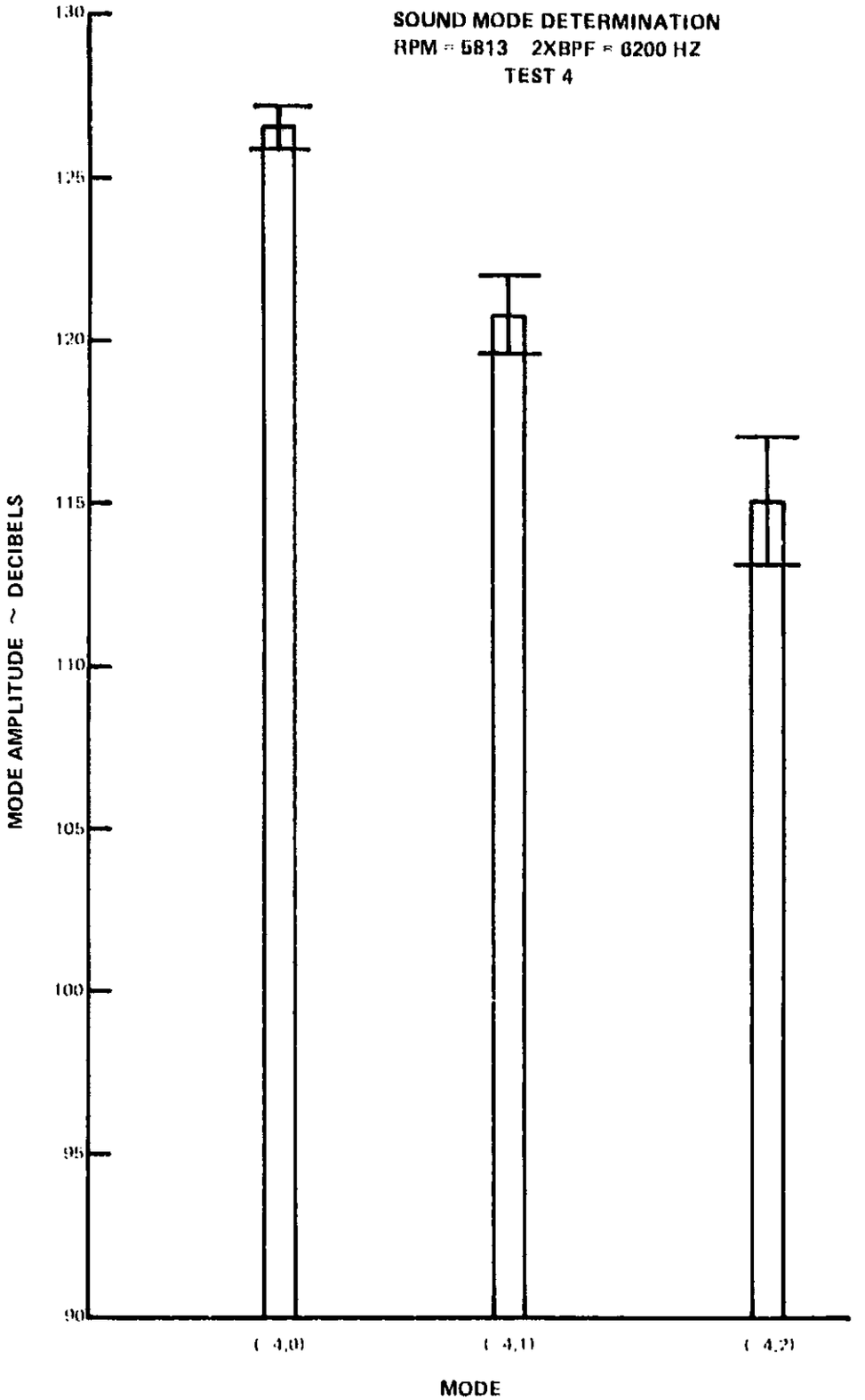

Figure 3.4-13 Sound Modal Amplitudes and Standard Deviations Mode Structure Configuration No. 4

TABLE 3.4-18

DIFFERENCE BETWEEN PREDICTED AND MEASURED

DUCT ACOUSTIC PRESSURE

(PREDICTED MINUS MEASURED)

CONFIGURATION NO. 4

Microphone No.	Amplitude Delta (dB)	Phase Delta (deg)
1	2.7	33.4
2	-3.4	33.6
4	12.2	-32.1
5	0.3	17.6
6	-4.2	-0.8
7	-3.5	16.0
8	5.6	-8.5
	$\sigma_{\Delta B} = 3.5$ dB	$\sigma_{\Delta\psi} = 25.5$

Additional predictions with more than three modes were not conducted for this case. However, it is reasonable to assume that the inaccuracies at the check microphones is due to the significant acoustic energy levels in some of the 50 modes not considered in the modal calculation.

Mode Structure Configuration No. 5

The fifth modal structure considered was that generated at BPF (1813 Hz) by the wake of a single rod interacting with the rotor operating at a speed of 3400 rpm. An acoustic spectrum at microphone location No. 10, for this configuration is shown in Figure 3.4-14. This case was included to evaluate the method for predicting all the incident propagating modes in the duct where the mode amplitudes are expected to be comparable. The propagating modes at this frequency are the same as those for configuration No. 1, and these seven microphone locations for this case are predicted by the MLP to be at the same locations as in configuration No. 1. Also, the same three check microphones were used for this case. Table 3.4-19 presents the measured amplitudes and phases at the ten microphone locations and the calculated modal amplitudes, phases and standard deviations are presented in Table 3.4-20. The mode amplitudes and amplitude standard deviations are illustrated in Figure 3.4-15. The accuracy of the method at the three check microphones is illustrated in Table 3.4-21 in the same manner as in previous cases.

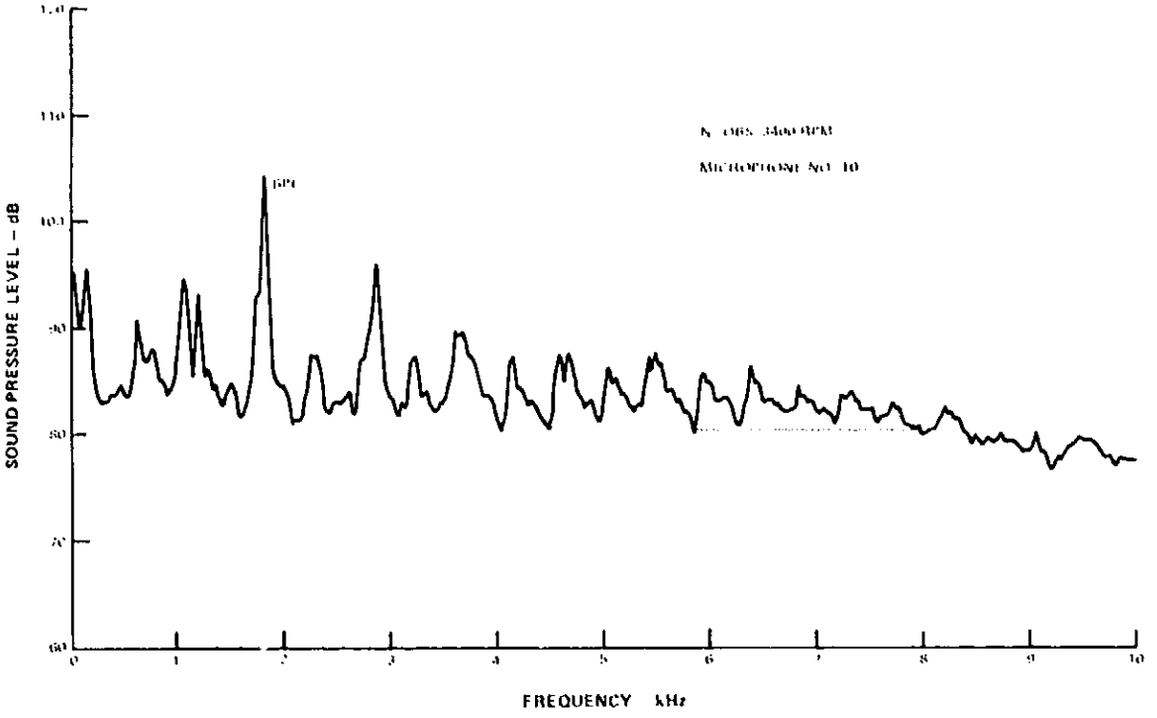

Figure 3.4-14 Overall Spectrum Generated at 3400 RPM at Microphone Location No. 10 Mode Structure Configuration No. 5

TABLE 3.4-19
MEASURED DUCT ACOUSTIC PRESSURE
(RPM = 3400 BPF = 1813 Hz)

CONFIGURATION NO. 5

Microphone No.	Coherent Resultant Amplitude (dB)	(dynes/cm^2)	(lbf/in.^{2})	Phase (deg.)
1	79.3	1.856	0.2691×10^{-4}	255.7
2	105.8	38.90	5.643×10^{-4}	220.2
3	86.7	4.288	0.6287×10^{-4}	283.8
4	102.6	26.97	3.911×10^{-4}	275.5
5	103.6	30.34	4.400×10^{-4}	77.7
6	95.6	12.12	1.757×10^{-4}	1.0
7	105.8	39.19	5.684×10^{-4}	57.4
8	98.7	17.15	2.488×10^{-4}	344.3
9	100.7	21.77	3.157×10^{-4}	350.5
10	102.9	27.98	4.057×10^{-4}	53.7

TABLE 3.4-30

CALCULATED MODE STRUCTURE AND ERROR
(SEVEN MODE INPUT TO MCP)

CONFIGURATION NO. 5

Mode	Amplitude (dB)	Error (dB)	Phase (deg)	Error (deg)
(-3,0)	105.4	0.6	25.0	3.8
(-2,0)	99.7	0.7	175.8	6.9
(-1,0)	80.9	4.9	73.3	67.0
(0,0)	85.0	3.3	113.4	25.0
(1,0)	89.7	3.0	125.6	18.5
(2,0)	87.1	4.2	211.8	32.2
(3,0)	105.5	0.5	358.7	3.1

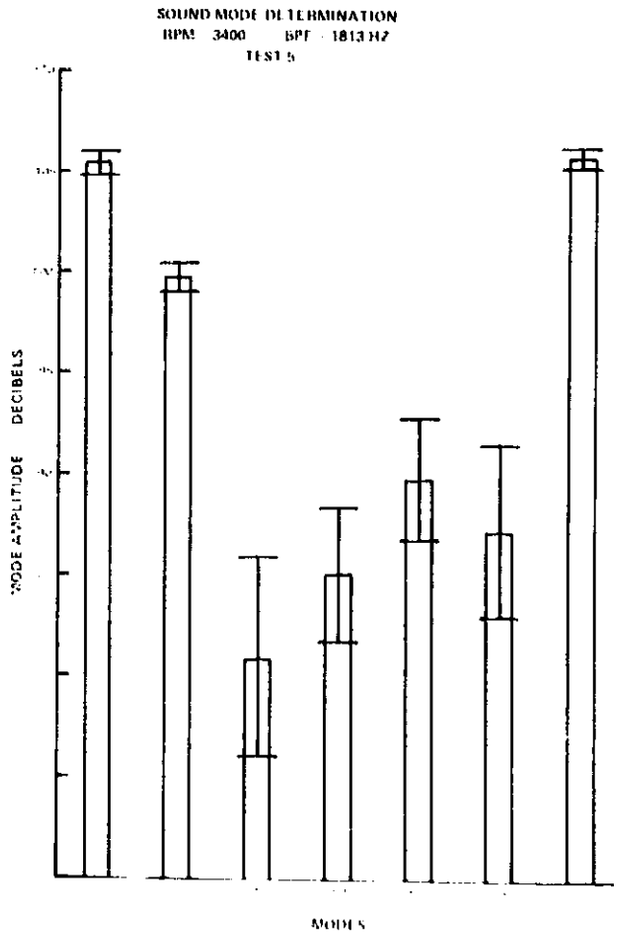

Figure 3.4-15 Sound Modal Amplitudes and Standard Deviations Mode Structure Configuration No. 5

TABLE 3.4-21

DIFFERENCE BETWEEN PREDICTED AND MEASURED

DUCT ACOUSTIC PRESSURE

(PREDICTED MINUS MEASURED)

CONFIGURATION NO. 5

Microphone (No.)	Amplitude Delta (dB)	Phase Delta (deg)
8	5.2	-22.7
9	0.1	-16.9
10	0.2	6.1

The first point to observe is that the modal structure is such that the higher sound pressure levels are in modes close to cutoff. This result is not altogether unexpected. It was shown, for example, by Pickett (ref. 16) that for rotor-turbulence interaction, the higher amplitude random modes are those close to cutoff. A similar model (used for stator-wake-rotor interaction) for a steady distortion that excites all the duct modes, shows essentially the same result.

A possible explanation for the 5.2 dB difference between the predicted and measured sound field at microphone location No. 8 is that the measured resultant amplitude at that location is the smallest of the measured amplitudes at the three check microphone locations. The reliability in predicting low resultant sound fields must itself be low as can be seen from the following argument: If the low resultant sound field amplitude is considered to be a small complex vector that is the resultant of a series of large vectors that represent each mode, then if the large complex vectors are slightly perturbated in amplitude and phase, it is not difficult to see that large percentage changes can be experienced by the small resultant vector.

In an effort to obtain a better estimate of the sound mode structure in this case, it was decided to apply the matrix inversion method to determine the amplitude and phase of the reflected modes that may have a significant portion of the acoustic energy. The reflected (-3, 0) and reflected (3, 0) modes were included in the selection due to an observation that (-3, 0) and (3,0) modes had a significant portion of the acoustic energy and with a cutoff ratio near one were expected to be reflected. Again seven modes were selected so as to group about the dominant modes near cutoff. The modes selected include: (-3, 0) reflected, (3, 0), (-2, 0), (1, 0), (2, 0), (3, 0), and (3, 0) reflected.

Acoustic pressure measurements at seven microphone locations are required for the determination of the sound field based on the above mode group. For this study, five sets of seven microphone locations were chosen from the ten available locations so that the matrix inversion method could be applied five times. This was done by running the MIP for various combinations of seven out of ten until a low conditioning number was obtained. It was found that the five sets of seven microphone locations conditioned the equation system so as to yield a conditioning number between 1.5 to 1.7.

The calculated amplitudes of the seven modes for each of the five cases are listed in Table 3.4-22. In addition, the mean and standard deviation of the amplitude for each mode were calculated and presented in this table. It can be seen that the mean amplitude of the incident modes with a cutoff ratio near unity have the highest sound pressure level. Comparison with the mode structure obtained without including reflected modes shows that the (3, 0) mode compares well to within 0.1 dB. Also, the amplitude of the (-3, 0) mode is 105.4 dB for the case that assumed reflected waves were insignificant and is within the standard deviation of the mean amplitude for the (-3, 0) mode when two reflected modes were included in the matrix inversion method. A final point is that the mean amplitude of the reflected modes is an order of 13 dB below the same incident modes that controlled a significant portion of the duct sound field. The inclusion of reflected modes in the calculation procedure did not explain the observed discrepancy between the predicted and measured sound field at the check microphones. However, in each of the five cases the accuracy at a check microphone deteriorated when the measured resultant pressure was small, and thus, reaffirmed the above explanation.

TABLE 3.4-22

CALCULATED MODE STRUCTURE
(SEVEN MODE INPUT TO MCP)

REFLECTED MODE STUDY
CONFIGURATION NO. 5

Case	Mode						
	(-3, 0) R	(-3, 0)	(-2, 0)	(1, 0)	(2, 0)	(3, 0)	(3, 0) R
1	86.5	105.8	101.3	83.6	89.3	106.4	91.3
2	85.4	105.6	101.1	83.9	89.0	106.4	90.2
3	92.7	102.0	101.8	86.7	94.0	104.9	93.2
4	94.4	107.6	101.5	88.1	93.7	104.2	93.0
5	91.2	102.9	101.9	84.5	94.5	104.9	94.6
Mean	90.7	103.8	101.5	85.5	92.4	105.4	92.6
Standard Deviation	3.1	1.8	0.3	1.8	2.2	0.9	1.6

Mode Structure Configuration No. 6

The final modal structure considered was that generated at BPF (1995 Hz) by the wake of the single rod interacting with the rotor operating at a speed of 3740 rpm. This configuration was chosen to determine the effect of a ten percent speed change on the method to determine mode structures with microphone locations chosen for the original speed and frequency. The same seven modes as in configuration No. 1 and No. 5 were generated in the duct, and at the frequency of 1995 Hz, the seven microphone locations as used in the previous configuration were found by the MIP to yield a conditioning number of 3.1. This value is comparable to those obtained where the MIP is used to select the microphone locations; so no problems in method accuracy were anticipated. Data were taken at microphones No. 1 through No. 10 and are presented in Table 3.4-23. The calculated modal amplitudes, phases, and standard deviations are presented in Table 3.4-24 and the amplitudes and amplitude standard deviations are illustrated in Figure 3.4-16. Finally, the comparison of predicted and measured sound field at the three check microphones is shown in Table 3.4-25.

TABLE 3.4-23
MEASURED DUCT ACOUSTIC PRESSURE
(RPM = 3740 BPF = 1995 Hz)

CONFIGURATION NO. 6

Microphone No.	Coherent Resultant Amplitude (dB)	(dynes/cm^2)	(lbf/in.^{2})	Phase (deg.)
1	91.8	7.769	1.127×10^{-4}	49.3
2	95.7	12.24	1.776×10^{-4}	2.3
3	85.9	3.940	0.5715×10^{-4}	357.7
4	104.2	32.48	4.711×10^{-4}	42.4
5	100.4	20.92	3.034×10^{-4}	167.4
6	100.4	20.89	3.030×10^{-4}	23.0
7	103.3	29.32	4.253×10^{-4}	172.5
8	102.7	27.34	3.965×10^{-4}	27.0
9	91.7	7.707	1.118×10^{-4}	358.3
10	94.4	10.53	1.527×10^{-4}	107.0

TABLE 3.4-24
CALCULATED MODE STRUCTURE AND ERROR

CONFIGURATION NO. 6

Mode	Amplitude (dB)	Error (dB)	Phase (deg)	Error (deg)
(-3,0)	103.2	0.8	36.8	4.0
(-2,0)	101.6	0.8	209.2	3.0
(-1,0)	97.1	1.0	357.0	7.3
(0,0)	91.1	1.5	177.8	15.6
(1,0)	94.7	1.5	175.9	15.7
(2,0)	99.7	1.3	180.3	8.0
(3,0)	97.3	1.6	49.5	7.0

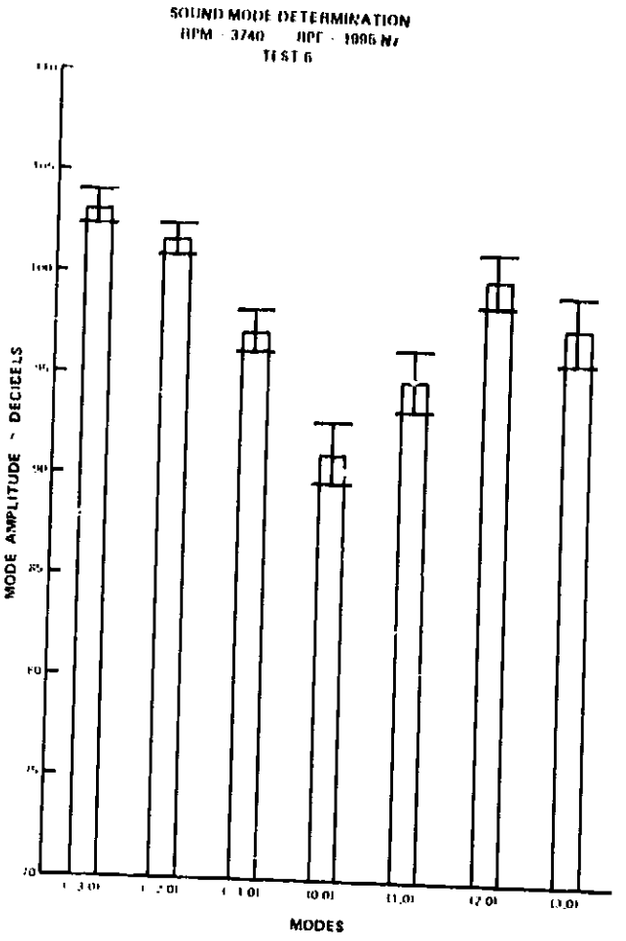

Figure 3.4-16 Sound Modal Amplitudes and Standard Deviations - Mode Structure Configuration No. 6 –

TABLE 3.4-25
DIFFERENCE BETWEEN PREDICTED AND MEASURED
DUCT ACOUSTIC PRESSURE
(PREDICTED MINUS MEASURED)

CONFIGURATION NO. 6

Microphone No.	Amplitude Delta (dB)	Phase Delta (deg)
8	-1.0	8.0
9	-5.4	15.1
10	-0.2	- 3.3

Results for this case are similar to those observed in configuration No. 5, although it can be seen from Tables 3.4-19 and 3.4-23 that the ten percent rotor speed difference between tests resulted in significant changes in measured amplitudes and phases at the 10 microphone locations. Again it is difficult to assess the accuracy of the method for this case, but it can be seen to be no worse than for configuration No. 5, despite the speed change. Again, a possible explanation for the 5.4 dB difference between the predicted and measured sound field at microphone location No. 9 is that the measured resultant amplitude at that location is the smallest of the measured amplitudes at the three check microphone locations.

3.4.7 Summary of Test Results and Assessment of Impact of Extraneous Modes on Method Accuracy

In the previous section, it was shown how the modal calculation method was applied to six different fan duct modal structures. In the first case, all incident propagating modes that could be supported by the duct were included in the modal calculation. In subsequent cases a subset of the total number of modes that could be supported by the duct was selected as predicted by the Tyler-Sofrin theory and was assumed to contain the bulk of the propagating acoustic energy. In the second and third cases considered, this subset was enlarged to include nine propagating duct modes in an effort to improve the accuracy of the results. The amplitudes and phases of the selected number of modes were calculated using as input the measured sound field at an equal number of microphones in the duct as modes to be calculated. The calculated modal structures were then used to predict the amplitude and phase of the sound field at other duct locations where measurements were also made.

For the first test case where the structure of all seven incident modes was calculated and for the additional test of the second case where the structure of nine modes was calculated, it was seen that the resultant sound field was predicted within +1.7 dB and -0.8 dB for case one and within -0.5 dB and -1.9 dB for case two. An alternate separate check could be provided in each of these two cases, since the amplitude and phase of the single dominant mode could be calculated accurately based on an average of all the in-duct microphone measurements. A comparison of the calculated amplitude and phase of the dominant mode using the modal calculation method with that obtained from an average of all the microphones, showed much better agreement. For this method of comparison, agreement was within 0.2 dB in amplitude and 1.2° in phase for case one and within 0.6 dB in amplitude and 10.5° in phase for case two. Although the phase is somewhat off in case two, it is apparent that for the first two cases, the amplitude and phase of the dominant mode was calculated quite accurately using the modal calculation method. Since the prediction of the resultant sound field based on the calculated modal structure, however, is seen to differ from the measured sound field by almost two dB, it can be seen that using the calculated mode structure to predict the total sound field at other duct measurement locations is a stringent test of the modal calculation method.

In case two, the amplitude and phase of the dominant mode was accurately determined despite, in the first attempt, the presence of 19 extraneous modes not included in the modal calculation and in the second attempt, 11 extraneous modes. In the third test case considered, the amplitude and phase of two modes, (-2,0) and (-2,1), were calculated and fourteen extraneous modes were present. For this case the total sound field at other duct locations was predicted within three dB, with a standard deviation of 1.5 dB. When the number of

modes included in the calculation was increased to nine, so that only seven extraneous modes were present, the accuracy in predicting the sound field at other duct locations was essentially unchanged. The calculated amplitude of the (-2,0) mode was 132.5 dB for the two mode calculation and 134.1 dB for the nine mode calculation, and the amplitude of the (-2,1) mode was 128.8 dB for the two mode calculation and 129.4 dB for the nine mode calculation. The differences between the two and nine mode calculations are fairly small (within a standard deviation as obtained from the nine mode calculation), indicating that either calculation could be used to determine the structure of the (-2,0) and (-2,1) modes with reasonable accuracy.

For the fourth test case, where the structure of three modes was determined, the amplitude of the total sound field at other duct locations based on the calculated mode structure, was predicted to be as much as 12.2 dB different from that measured, with a standard deviation of 3.5 dB. The significant difference between test case four and the other three cases was that in test case four, the number of extraneous modes supportable by the duct, but not included in the modal calculation was much greater than in the other three cases. In test case four, fifty incident extraneous modes could propagate in the duct in addition to the three used in the modal calculation method based on an application of the Tyler-Sofrin analysis to the fan design. Clearly the impact of these extraneous modes greatly affected not only the calculation of the structure of the three modes, but also the prediction accuracy of the total sound field at other duct locations.

The accuracy of the method when applied to test cases five and six is more difficult to determine. In these test cases, a single rod was placed upstream of the rotor with the purpose of generating seven comparable incident modes at two slightly different frequencies. Modes with a cutoff ratio near unity were expected to contain higher sound pressure levels than the other incident modes. It was shown by Pickett (ref. 16) that for rotor-turbulence interaction, the higher amplitude modes are those close to cutoff. A similar model (used for stator-wake rotor interaction) for a steady distortion that excites all the duct modes shows essentially the same result. For the frequencies considered, the duct was able to support 7 modes, so there were no extraneous modes for these cases. The calculated mode structures were used to predict the sound fields at three other measurement locations. It was found that in both cases, two out of the three predictions were reasonably accurate, but the third prediction was on the order of 5 dB different from the measured level. Because of the widely differing results from only three check locations, it is not possible to make a definitive statement on the method accuracy for these two cases. As explained in the last section, however, a possible reason for the large difference at a single location for each case, is that at those locations, the amplitude of the total measured sound field was smaller than for the other two check microphone locations. When the resultant amplitude at any duct location is small but caused by the confluence of seven modes, as in this case, and when the amplitudes of these modes are comparable, inaccuracies can be expected in predicting the total sound field at those duct locations based on the calculated mode structure. This is suggested as a possible explanation of the poor agreement between measured and calculated levels at the third microphone location.

In order to explore further the effect on the method accuracy of extraneous modes, an order-of-magnitude analysis will now be considered. The contribution of extraneous modes to the amplitude and phase of the resultant sound field at any duct location can be considered equivalent to a measurement system error. The magnitude of this error at any location is the resultant of all the extraneous modes at that location. The order-of-magnitude estimate of the variance of the resultant of the extraneous modes is obtained by assuming that the number of extraneous modes is large and invoking a statistical argument. If the total number of modes propagating in the duct is N_T and the number of modes used in the modal calculation is N, then the number of extraneous modes is $(N_T - N)$. Since the mean amplitude of each extraneous mode as measured at the various duct measurement locations is $A_{I;M}E_M$ and if $(N_T - N) >> 1$, it is shown in Appendix E that so long as the phases of the extraneous modes are considered to be uniformly distributed in $[0, 2\pi]$, the variance of the resultant of all the extraneous modes is $(A_{I;M}E_M)^2 (N_T - N)$, where the average is taken over all the extraneous modes. Thus, it can be seen from this analysis that the expected resultant amplitude of the extraneous modes at any duct location increases significantly as the amplitudes and number of extraneous modes increases.

In summary then, the modal calculation method presented in this report can be expected to be accurate only for test cases where either the amplitudes of the extraneous modes are much less than those being calculated, or the number of extraneous modes is small, which is equivalent to selecting the number of microphones used to obtain data during the test to be comparable to the total number of modes propagating in the duct.

In the next section the experimental requirements are determined for the application of the modal calculation method to specific applications. An approximate procedure for defining these experimental requirements is described and is applied to an example of a fan design that has been run on the NASA 1/2-meter (20-in.) Fan Rig. The general utility of the method also is discussed.

3.5 EXPERIMENTAL REQUIREMENTS FOR APPLICATION OF METHOD

3.5.1 Overview

In order to apply the methods developed it is desirable to have, a priori, a procedure which for a given problem and desired calculation accuracy, would provide a guide to the number of microphones and measurement accuracy required. Such a procedure should be simple to apply and should not require input from either the MCP or MLP. To develop such a procedure, approximate expressions based on an order-of-magnitude analysis for the MCP influence coefficients were derived. These approximate expressions were used to generate a set of parametric curves from which an estimate can be obtained of the required measurement accuracies that will yield a desired calculated modal amplitude and phase accuracy. Additionally, an approximate expression was derived that relates modal amplitude and phase errors to the number of extraneous modes [i.e., the difference between the total number of modes that can propagate in a duct at a given frequency minus the number of modes (i.e., microphone inputs) used in the modal calculation].

The derivation of these expressions and the use of these expressions in the development of the procedure to define experimental requirements are described in the following sections.

The objective of this part of the program is summarized as follows:

To develop a procedure that can be used to provide:

1) an estimate of the number of microphones required to calculate coherent fan modal structure to within a specified accuracy for a specific application.

2) an estimate of the experimental accuracy required to ensure that calculated modal amplitudes and phases are within a specified accuracy for a specific application.

3.5.2 Analysis For Influence Coefficients

Objective

To derive a set of order-of-magnitude expressions for the influence coefficients, equation (3.2-18) and to check them against those values obtained from the analytical and experimental test cases described in sections 3.2 and 3.4, respectively.

Analysis

In section 3.2.4 and Appendix B, closed form expressions were derived for a set of influence coefficients that are used to determine the first-order errors in calculated mode amplitude and phase due to errors in the knowledge of microphone location and errors in acoustic pressure measurements. It is shown in Appendix D that by assuming: 1) the number of modes, N, being determined is large (i.e., $N \gg 1$) and 2) the large set of deterministic phase angles associated with the complex matrix elements of the modal calculation algorithm can be formally replaced by a set of statistically independent and random phase angles uniformly distributed in $[0, 2\pi]$, then order-of-magnitude expressions for the variances ($\sigma^2_{\tilde{A}_M}$ and $\sigma^2_{\tilde{\phi}_M}$) of the calculated modal amplitudes (A_M) and phases (ϕ_M) can be derived in terms of the variances in measured acoustic pressure amplitudes and phases ($\sigma^2_{\tilde{B}}, \sigma^2_{\tilde{\psi}}$), and the variances in locating microphones in the duct ($\sigma^2_{\tilde{X}}, \sigma^2_{\tilde{r}}, \sigma^2_{\tilde{\theta}}$).

The assumptions used in the analysis would seem intuitively reasonable so long as the number of modes being calculated is large, but the justification required a comparison with experience, which will be considered presently.

Using Appendix D, we can write for the expected values of the variances of A_M and ϕ_M:

$$\frac{E_X\left\{\sigma^2_{A_M}\right\}}{A^2_M} \quad E_X\left\{\sigma^2_{\phi_M}\right\} \quad \frac{G(\sigma^2_B, \sigma^2_\psi, \sigma^2_X, \sigma^2_\theta, \sigma^2_r)}{A^2_M \; I^2_M} \qquad (3.5\text{-}1)$$

where $G(\sigma^2_B, \sigma^2_\psi, \sigma^2_X, \sigma^2_\theta, \sigma^2_r) = \sigma^2_B + B^2_n \sigma^2_\psi + \sum_{s=1}^{N} \left\{A^2_s F^2_s (k^2_{X_s} \sigma^2_X + m^2_s \sigma^2_\theta + k^2_{rs} \sigma^2_r)\right\}$,

$B^2_n \quad \frac{1}{N} \sum_{n=1}^{N} B^2_n$ and s_{ns} is defined in equation (B15), and the remaining notation is defined in Appendix A

To determine how well the expressions of equation (3.5-1) represent calculated values, these expressions were evaluated by comparing the predictions from equation (3.5-1) with calculations of modal amplitude and phase standard deviations based on the influence coefficients. These comparisons were made using the ten analytical test cases used in Section 3.2 to check out the computer programs and an equal number of experimental cases from the test program presented in section 3.4. Considering first only acoustic pressure amplitude measurement errors, equation (3.5-1) can be written as:

$$\frac{E_x\left\{\sigma_{A_m}^2\right\}}{A_m^2} \quad \frac{\bar{B}_n^2}{\sigma_B^2} \quad \frac{1}{2}\left[\frac{A_m^2 F_m^2}{\bar{B}_n^2}\right]^{-1} \tag{3.5-2}$$

where $\bar{B}_n$ is the root mean square amplitude of the resultant sound field at the measurement locations, and $A_m F_m$ is the amplitude at the duct wall due to the mth mode.

Using the calculated influence coefficients from the 10 analytical and 10 experimental test cases, values $\sigma_{A_m}^2/A_m^2 \times \bar{B}_n^2/\sigma_B^2$ were obtained for each mode in each case. As shown in Figure 3.5-1, these values were plotted on a graph as a function of $A_m^2 F_m^2/\bar{B}_n^2$, which is a ratio of the amplitude at the duct wall due to the mth mode and the mean amplitude of the resultant sound field at the measurement locations. Superposed on this plot is the equation given by (3.5-2). It can be seen for this case that the analysis predicts the proper order-of-magnitude, since most of the data falls within an order-of-magnitude of the line given by equation (3.5-2). Comparisons for phase measurement errors and microphone location errors show similar results. Figure 3.5-2 shows the comparison of approximate and exact values for the ratio of variances of calculated modal phase and measured phase. For this case, equation (3.5-1) for the phase variance based on the order-of-magnitude analysis reduces to:

$$\frac{E_x\left\{\sigma_{\phi_m}^2\right\}}{\sigma_\psi^2} \quad \frac{1}{2}\left[\frac{A_m^2 F_m^2}{\bar{B}_n^2}\right]^{-1} \tag{3.5-3}$$

The use of equations 3.5-1 in the development of the expressions for errors due to extraneous modes and expressions for the definition of measurement accuracy is described in sections 3.5.3 and 3.5.4, respectively.

3.5.3 Approximate Analysis For Errors Due to Extraneous Modes

To obtain an order of-magnitude expression for determining the errors in calculated modal amplitude and phase attributable to the presence of extraneous modes, use will be made of the approximate expressions for the influence coefficients, equation (3.5-1) and the analysis for the expected contribution to the total sound field of the extraneous modes presented in

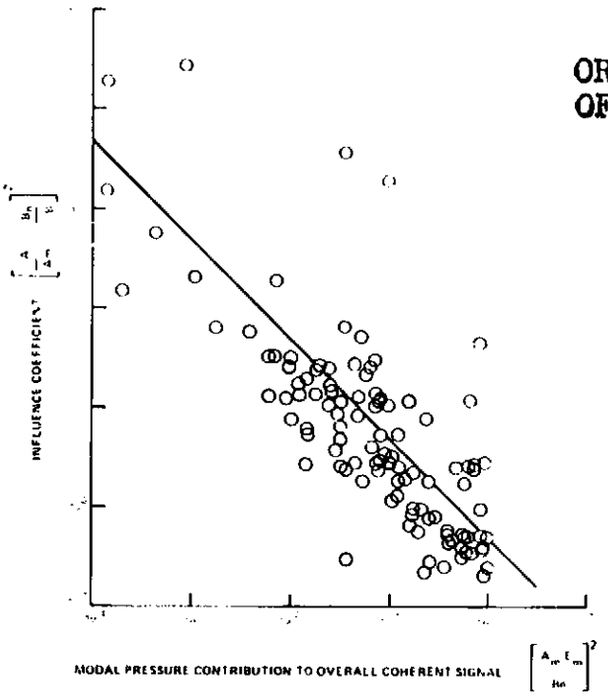

Figure 3.5-1 Comparison Between Calculated and Order of Magnitude Analysis of Influence Coefficient

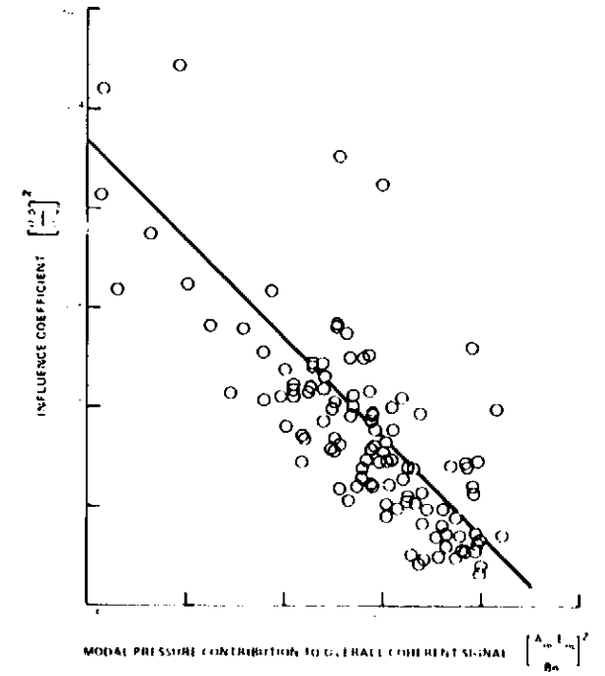

Figure 3.5-2 Comparison Between Calculated and Order of Magnitude Analysis of Influence Coefficient

Appendix F. The analysis in Appendix F shows that the variance of the resultant amplitude of the extraneous modes is proportional to the mean square amplitude of the extraneous modes times the number of extraneous modes. That is:

$$\sigma_B^2 = \left\{ \overline{F_m^2 A_{Fm}^2} \right\} (N_T - N) \qquad (3.5\text{-}4)$$

where N_T is the total number of modes supportable by the duct, N is the number of modes assumed to contain the bulk of the acoustic energy, and $\left\{ \overline{F_m^2 A_{Fm}^2} \right\}^{1/2}$ is the rms value of the extraneous modes at the measurement locations.

Now, the resultant amplitude of the extraneous modes can be considered to be equivalent to an error in acoustic measurement. Thus, assuming a perfect measuring system, the variance of the pressure measurement, σ_B^2, in the sensitivity analysis (equation 3.5-2) can be considered to be a pressure measurement error caused by the number of extraneous modes. Substituting into equation (3.5-2) yields equation (3.5-5)

$$\frac{E_x \{ \sigma_{A_m}^2 \}}{A_M^2} = \frac{1}{2} \frac{\overline{A_{EM}^2 E_M^2}}{A_m^2 E_m^2} (N_T - N) \qquad (3.5\text{-}5)$$

In equation (3.5-5), $\dfrac{F_m^2 A_m^2}{F_m^2 A_{Fm}^2}$ can be considered to be the square of the signal to noise ratio, since $F_m A_m$ is the acoustic amplitude at the measurement location attributable to the modes that are due to be calculated (and which are assumed to contain the bulk of the acoustic energy) and $\sqrt{\overline{F_m^2 A_{FM}^2}}$ is the overall contribution due to the extraneous modes.

Experience gained from the experimental portion of the program demonstrates that the method accuracy deteriorates as the number of extraneous modes increases, providing qualitative substantiation of equation (3.5-5). The expected error of the calculated mode amplitude in decibels can be obtained from

$$\Delta\, dB\Big|_{A_M} = 20 \log_{10} \left[1 + \frac{E_x \{ \sigma_{A_m} \}}{A_m} \right]$$

whereupon, using equation (3.5-5),

$$\Delta\, dB\Big|_{A_M} = 20 \log_{10} \left[1 + \frac{1}{\sqrt{2}} \frac{\sqrt{A_{EM}^2 E_M^2}}{A_M E_M} \sqrt{N_T - N} \right] \qquad (3.5\text{-}6)$$

In Figure 3.5-3, ΔdB_{Am}, which can be considered to be the order-of-magnitude error in the calculation of the amplitude of the Mth mode, is plotted against the number of extraneous modes (N_T-N) for a range of signal to noise ratios $\frac{F_m A_m}{\sqrt{F_m^2 A_{Fm}^2}}$.

Following a similar type of analysis, the order of magnitude error in the calculated phase of the Mth mode can be determined. That result also is plotted in Figure 3.5-3.

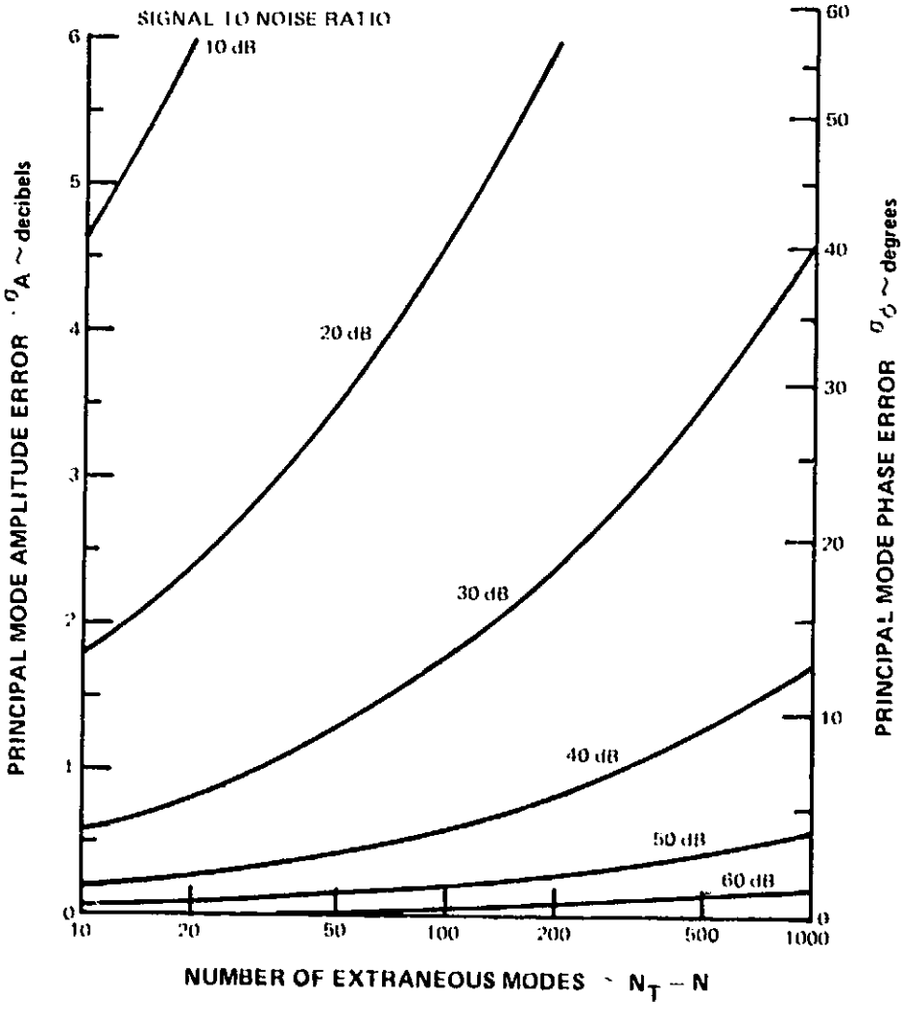

Figure 3.5-3 Assessment of Method Utility

3.5.4 Approximate Analysis for Definition of Required Measurement Accuracy

The order-of-magnitude estimates of the influence coefficients can also be used to determine the experimental accuracy requirements to ensure results within a specified error range for a specific application. The required acoustic pressure measurement accuracy will be considered first. Assuming only acoustic pressure amplitude measurement errors, equation (3.5-1) becomes:

$$\frac{E_x\{\sigma_{A_m}^2\}}{A_m^2} = \frac{1}{2}\frac{\sigma_B^2}{A_m^2 E_m^2}$$

The expected error in modal amplitude, expressed in decibels, can be shown in a similar manner to that presented in equation (3.5-6) to be:

$$\Delta dB|_{A_m} = 20\,Log_{10}\left[1 + \sqrt{\frac{1}{2}\frac{\sigma_B^2}{A_m^2 E_m^2}}\right] \qquad (3.5\text{-}7)$$

In anticipation of developing a procedure for estimating the instrumentation requirements, a desired accuracy (or maximum error) for the calculated modal amplitude (and possible phase) will be assumed given. This same error will be used to estimate the number of allowable extraneous modes (or, by application of Figure 3.5-3, the number of microphones required), the allowable error in pressure amplitude and phase measurement, and the allowable error in microphone location. The interpretation of these allowable errors is discussed in section 3.5.5.

Proceeding we can combine equations (3.5-6) and (3.5-7) to give:

$$\frac{\overline{E_{mi}^2 A_{i\,m}^2}}{L_{mn}^2 A_{mi}^2}\left(N_i - N\right) = \frac{\sigma_B^2}{\overline{B_{mi}^2}}\frac{\overline{B_m^2}}{A_{mn}^2 E_{mn}^2} \qquad (3.5\text{-}8)$$

Since N_I and N have already been assumed large, it will be further assumed that the mean-square amplitude of the measured pressure, $\overline{B_{mi}^2}$, is of the same order-of-magnitude as the sum of the expected mean square resultant due only to the extraneous modes and the expected mean-square resultant due only to those modes being calculated. That is:

$$\overline{B_{mi}^2} \approx N\,\overline{A_{mi}^2 L_{mn}^2} + (N_i - N)\,\overline{A_{mn}^2 E_{mn}^2} \qquad (3.5\text{-}9)$$

Clearly, this approximation will be reasonable if the contribution from the extraneous mode is much smaller than the contribution from the modes being used in the modal calculation.

This approximation will deteriorate however, if the two contributions are comparable. Substituting equation (3.5-9) in equation (3.5-8) yields an equation from which a set of parametric curves can be obtained demonstrating, for a range of signal-to-noise ratios (i.e., ratio of the amplitude of dominant modes to the rms acoustic amplitudes of extraneous mode), when extraneous mode contributions and pressure measurement errors cause an equal error in the calculated mode amplitude. This set of parametric curves is shown in Figure 3.5-4. Also, it will be seen that, following a similar analysis, the same curves can be used to relate extraneous modes and measured phase errors in the same manner. Thus, by way of example, if the contributions from the average of the extraneous modes are about 30 dB down from the dominant modes, and if the ratio $(N_T - N)/N$ takes the value 50, the error introduced in the calculation of the mode amplitudes will be equivalent either to a 1.7 dB error in amplitude measurement or a 13° error in phase measurement by the microphone system.

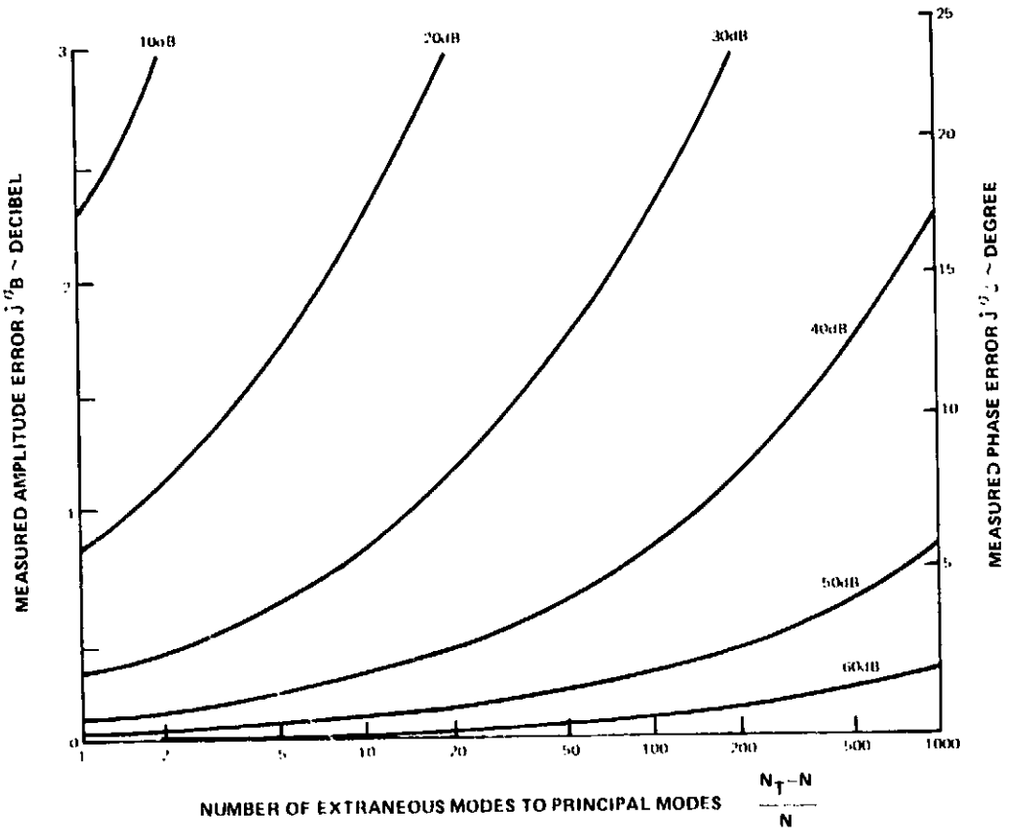

Figure 3.5-4 Accuracy Requirements of Pressure Measurements

Using a similar analysis, a set of parametric curves can be generated that demonstrate, for a given signal to noise ratio, when extraneous mode contributions and axial and circumferential microphone location errors cause an equal error in the calculated mode amplitude and phase. The analysis for relating axial location errors with the number of extraneous modes is as follows: Assuming perfect measurement and errors only in axial location, equation (3.5-1) becomes for the error in calculated modal amplitude

$$\frac{E_x\{\tau_{A_{mn}}^2\}}{A_{mn}^2} = \frac{1}{2}\frac{\tau_x^2}{A_{mn}^2 l_{mn}^2}\sum_{s=1}^{N} k_{x_s}^2 A_s^2 E_s^2$$

$$\text{or} \quad \frac{E_x\{\tau_{A_{mn}}^2\}}{A_{mn}^2} = \frac{1}{2}\cdot\frac{N\tau_x^2}{A_{mn}^2 E_{mn}^2}\,\overline{k_{x_s}^2 A_s^2 E_s^2} \tag{3.5-10}$$

$$\text{where} \quad \overline{k_{x_s}^2 A_s^2 E_s^2} = \frac{1}{N}\sum_{s=1}^{N}\overline{k_{x_s}^2 A_s^2 E_s^2}$$

If $E_x(\tau_{A_m}^2)$ is eliminated from equations (3.5-5) and (3.5-10) a relation is obtained between the error in axial microphone location and the number of extraneous modes that give the same error in calculated modal amplitude. Thus,

$$E_{mn}^2 A_{mn}^2 (A_T - 1) = N\tau_x^2 \overline{k_{x_s}^2 A_s^2 E_s^2} \tag{3.5-11}$$

In order to pursue the order-of magnitude analysis, it will be assumed that k_{x_s} and $A_s E_s$ are statistically independent. Then

$$\overline{k_{x_s}^2 A_s^2 E_s^2} = \overline{k_{x_s}^2}\cdot\overline{A_s^2 E_s^2}$$

whereupon,

$$\tau_x^2\,\overline{k_{x_s}^2} = \frac{A_T - 1}{N}\cdot\frac{E_{mn}^2 A_{mn}^2}{E_s^2 A_s^2} \tag{3.5-12}$$

For a range of signal to noise ratios $\left(E_s^2 A_s^2/E_{mn}^2 A_{mn}^2\right)$, equation (3.5-12) is used to obtain Figure 3.5-5 which is a plot of the normalized axial location error versus the ratio of extraneous modes to calculated modes. Superposed on the same figure are the circumferential location errors versus the ratio of extraneous modes to calculated modes that was obtained by a similar analysis.

Figure 3.5-5 can thus be used to show, for a range of signal to noise ratios, when extraneous mode contributions and axial and circumferential microphone location errors give rise to an equal error in the calculated mode amplitude. A similar relationship for errors in radial microphone location is not readily obtained because the appropriate influence coefficients contain radial derivatives of Bessel functions. Based on experience from this program, however, the errors introduced into the modal calculation by radial microphone location errors are always much smaller than those due to the other measurement and location errors considered here.

It is now possible using Figures 3.5-3, 3.5-4, and 3.5-5 to demonstrate a procedure for estimating the experimental accuracy that would be required in applying the method for determining coherent fan sound mode structure.

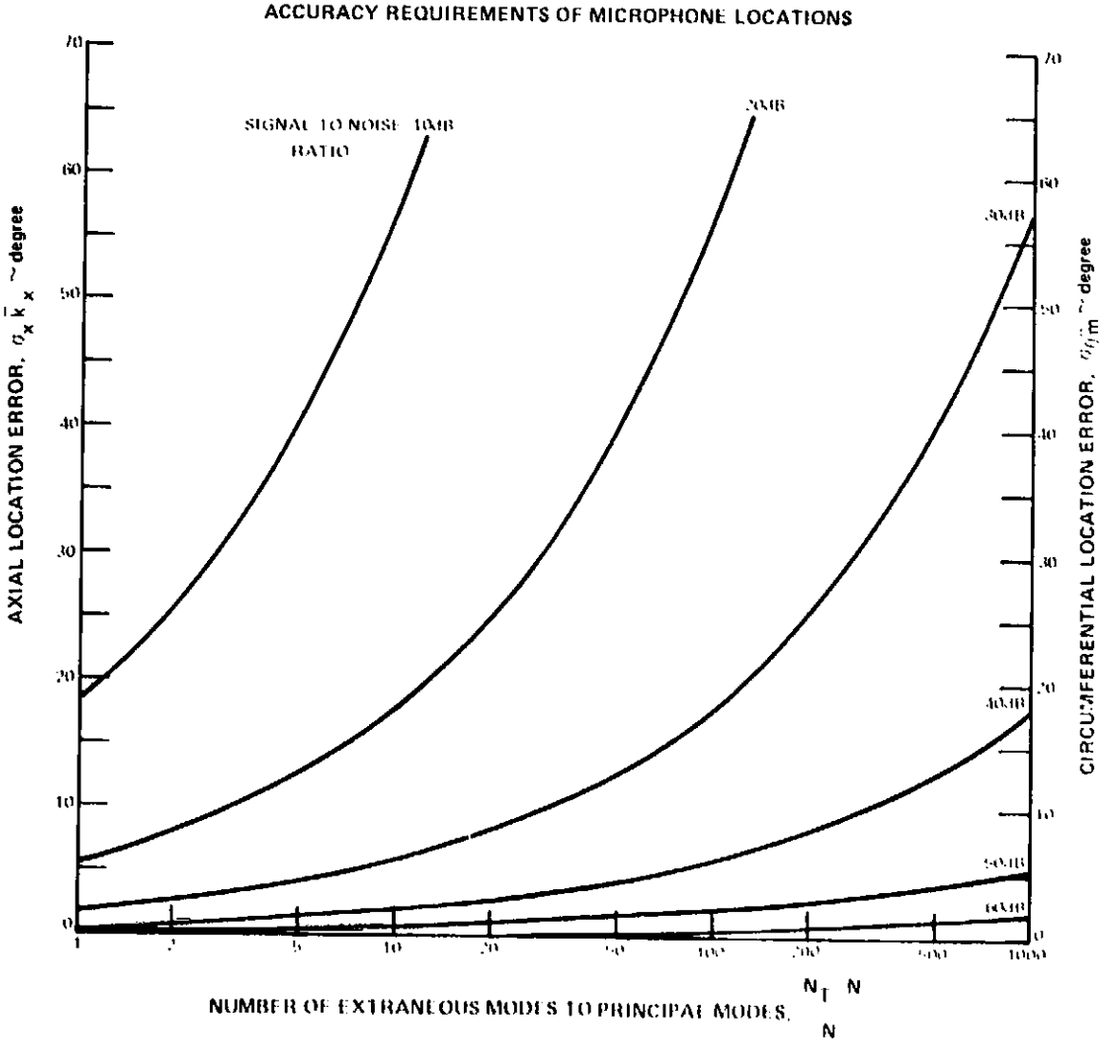

Figure 3.5-5 Accuracy Requirements of Microphone Location Measurements

3.5.5 Description of Procedures for Defining Experimental Requirements

Since Figures 3.5-3, -4 and -5 were based on order of magnitude analysis, they can at best be used as an approximate guide in selecting numbers of microphones and measurement and position accuracies. In lieu of any prior experience, the procedure to be described can be used as a guide in defining the instrumentation requirements. Once a test has been completed and the MCP has been used to calculate modal amplitudes and phases, the influence coefficients (that are also calculated by the MCP), can be used to quantify more accurately the errors in calculated modal amplitudes.

The procedure to be described shortly consists of 5 steps. First a value of the desired accuracy, or maximum error, in the calculated modal structure is selected. The second step provides an estimate of the total number of microphones required to provide the desired calculated modal amplitude and phase accuracy, assuming there are no measurement or position errors. The third step provides an estimate of the allowable error in measured amplitude and phase, consistent with the requirements of step one, assuming all microphones are perfectly located and there are no extraneous modes. Step 4 provides an estimate of the allowable error in the microphone positions, consistent with the requirements of step 1, assuming that there are no extraneous modes or instrumentation measurement errors. In step 5, the allowable errors in measured pressure amplitude and phase are compared with the estimated instrumentation system measurement errors that would be expected in conducting the test. Similarly, the allowable position errors calculated in step 4 are compared with the actual position errors that would be expected in locating the microphones for the test. If the actual errors are an order or magnitude (or more) less than the allowable errors, then the accuracy selected in step 1 can probably be achieved by use of the number of microphones defined in step 2. If on the other hand, the actual errors are comparable to the allowable errors that yield calculation errors of the modal coefficients on the order of that specified in step 1, then these calculation errors will accumulate from each source, and the total error in the calculated modal amplitude and phase will be larger than that specified in step 1. In this eventuality, an assessment of the modal calculation accuracy can be obtained only after the test has been conducted.

In the following, the above steps are outlined:

Step 1: Select desired accuracy for modal amplitude and phase calculations, in dB and degrees.

Step 2: For a given duct geometry and sound frequency, the total number of modes supportable by the duct can be calculated. For the particular accuracy in calculating the dominant mode specified in Step 1, the number of allowable extraneous modes can be determined from Figure 3.5-3 as a function of signal-to-noise ratio* (defined as the ratio of the amplitude of the principle modes as measured at the duct wall to the mean amplitude of the extraneous modes as measured at the duct wall). Thus, the number of allowable extraneous modes to achieve the desired accuracy in the modal calculation can be determined, from which the number of microphone measurements that need to be made also can be determined by subtracting the number of allowable extraneous modes from the total numbers of modes supportable by the duct.

*Based on experience or a conservative "best guess", a value for the signal to noise ratio must be estimated

Step 3: The allowable pressure measurement accuracy is determined as follows.

From the known ratio of the number of extraneous modes to the number of modes to be used in the modal calculation, $(N_T - N)/N$ and the estimated signal to noise ratio, the order-of-magnitude allowable error in measured acoustic amplitude and phase, consistent with the requirements of step 1 can be determined from Figure 3.5-4.

Step 4: The allowable microphone location accuracy is determined as follows:

From step 2 the number of microphone measurements required is known. A set of modes must next be identified, which will be input to the MCP. The modes selected should be those that are considered to contain the bulk of the propagating acoustic energy. It is therefore suggested that the particular modes chosen be based on an application of the Tyler-Sofrin analysis to the fan design together with the experience presented in Section 3.4.4 for enlarging beyond this number, to achieve the set of modes required for the calculation. From this set of modes and for the specified frequency, the average values of the axial wave number $\bar{k}_{xs}$ and the circumferential mode number $\bar{m}$ can be calculated or estimated. From the estimated signal to noise ratio and the known ratio $(N_T-N)/N$, Figure 3.5-5 can be used to determine the standard deviations of the allowable error in axial and circumferential location (σ_x and σ_θ) that would give rise to errors in the calculated modal structure, comparable to the accuracy selected in step 1.

Step 5: In the final step of the procedure, the allowable errors calculated in steps 2 through 4 should be evaluated. First the allowable errors in measured pressure amplitude and phase are compared with the instrumentation system measurement errors. Similarly, the allowable position errors, calculated in Step 4, are compared to the actual position errors. If the actual errors in all cases are an order of magnitude (or more) less than the allowable errors, then the accuracy selected in step 1 can probably be achieved by use of the number of microphones determined in step 2. If on the other hand, the actual errors are comparable to the allowable errors that yield calculated errors in the modal coefficients on the order of that specified in step 1, then these calculated errors will accumulate from each source (extraneous modes, pressure amplitude and phase measurement errors and position errors) and the total error in modal amplitude and phase will be larger than that specified in step 1. In this eventuality, this simple method underestimates the actual error and the influence coefficients are required and an assessment of the modal calculation accuracy will be obtained only after the test has been conducted.

In applying the procedure presented here, it should be remembered that Figures 3.5-3, 3.5-4 and 3.5-5 were obtained from order of-magnitude expressions of the influence coefficients of (3.2-18). Thus, care should be exercised in interpreting the particular values presented in these figures. This procedure can only be considered as a guide to the user. The actual sensitivity of the method as applied to specific applications can be determined best after the test has been conducted by use of the influence coefficients provided by the MCP.

3.5.6 Application of Mode Calculating Procedure to a NASA Fan Design

Objective

To provide an example of the application of the procedure for determining the experimental accuracy requirements, section 3.5.5, using an existing fan design that has been run on the NASA 50cm (20 inch) diameter fan rig.

Application

To illustrate the application of the procedure for determining the required experimental accuracy for a specific application, a particular fan design will be used that has been run on the NASA 50cm (20 in.) diameter fan rig at the Lewis Research Center. The particular fan stage chosen, designated rotor 55, has a 15 bladed rotor, 25 fan exit guide vanes, and has a design speed of 8020 rpm. At a typical approach speed, the Tyler-Sofrin theory would predict that at twice blade passing frequency the rotor-stator interaction will generate five modes: (5,0), (5,1), (5,2), (5,3), (5,4). Typically, however, the duct could support at that frequency on the order of one hundred incident acoustic duct modes.

If the desired accuracy for predicting the dominant modes in the duct is set at approximately ±2 dB, (Step 1), and if it is assumed that the mean amplitude of the modes omitted from the calculation procedure (i.e., the extraneous modes) are about 20 dB down from the dominant modes, then it can be seen from Figure 3.5-3 that the allowable number of extraneous modes has to be about 12. This quick analysis illustrates that, providing the assumptions made are reasonable, a ±2 dB accuracy in the calculation of the dominant modes can be achieved only if 88 (i.e., 100 − 12) microphones are used to obtain data (Step 2). Note that with the same assumptions, a ±3 dB accuracy in the modal calculation could be obtained with about 60 microphone measurements.

If the rotor-stator spacing for this fan design was reduced so that a strong interaction tone was generated, and if care was taken to control inflow distortions, it is conceivable that the mean amplitude of the extraneous modes will be 25 dB to 30 dB down from the five dominant modes due to the interaction. In this case, it can be seen from Figure 3.5-3 that an accuracy with ±2 dB could be expected with as few as five microphones.

For purposes of proceeding with the illustration, it will be assumed for Step 1 that a ±2 dB accuracy in the modal calculation procedure is desired and that the mean amplitude of the modes is about 30 dB down from the dominant modes. From Step 2, using Figure 3.5-3, it follows that five microphones should be used. The allowable error of the acoustic measurements (Step 3) can be determined from Figure 3.5-4. From the assumption stated above, $(\frac{N_T - N}{N}) = 19$. From Figure 3.5-4 it can be seen that the allowable error in pressure amplitude measurement should be 1.1 dB, and the allowable error in pressure phase measurement is about eight degrees.

The allowable error in locating microphones on the duct wall in this case is obtained (Step 4) from Figure 3.5-5. Again, based on the assumptions stated above, and since m is five and k_{x_S} is on the order of 83 degrees-per-cm for the case being considered, it can be seen from Figure 3.5-5 that the allowable error in placing microphones at specific axial and circumferential locations is on the order of $8/k_{x_S} \approx 0.1$ cm and $8/m = 1.6$ degrees respectively.

As required by Step 5, the allowable measurement and placement errors are compared with estimates of the actual measurement and placement errors that would be expected when conducting the test. Clearly, the microphone location errors met in practice would be much less than the 0.1 cm in axial direction and the 1.6 degrees in circumferential direction. Also, the measured acoustic pressure amplitudes and phase errors should be able to be held within values well below 1.1 dB and 8 degrees, respectively. Thus in the situation described in this section, the acoustic measurement and location accuracy requirements are reasonable, and the desired modal calculation accuracy of ±2 dB (Step 1) should be achieved. If more modes (requiring more microphones) are included in the modal calculation method, the calculation accuracy will improve. This improvement would continue with the addition of more microphones until eventually, the measurement system accuracy would determine the modal calculation accuracy.

Based on this illustration of the procedure that can be used to provide an approximate guide of the number of microphones and the measurement accuracy experimentally required for a specific application, it is recommended that a test of the modal calculation method be conducted on the NASA 50cm (20 in.) diameter rig. The number of microphones used during the test and the number of modes used in the modal calculation, could be increased further reducing the contamination from extraneous modes and thereby achieving a greater accuracy in the modal calculation.

4.0 DISCUSSION OF OVERALL PROGRAM RESULTS

During this program, two studies were performed for the calculation of the modal structure in the inlet of a turbofan engine using in-duct measurement as the calculation input. For the first study, experimental and computational procedures and two computer programs were developed for the calculation of the amplitudes and phases of the coherent propagating sound modes. In addition, an experimental program was run to provide verification of the procedure. For the other study, procedures were identified for the determination of the expected amplitudes of the duct modes resulting from a random noise generating mechanism. In fact, these procedures are sufficiently general and could be applied to any duct sound field. These overall program results will be discussed separately for each of the two cases.

4.1 COHERENT MODE STRUCTURES

The computational procedure to calculate the amplitudes and phases of the coherent mode structure in the inlet duct of a specific fan design is based on two computer programs, the Microphone Location Program (MLP) and the Modal Calculation Program (MCP). First, in those cases where the number of propagating modes is greater than the number of microphones to be used, a subset of modes is selected from all the propagating modes supportable by the inlet duct that are considered to contain the bulk of the acoustic energy in the duct sound field. This selection can be based on an application of the Tyler-Sofrin analysis. With the number of modes to be calculated identified, the MLP is used to determine locations for an equal number of microphones within the duct that ensures numerical stability of the subsequent modal calculation. So long as specific criteria are satisfied that ensure numerical stability in the modal calculation, the microphone locations are restricted only to axial and circumferential wall measurements. For many situations, however, to provide sufficient stability, input measurements are required from all three dimensions within the duct; and in those cases the MLP will select such positions. The MCP, using data from these microphones as input calculates the amplitude and phase of each of the modes comprising the chosen set of modes.

In addition, the MCP calculates a set of influence coefficients that can be used to calculate the first order error in modal amplitude and phase that would result from errors in the knowledge of the measuring location and in the measured phase angles and pressure amplitudes. Finally, if the standard deviations due to measurement and microphone location errors are input to the MCP, the standard deviations of the resulting errors in each of the calculated modes is computed.

The method for determining coherent mode structures was checked out using ten arbitrarily chosen analytical test cases, and subsequently, in a set of experiments to determine six different modal structures generated in the inlet of the Pratt & Whitney Aircraft 25cm (10 inch) research fan rig. Experimental procedures that were established on the basis of the analytical method were also checked out during this set of experiments.

Results from these experiments demonstrated that the method for determining coherent mode structures is suitable for relatively simple mode structures when the number of microphones used to provide data input to the MLP is comparable to the number of incident

propagating modes in the duct. In one case, the structure of seven modes was identified using seven microphones, and it was determined that the dominant mode was calculated to within an accuracy of 0.2 dB in amplitude and 0.9 degree in phase. In other cases, where the structure of up to nine modes was determined, and the number of microphones used in the test was on the order of one half the total number of incident modes that could propagate, the structure was determined with an accuracy that allowed the sound field to be predicted to within a standard error of 1.5 dB at other duct locations based on the calculated modal structure. In yet another case where the structure of three modes was determined using three microphones but where the duct could support 8.3 propagating incident modes, the sound field at other duct locations was poorly predicted — within a standard error of 3.8 dB — based on the calculated mode structure.

Based on these experimental and analytical test cases and on a complementary analytical study, it was found that the accuracy of the method depends on the number and average amplitude of the extraneous modes, (i.e., the difference between the number of modes supportable by the duct, and the number of modes used as input to the MCP) as well as the measurement and position accuracies. An approximate procedure was developed to help guide the experimentalist in identifying the number of microphones that would be required to achieve a desired accuracy. Since the procedure was based on an order of magnitude analysis, it should be used only as a guide.

4.2 RANDOMLY GENERATED MODE STRUCTURES

By using the property that any acoustic field in a duct (random or coherent) at any instant of time must exhibit 2π periodicity in the angular coordinate, it was shown that a modal Power Spectral Density function (PSD) could be generated that depended on frequency and integer values of the wave (or mode) number in the circumferential direction. This definition of the Modal PSD also permitted interpretation of random acoustic fields for the annular ducts in terms of spinning mode concepts similar to those evolved for coherent acoustic fields.

Two approaches for measuring the modal PSD in thin annular ducts were derived. The first evolved from the development of the modal PSD concept and requires cross spectral analysis of microphone signals for its implementation. A second approach was also derived, using phased array measurement and data reduction concepts. This second method does not require cross spectral properties for its implementation and should therefore be easier to use.

An outline of the array method is as follows. For a specific annular duct geometry and frequency range of interest, a minimum number of microphones is selected in order to satisfy the Nyquist criterion (in frequency and mode number space). These microphones are then placed equidistant in one axial plane on the duct wall. During the test, the outputs from these microphones are recorded on analog tape and or subsequently digitized. The sound field is then discriminated into acoustic waves with specific spin rates. The discrimination can be achieved when processing the data by just passing the signal from each microphone through a narrow band filter to select signals at a prescribed frequency, and then subsequently delaying each signal output by a given increment in time and then averaging the signals to yield a single output signal.

In effect, this process enhances acoustic waves of a given frequency rotating at a specific spin rate along the duct wall and suppresses the input to the signal from waves rotating at other spin rates. Since the spin rate is given by ω/m (where ω is the radian frequency of interest and m is the circumferential mode number), once the spin rate or delay time has been selected, the output signal consists of contributions only from acoustic waves with a specific circumferential mode number. The process can then be repeated for a range of delay rates to generate the contribution to the modal PSD (at the selected frequency) of waves with other circumferential mode numbers. Repetition of the process at other frequencies leads to a complete definition of the modal PSD.

This method for the determination of randomly generated mode structures is in fact quite general, and the method can be applied equally well to coherent sound fields. For thin annular ducts, the spin rate can be related to the propagation angle of the mode. If the method is applied to a coherent sound field whose frequency spectrum consists of a fundamental time and its harmonics, application of the procedure permits the modal energy of all modes spinning out a given rate to be determined by simply processing the unfiltered signals in the manner described previously.

When applied to thee dimensional ducts, the method will determine only the circumferential mode structure at the duct wall, so in its present form it can give no information about the radial modal structure.

5.0 CONCLUSIONS

1. The method has been assessed experimentally for sample modal structures and is reasonably accurate when the number of available microphone measurements is comparable to the total number of propagating modes in the duct. For the experiments in this program, up to ten microphones were used for the modal calculation. The accuracy deteriorates as the number and average amplitude of those modes not included in the modal calculation increases.

2. A procedure has been established to estimate for a specific potential application, the number of microphone systems that would be needed and the acoustic pressure measurement and microphone location accuracy that would be required to achieve a desired accuracy in the calculation of the amplitudes and phases of the dominant propagating modes.

3. Two approaches have been defined for measuring the modal PSD of a random sound field in two dimensional annular ducts; one requires cross-spectral analysis of the microphone signals, whereas the other depends on processing through the use of incremental delays, the outputs from a circumferential array of microphones whose signals have been narrow-band filtered.

6.0 RECOMMENDATIONS

Based on the work conducted under this contract, the following recommendations are suggested for continuing the development of methods for determining fan sound mode structures:

1. The method for determining coherent fan sound mode structures should be evaluated on a high speed fan rig, such as the NASA 50 cm (20 in.) fan rig. The fan design should be such that a strong rotor-stator interaction tone noise is generated, and provision should be made for minimizing the levels of inflow turbulence and steady distortion. In this way, the amplitudes of extraneous modes not included in the modal calculation will be minimized.

2. Develop and experimentally assess circumferential microphone array methods that can be used to determine the pressure amplitude at the wall to define discrete coherent and/or random fan duct sound fields in terms of circumferential mode orders. This would provide guidance in selecting the dominant modes for use in the modal calculation program (MCP) developed under this contract.

3. Apply the circumferential array method, together with the existing P&WA/NASA procedure (MLP and MCP), to the problem of determining the amplitude and phase of the dominant modes in terms of both circumferential and radial order when a relatively large number (i.e., 60) of discrete coherent duct modes are present in the P&WA 10-inch circular duct.

4. The method for determining the amplitude frequency spectrum of coherent and/or randomly generated sound modes in a thin annular duct, using a circumferential array of microphones should be developed and assessed experimentally on a small-scale, low-speed fan rig such as the Pratt & Whitney Aircraft 25 cm (10 in.) fan research rig.

5. The microphone array method should be extended to include axial arrays so that the radial structure of coherent and randomly generated modes can be determined in three-dimensional ducts.

REFERENCES

1. Tyler, J.M. and Sofrin, T.G.: " Axial Flow Compressor Noise Studies," *Trans. SAE*, 70, p. 309, (1962).

2. Sofrin, T.G. and McCann, J.C.: "Pratt & Whitney Aircraft Experience in Compressor Noise Reduction," For Presentation at 72nd Meeting of Acoustic Soc. Amer., Los Angeles, CA, Nov. 1966.

3. Mugridge, B.D.: "The Measurement of Spinning Acoustic Modes Generated in an Axial Flow Fan," *J Sound and Vibration*, 10 (2), 1969, pp 227-249.

4. Bolleter, U. and Chanaud, R.C.: "Propagation of Fan Noise in Cylindrical Ducts," *J. Acoustical Soc. Amer.*, Vol. 49, No. 3, (Part 1), 1971.

5. Moore, C.J. "In-Duct Investigation of Subsonic Fan 'Rotor Alone' Noise," *J. Acoustic Soc. Amer.*, Vol. 51, #5 (Part 1), 1972.

6. Bolleter, U. and Crocker, M.,: " Theory and Measurement of Modal Spectra in Hardwall Cylindrical Ducts," *J. Acoustic Soc. Amer.*, Vol. 51 #5, (Part 1), 1972.

7. Plumblee, H.E.; Dean, P.D.; Wynne, G.A.; and Burrin, R.H.: "Sound Propagation in and Radiation from Acoustically Lined Ducts: A Comparison of Experiment and Theory," NASA, Washington, NASA CR-2306, Oct. 1973.

8. Kraft, R.E. and Posey, J.W.: "A Preliminary In-Duct Measurement of Spinning Modes in the Inlet of a Rotating Vehicle," Presented at 91st Meeting of Acoustical Soc. Amer. Washington D.C., April 1976.

9. Pickett, G. F.; Wells, R. A.; and Love, R. A: "Computer Program User's Manual Modal Calculation Program," NASA Lewis Research Center, NASA CR-135295, (1977).

10. Resanoff, R. A. and Ginsburg, T. A.: "Matrix Error Analysis for Engineers," AFFDL-TR-66-80, p. 889.

11. Pickett, G. F.; Wells, R. A.; and Love, R. A.: "Computer Program User's Manual Microphone Location Program," NASA Lewis Research Center, NASA CR-135294, (1977).

12. Lee, Y. W.: *Statistical Theory of Communication*, John Wiley, New York, 1960.

13. Collin, R. F. and Zucker, F. J.: *Antenna Theory*, McGraw-Hill, New York, 1969.

14. A. Silverstein et al: "Downwash and Wake Behind Plain and Flapped Airfoils," NACA Report 651, 1939.

15. Schubauer, G. B.; Spangenberg, W. A.; and Klebanoff, P. S.: "Aerodynamic Characteristics of Damping Screens," NACA TN 2001, January 1950.

16. Pickett, G. F.: "Effect of Non-Uniform Inflow on Fan Noise," *J. Acous. Soc. Amer.*, 55, S3(A), Spring 1974.

APPENDIX A - NOTATION

English Symbols

Symbol		Description
$A_{m\mu}$		amplitude of modal pressure
a_k		distortion harmonics of downstream flow
$a_m(t)$		random time function
$a_m a_m(t)$ $b_m b_m(t)$ $a_m b_m(t)$	–	cross correlation functions
B	–	number of rotor blades
B_n	–	amplitude of measured pressure
b_ℓ		distortion harmonics of inflow
$b_m(t)$	–	random time function
C_D		drag coefficient
C_m	–	complex amplitude
C_{mn}	–	modal amplitude complex coefficient
C_{nm}	–	cofactor of an element in Hnm
c		stator vane cord
c	–	speed of sound
dp,dz,dx,etc.		errors in indicated variables
$^{r}dA_m$, $^{x}dZ_m$,etc.		error in variable due to error in superscript variable
$E_{m\mu}$		characteristic radial function
Ex ( )		expected magnitude

APPENDIX A - NOTATION (Continued)

Symbol	Description
$\mathcal{F}_J$	Fourier transform operator
$f(r, \theta, x, t ; w)$	incoherent noise filtered at frequency ω
$f_j(\frac{x}{c}, C_D, y)$	wake deficit from airfoil
$f_n(t)$	array signal average
H	complex matrix giving p in terms of Z
h_{nm}	amplitude of elements of H
k	loss factor
k	integer
k_s	characteristic radial eigenvalue
$k_{m\mu}$	characteristic radial eigenvalue
$\bar{k}_{ns}$	defined by eqn. B-15
k_x	axial wave number
ℓ	number of calculated modes
M	specific value of m
Mx	axial Mach number
m	circumferential mode number
m*	highest propagating circumferential mode number
N	number of detectors in array
N	number of calculated modes
N	number of rotor revolutions
N_T	number of duct supported modes

APPENDIX A – NOTATION (Continued)

Symbol		Description
$P(r, \theta, x, t;\omega)$		complex measured (local) pressure
$< P >$		average pressure for N averages
P_A		probability distribution density about mean A
ΔP	-	pressure difference
Q	-	Inverse of H giving Z in terms of Q
q	-	dynamic head
q_{mn}		amplitude of elements of Q
$R(\sigma, \tau)$		cross correlation function
Re		real part
$R_{jk}(\tau)$	-	cross correlation function
$R_\theta(\theta;\sigma\tau)$		partial cross correlation function
r	-	radial coordinate
r		radius of narrow annular duct
$S(m,\omega)$		modal power spectral density
$S_m^+(\|\omega\|), S_m^-(\|\omega\|)$	-	modal component psd functions
$S_{jk}(\omega)$		cross power spectral density
$S_\eta(\omega)$		array signal psd
$S_\sigma(\sigma,\omega)$		space average cross psd function
t		time coordinate
U		mean inflow velocity
u		stator wake deficit

APPENDIX A – NOTATION (Continued)

Symbol	Description
$U_n(\omega)$, $V_n(\omega)$	combinations of spectral functions defined by eqs. 3.3-16
V	flow velocity downstream of stator
V	number of stator vanes
x	coordinate in direction of axis
y	transverse coordinate of stator wake
Z	complex modal pressure
Z	array factor
$\|z\|$	magnitude of array of factor; array response or array response function

Greek Symbols

Symbol	Description
α_{nm}	phase of elements of H
β	array factor argument, $\beta = (m - \omega\eta)$
β_{mn}	phase of elements of Q
γ_j	sum of phase angles
Δ_{nn}	determinant of a N x N matrix
δ ( )	delta function defined by properties: $\sum_{n=0}^{\infty} C_n \delta(m-n) = C_m$ for m = 0, 1, 2, $\sum_{n=1}^{\infty} C_n \delta(m+n) = C_{\|m\|}$ for m = 1, 2,

Greek Symbols (Continued)

Symbol	Description
δ_j	sum of phase angles
η	defined by eqn. B-19
η	array delay rate, $\Delta t/\Delta\theta$
θ	angular coordinate, radians
μ	radial mode index
σ	hub-to-tip ratio
σ	angular separation of detector pair
σ_A, σ_X, σ_Γ, etc.	standard deviation of errors of subscript variables
τ	period of one revolution of the rotor
τ	delay time
$\Phi_m(\omega)$	combination of $\phi_m{}^a(\omega)$, $\phi_m{}^b(\omega)$ psds
ϕ	phase of modal pressure
$\phi_m^a(\omega)$, $\phi_m^b(\omega)$	power spectral densities of $a_m(t)$, $b_m(t)$
$\Psi_m(\omega) = i\,\Psi'_m(\omega)$	combination of $\psi_m^{ab}(\omega)$, $\psi_m^{ba}(\omega)$ cross psds
ψ_η	phase of measured pressure
$\psi_m^{ab}(\omega)$, $\psi_m^{ba}(\omega)$	cross psd functions of $a_m(t)$, $b_m(t)$
Ω	mode spin velocity
ω	radian frequency

Greek Symbols (Continued)

Indicies

Symbols	Description
i, k, l, n	integer
M	indicating specific modes
n, m, s	number of modes
N	number of microphone locations
n	specific microphone location
x, r, θ	axial, radial, and circumferential coordinates

Notation

Symbols	Description
$\{\ \}$	optional usage for column matrix
$[\ ]$	optional usage for square matrix

APPENDIX B
DERIVATION OF INFLUENCE COEFFICIENTS

It was shown by equation (3.2-17) that the combined effects of acoustic pressure and microphone placement errors on the mode coefficients (z) can be expressed in matrix notation as:

$$dz = Q\,dp - Q'\,dx \tag{B1}$$

To facilitate the determination of the specific effects on mode amplitude and phase due to changes in amplitude and phase of the N measured pressures, and due to errors in the coordinate (x, γ, θ) of the N microphone locations, the two terms on the RHS of equation (B1) will be considered separately. The total effect can then be obtained by linearly superposing the two separate effects.

B.1 EFFECT OF PRESSURE AMPLITUDE AND PHASE ERRORS

Consider

$$dz = Q'\,dp \tag{B2}$$

Each pressure p_n at the n^{th} microphone location has amplitude B_n and phase angle ψ_n subject to independent errors dB_n and $d\psi_n$, and these errors affect all elements Z_m. The left hand side of equation (B2) can be expressed in terms of these errors through the appropriate partial derivatives to give the following:

$$\{dz_M\} = \left[\frac{\partial z_M}{\partial B_n}\right]\{dB_n\} + \left[\frac{\partial z_M}{\partial \psi_n}\right]\{d\psi_n\} \tag{B3}$$

$\{dB_n\}$ and $\{dZ_M\}$ are column matrices indicating the independent pressure amplitude errors and the resulting (complex) errors in the modal coefficients. The square matrix $\left|\frac{\partial Z_M}{\partial B_n}\right|$ has elements $\frac{\partial Z_M}{\partial B_n}$ which represent the effect of the n^{th} pressure amplitude error on the M^{th} modal coefficient. This matrix, and the companion $\left|\frac{\partial Z_M}{\partial \psi_n}\right|$ are to be found in terms of the right hand side of equation (B2). Considering without loss in generality the change in one of the components (the M^{th}) of the column matrix dz, equations (B2) and (B3) give:

$$dz_M = \sum_{n=1}^{N} q'_{Mn}\,dp_n \tag{B4}$$

$$dz_M = \sum_{n=1}^{N}\left(\left(\frac{\partial z_M}{\partial B_n}\right)dB_n + \left(\frac{\partial z_M}{\partial \psi_n}\right)d\psi_n\right) \tag{B5}$$

Putting $dp_n = \frac{\partial P_n}{\partial B_n} dB_n + \frac{\partial P_n}{\partial \psi_n} d\psi_n$ in equation (B4) and eliminating dz_M between equations, (B4) and (B5) give:

$$\sum_{n=1}^{N} \frac{\partial z_M}{\partial B_n} dB_n + \sum_{n=1}^{N} \frac{\partial z_M}{\partial \psi_n} d\psi_n = \sum_{n=1}^{N} Q_{Mn} \frac{\partial P_n}{\partial B_n} dB_n + \sum_{n=1}^{N} Q_{Mn} \frac{\partial P_n}{\partial \psi_n} d\psi_n \quad \text{(B6)}$$

Since the dB_n and the $d\psi_n$ are all independent variables, the only way this equation can be satisfied for arbitrary values of dB_n and $d\psi_n$ is if corresponding coefficients of each dB_n and $d\psi_n$ on each side of equation (B6) are equal.

Thus

$$\frac{\partial z_M}{\partial B_n} = Q_{Mn} \frac{\partial P_n}{\partial B_n}$$

$$\frac{\partial z_M}{\partial \psi_n} = Q_{Mn} \frac{\partial P_n}{\partial \psi_n} \quad \text{(B7)}$$

Now expressing the complex quantities z_M and p_n in polar form and taking the derivatives required in equation (B7):

From $Z_M = A_{Me}^{\ i\phi_M}$

$$\frac{\partial z_M}{\partial B_n} = \frac{\partial A_M}{\partial B_n} e^{i\phi_M} + A_M i \frac{\partial \phi_M}{\partial B_n} e^{i\phi_M}$$

$$= \left(\frac{\partial A_M}{\partial B_n} + i A_M \frac{\partial \phi_M}{\partial B_n}\right) e^{i\phi_M} \quad \text{and} \quad \text{(B8)}$$

$$\frac{\partial z_M}{\partial \psi_n} = \left(\frac{\partial A_M}{\partial \psi_n} + i A_M \frac{\partial \phi_n}{\partial \psi_n}\right) e^{i\phi_M}$$

and from $p_n = B_n e^{i\psi_n}$,

$$\frac{\partial P_n}{\partial B_n} = e^{i\psi_n}$$

$$\frac{\partial P_n}{\partial \psi_n} = i B_n e^{i\psi_n} \quad \text{(B9)}$$

Substituting equations (B8) and (B9) in equation (B7) and writing $Q_{Mn} = q_{Mn} e^{ib_{Mn}}$

$$\left(\frac{\partial A_M}{\partial B_n} + i A_M \frac{\partial \phi_M}{\partial B_n}\right) e^{i\phi_M} = g_{MN} e^{i(\psi_n + \beta_{Mn})}$$

$$\left(\frac{\partial A_M}{\partial \psi_n} + i A_M \frac{\partial \phi_M}{\partial \psi_n}\right) e^{i\phi_M} = g_{MN} i B_n e^{i(\psi_n + \beta_{Mn})} \qquad \text{(B10)}$$

Equating real and imaginary parts gives the following results for the four influence coefficient matrices:

$$\left[\frac{\partial A_M}{\partial B_n}\right] = \left[g_{MN} \cos(\beta_{Mn} + \psi_n - \phi_M)\right]$$

$$\left[\frac{\partial A_M}{\partial \psi_n}\right] = -\left[B_n g_{MN} \sin(\beta_{Mn} + \psi_n - \phi_M)\right]$$

$$\left[\frac{\partial \phi_M}{\partial B_n}\right] = \left[\frac{1}{A_M} g_{MN} \sin(\beta_{Mn} + \psi_n - \phi_M)\right]$$

$$\left[\frac{\partial \phi_M}{\partial \psi_n}\right] = \left[\frac{B_n}{A_M} g_{MN} \cos(\beta_{Mn} + \psi_n - \phi_M)\right] \qquad \text{(B11)}$$

These are four of the influence functions presented in equation (3.2-18). The remainder are influence functions related to errors in microphone location and this subject is considered next.

B.2 EFFECT OF MICROPHONE LOCATION ERRORS

The effect of errors dx_n, dr_n, and $d\theta_n$ in the coordinates of the microphone location are represented by the second term on the RHS of equation (B1).

i.e., (B12)

It should be noted that the column matrix produced by the product $dH \cdot z$ can be considered to be similar to a set of pressure errors, since $dH \cdot z$ premultiplied by Q is similar to the set of relations for dz (= Qdp) that has just been analyzed. Therefore, the analysis given in the preceeding section apply equally well here. The only complications result from having to formulate explicit expressions for $dH \cdot z$ instead of starting with given values of dp. Instead of seeking directly expressions for the partial derivatives of z with respect to r_n, x_n, and θ_n, it is more straightforward to find dz in terms of dr_n, dx_n, and $d\theta_n$ and to finally equate coefficients of the differentials in order to obtain expressions for the derivatives.

In obtaining an expression of dH, two features exist that simplify the algebra. First, the equation system (B12) is linear in the elements of dH, so that the contributions of errors dr_n, dx_n, and $d\theta_n$ may be obtained separately and then superposed. Secondly, the dr_n, dx_n, and $d\theta_n$ errors of positions of the n^{th} microphone location affect only the elements dH in the n^{th} row, the other elements of the dH matrix being zero. These features allow explicit expressions for the partial derivatives to be obtained.

The contributions to dH due to dr_n, dx_n, and $d\theta_n$ will be denoted by ${}^{r}dH_{ns}$, ${}^{x}dH_{ns}$, ${}^{\theta}dH_{ns}$, where the subscript n denotes that only the n^{th} row of $[dH_{nM}]$ is affected. The subscript s replaces the M subscript to denote successive elements in this n^{th} row. This replacement is necessary to avoid subsequent confusion when it becomes necessary to perform summations with respect to an index denoting these successive n^{th} row elements — the index M is reserved to specify a particular mode coefficient, z_M and should not also be employed as a dummy or summation index.

The column matrix dH.z due to errors in location of the n^{th} microphone only can be written out in full as:

$$\{dZ\} = \begin{pmatrix} 0 & 0 & \cdots & 0 & \cdots & 0 \\ 0 & 0 & \cdots & 0 & \cdots & 0 \\ \vdots & & & & & \\ dH_{n1} & dH_{n2} & \cdots & dH_{ns} & \cdots & dH_{nN} \\ 0 & 0 & \cdots & 0 & \cdots & 0 \end{pmatrix} \begin{Bmatrix} z_1 \\ z_2 \\ z_s \\ z_N \end{Bmatrix} = \begin{Bmatrix} 0 \\ 0 \\ \vdots \\ \sum_{s=1}^{N} dH_{ns} z_s \\ \vdots \\ 0 \end{Bmatrix} \qquad \text{(B13)}$$

Since the partial product $dH \cdot z$ is a column of zeros everywhere except in the n^{th} row, the results dZ_M will be the column matrix formed from the n^{th} column elements of $[Q_{Mn}]$, all multiplied by the common scalar $\Sigma\ dH_{ns} Z_s$. Accordingly, the elements dZ_M resulting from position errors in the n^{th} location can be denoted by ndzm and are simply given by:

$$^{n}dZ_M = Q_{Mn} \sum_{s=1}^{N} dH_{ns} z_s \qquad \text{(B14)}$$

Equation (B14) is the essential result of the analysis. Further work only involves algebraic detail in obtaining ${}^{r}dH_{ns}$, ${}^{x}dH_{ns}$, ${}^{\theta}dH_{ns}$, the specific differentials for errors dr_n, dx_n, $d\theta_n$, and then resolving the resulting ${}^{rn}dZ_M$, ${}^{xn}dZ_M$, ${}^{\theta n}dZ_M$ into amplitude and phase, ${}^{m}dA_M$, ${}^{m}d\phi_M$, etc., by the procedures described previously in the pressure error analysis. From equation (3.2-13) for the elements of the matrix H, there follows:

$$^{rn}dH_{ns} = \frac{\partial H_{ns}}{\partial r_n} dr_n = \left(k_s J_s'(k_s r_n) / Z_s(k_s r_n)\right) H_{ns}\, dr_n$$

$$= \xi_{ns} H_{ns}\, dr_n$$

$$\text{WHERE} \quad \xi_{ns} = k_s J_s'(k_s r_n) / Z_s(k_s r_n)$$

$$^{xn}dH_{ns} = \frac{\partial H_{ns}}{\partial x_n} dx_n = k_{xs} H_{ns}\, dx_n \qquad \text{(B15)}$$

$$^{\theta n}dH_{ns} = \frac{\partial H_{ns}}{\partial \theta_n} d\theta_n = i m_s H_{ns}\, d\theta_n$$

Substituting equation (B15) into (B14) gives:

$$ {}^{rn}d\hat{e}_u = -d_{rn}\, Q_{un} \sum_{s=1}^{N} \bar{h}_{ns} H_{ns} \hat{e}_s \qquad \text{(B16)} $$

If the complex quantities on the RHS of equation (B16) are then expressed in the polar forms:

$$ \begin{aligned} Q_{un} &= q_{un}\, e^{i\beta_{un}} \\ H_{ns} &= h_{ns}\, e^{i\alpha_{ns}} \\ \hat{e}_s &= A_s\, e^{i\phi_s} \end{aligned} \qquad \text{(B17)} $$

Then

$$ \begin{aligned} d\hat{e}_u &= \frac{\partial \hat{e}_u}{\partial A_u} dA_u + \frac{\partial \hat{e}_u}{\partial \phi_u} d\phi_u \\ &= (dA_u + i A_u d\phi_u)\, e^{i\phi_u} \end{aligned} \qquad \text{(B18)} $$

and

$$ \begin{aligned} {}^{rn}d\hat{e}_u &= d_{rn}\left(\frac{\partial A_u}{\partial r_n} + i A_u \frac{\partial \phi_u}{\partial r_n}\right) e^{i\phi_u} \\ {}^{hn}d\hat{e}_u &= d_{hn}\left(\frac{\partial A_u}{\partial h_n} + i A_u \frac{\partial \phi_u}{\partial h_n}\right) e^{i\phi_u} \\ {}^{\alpha n}d\hat{e}_u &= d_{\alpha n}\left(\frac{\partial A_u}{\partial \alpha n} + i A_u \frac{\partial \phi_u}{\partial \alpha n}\right) e^{i\phi_u} \end{aligned} $$

On substituting (B17) and (B18) into (B16) equating real and imaginary parts, and extracting the coefficients of dr_n, dx_n and $d\theta_n$, the following expressions are obtained for the influence coefficients or partial derivatives:

$$\frac{\partial A_{xx}}{\partial r_n} = \gamma_{xn} \sum_{s=1}^{N} k_{xs} h_{ns} A_s \cos \eta_{ns},$$

$$\frac{\partial A_{xx}}{\partial r_n} = \frac{1}{A_{xx}} \gamma_{xn} \sum_{s=1}^{N} k_{ns} n_{ns} A_s \cos \eta_s$$

$$\frac{\partial A_{xx}}{\partial x_n} = -\gamma_{xn} \sum_{s=1}^{N} k_{xs} h_{ns} A_s \cos \eta_{ns},$$

$$\frac{\partial A_{xx}}{\partial x_n} = \frac{1}{A_{xx}} \gamma_{xn} \sum_{s=1}^{N} k_{xs} h_{ns} A_s \cos \eta_{ns} \qquad \text{(B19)}$$

$$\frac{\partial A_{xx}}{\partial \theta_n} = -\gamma_{xn} \sum_{s=1}^{N} k_{xs} n_{ns} A_s \cos \eta_{ns},$$

$$\frac{\partial A_{xx}}{\partial \theta_n} = \frac{1}{A_{xx}} \gamma_{xn} \sum_{s=1}^{N} k_{xs} n_{ns} A_s \cos \eta_{ns}$$

WHERE $\eta_{ns} = \beta_{xn} - \alpha_{ns} + \phi_s - \phi_{xx}$

These six influence coefficients represent the balance of all the influence coefficients presented in equation (3.2-18)

APPENDIX C
THE EFFECT OF NONUNIFORM INFLOW ON ROTOR-IGV INTERACTION TONE NOISE

The duct sound field generated by rotor-IGV interaction consists of a set of duct modes that can be predicted by an application of the theory presented by Tyler & Sofrin (ref.1). Sofrin & McCann (ref. 2) extended this theory to include the effects of uniform axial flow. One of the main results from this work is that for a B bladed rotor and V inlet guide vanes, a set of circumferential acoustic duct modes at blade passing frequency harmonics are generated given by the expression $m = nB + kV$. In this expression, n denotes the particular harmonic of blade passing frequency and kV denotes the harmonics of inflow distortion due to the wakes of the IGV's interacting with the rotor. The range of k and the set of radial orders for each circumferential duct mode are bounded because at a given frequency, the duct can support only a finite set of propagating acoustic duct modes.

The purpose of this appendix is to demonstrate how the kinematics of fan noise generation due to inlet-guide-vane wake-rotor interaction can change when steady non-uniform fan inflow modulates the vane wakes, resulting in the generation of additional acoustic duct modes. It is sufficient to consider the effect of steady azimuthally non-uniform inflow to a fan with high hub-tip ratio where no high order radial modes are generated.

If the inflow upstream of the IGV's is given by $U(\theta)$, the flow distortion downstream of the rotor will be of the same general shape but with viscous wake deficits superimposed as shown schematically in Figure C1. Since the viscous wake deficit from each vane depends on the free stream velocity in the vicinity of that vane, the wake deficit from each vane will be different and can be denoted by $u_j(\theta, U_j(\theta))$ where j denotes the j^{th} IGV, and $U_j(\theta)$ is the free stream velocity in the vicinity of the vane.

If $U_j(\theta)$ is a slowly varying function of θ (relative to a vane gap), U_j can be taken to be a constant over the wake width from each vane and the non-uniform flow downstream of the IGV's can be written as:

$$V(\theta) = U(\theta) - \sum_{j=1}^{V} u_j(\theta, U_j) \qquad (C1)$$

Again, since $U(\theta)$ is assumed slowly varying, the wake deficit $u_j(\theta, U_j)$ can be represented by empirically derived formulae for wake deficits behind isolated airfoils. An example of such formula is that given by Silverstein et al. (ref. 14). The form of these formulae are similar and the wake deficit $u(y)$ can be written generally as

$$\frac{u(y)}{U} = f_j\left(\frac{x}{c}, C_D, y\right) \qquad (C2)$$

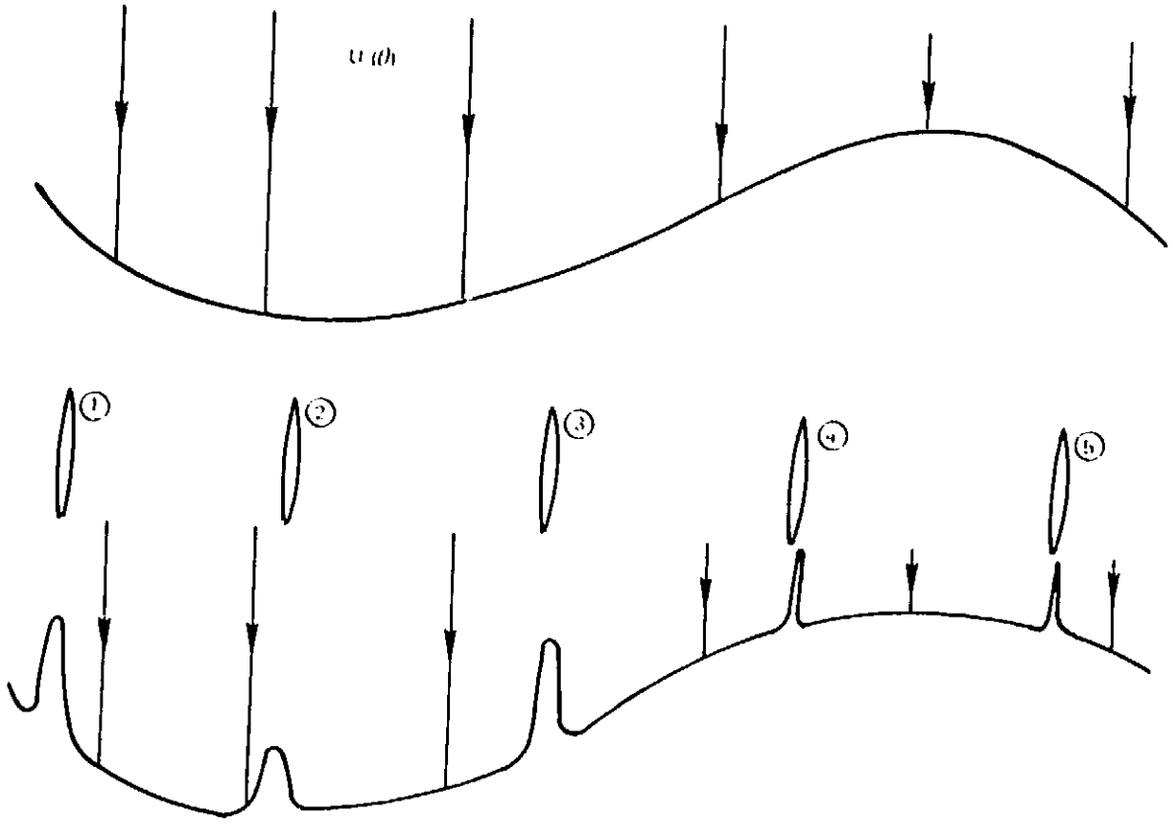

Figure C-1 Illustration of Viscous Wake Deficits Downstream of an IGV in Nonuniform Flow

where y is the transverse coordinate centered at the midpoint of the wake, x is the distance downstream of the IGV's, c is the chord of each vane, C_D is the drag coefficient for each vane, and U is the mean flow over the airfoil. Based on the above assumptions the velocity defect due to the j^{th} vane in the coordinate system of the duct, can be written as

$$\frac{u_j(\theta)}{U_j} = f_j\left(\frac{x}{c}, C_D, \theta\right)$$

or

$$u_j(\theta) = U(\theta) f_j\left(\frac{x}{c}, C_D, \theta\right) \qquad (C3)$$

since $f_j\left(\frac{x}{c}, C_D, \theta\right)$ is non zero only in the vicinity of the j^{th} vane.

Substituting (C3) in (C1),

$$V(\theta) = U(\theta)\left[1 - \sum_{j=1}^{V} f_j\left(\frac{x}{c}, C_D, \theta\right)\right] \qquad (C4)$$

Now for uniform flow $U(\theta) = U$, a constant, and

$$V_{uf}(\theta) = U\left[1 - \sum_{j=1}^{V} f_j\left(\frac{x}{c}, C_D, \theta\right)\right] \qquad (C5)$$

By Fourier expansion over the period of one vane, this expression can be written as

$$V_{uf}(\theta) = U\sum_{k=-\infty}^{\infty} a_k e^{ikV\theta}$$

where $V_{uf}(\theta)$ is the velocity downstream of the IGV's in uniform flow and the "a_k" can be considered to be distortion harmonics of the flow downstream of the IGV's

Using the result from (C5) in (C4), $f_j\left(\frac{x}{c}, C_D, \theta\right)$ can be eliminated. Thus, the distortions downstream of the IGV's for uniform and non uniform flow can be related as follows

$$V(\theta) = U(\theta)\ \frac{V_{uf}(\theta)}{U}$$

whereupon

$$V(\theta) = \frac{U(\theta)}{U} \sum_{K=-\infty}^{\infty} a_k e^{iK\nu\theta}$$

Now if the inflow distortion U (θ) is expanded in terms of a Fourier series with period 2π, U (θ) can be written as:

$$U(\theta) = U \sum_{\ell=-\infty}^{\infty}{}' b_\ell e^{i\ell\theta}$$

The inflow distortion interacting with the rotor is thus

$$V(\theta) = \sum_{\ell,K=-\infty}^{\infty}\sum a_K b_\ell e^{i(K\nu+\ell)\theta} \qquad \text{(C6)}$$

When the distortion given by (C6) interacts with the rotor, the circumferential duct modes generated are now given by

$$m = nB + kV + \ell$$

where ℓ represents the distortion harmonics in the flow upstream of the IGV's.

For low inflow harmonics of distortion (the case most likely to be met in practice due to ground effects, stand effects, etc.) the assumptions used to derive this result are good. The assumptions become weak for large values of ℓ because this would indicate rapid changes of U (θ) with θ. If the absolute magnitude of the inflow distortion harmonics, $|b_\ell|$, are monotonic decreasing, then the mode structure generated by rotor-IGV interaction with non-uniform inflow will consist of the primary circumferential mode given by $m = nB + kV$ (i.e., with $\ell=0$), and successively decreasing side modes about the primary, given by $m = nB + kV + 1$, $m = nB + kV + 2$, etc. This case is illustrated schematically in Figure C2.

Thus, nonuniform inflow imposed on a stator-rotor interaction, gives rise to side modes that would not exist if the inflow were uniform. It can be seen that this process can give rise to significant pressure levels in extraneous modes, not included in the modal calculation.

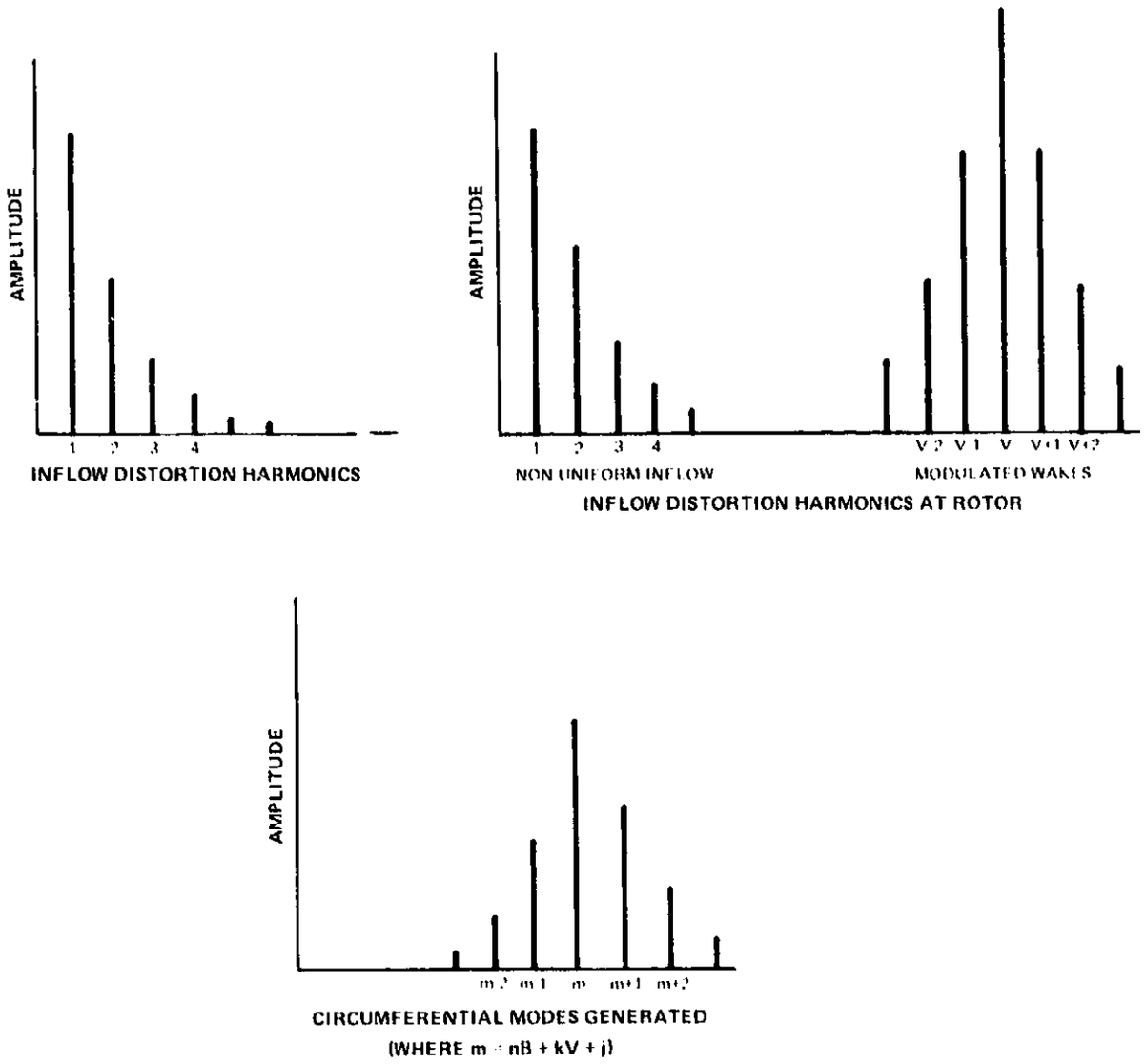

Figure C.2 Schematic of Circumferential Duct Modes Generated by Rotor-IGV Interaction With Nonuniform Axial Flow

APPENDIX D
ORDER-OF-MAGNITUDE ANALYSIS OF INFLUENCE COEFFICIENTS

In section 3.2.4 and Appendix B, closed form expressions were derived for the first order errors in calculated mode amplitude and phase due to errors in the knowledge of microphone location and errors in acoustic pressure measurements. These expressions, which are a set of partial derivatives, are termed influence coefficients. Since these coefficients are calculated along with every mode structure calculation, it is possible to use the values of the coefficients to determine the sensitivity of the method for fan sound mode structure determination for every modal calculation performed.

A need exists, however, to have some estimate of the sensitivity of the method for any given situation before conducting a test and before running the MCP. This estimate can be obtained from both a consideration of an order-of-magnitude analysis of the influence coefficients and a review of the experience gained (and reported on in section 3.5) from conducting this program. The objective of this Appendix is to present this order-of-magnitude analysis. The analysis will be presented separately for i) pressure amplitude and phase measurement errors, and ii) microphone location errors.

i) ANALYSIS OF PRESSURE AMPLITUDE AND PHASE ERRORS

Four influence coefficients ($\frac{\partial A_M}{\partial B_n}, \frac{\partial \phi_M}{\partial B_n}, \frac{\partial A_M}{\partial \psi_n}, \frac{\partial \phi_M}{\partial \psi_n}$) express the error in the calculated modal amplitudes and phases due to acoustic pressure measurement errors. The partial derivative,

$$\frac{\partial A_M}{\partial B_n} = \beta_{Mn} \cos(\beta_{Mn} + \psi_n - \phi_M) \qquad \text{(D1)}$$

obtained from equations (3.2-18), will be used to illustrate the order-of-magnitude analysis. The analysis for the other three partial derivatives is similar and not shown here. The combined standard deviation for a given pressure measurement standard deviation, taken to be the same at all locations, while assuming all other measurements are perfect, can be rewritten from (3.2-19) as:

$$\frac{\sigma_{A_M}}{A_M} = \frac{\sigma_B}{A_M} \sqrt{\sum_{n=1}^{N} \left(\frac{\partial A_M}{\partial B_n}\right)^2} \qquad \text{(D2)}$$

where σ_A and σ_B are the standard deviations of the amplitude error in the calculated mode and acoustic pressure measurement respectively.

It is convenient to initiate the order-of-magnitude analysis by examining the most probable magnitude of an element g_{Mn} in the inverse matrix $\underline{G}$. First, consider the original matrix $\underline{H}$ which can be written in full as:

$$H_{nM} = \begin{bmatrix} E_{11} e^{i\alpha_{11}} & E_{12} e^{i\alpha_{12}} & \cdots & E_{1M} e^{i\alpha_{1M}} \\ E_{12} e^{i\alpha_{21}} & E_{22} e^{i\alpha_{22}} & \cdots & E_{2M} e^{i\alpha_{2M}} \\ \vdots & \vdots & & \vdots \\ E_{n1} e^{i\alpha_{n1}} & \cdots & & E_{nM} e^{i\alpha_{nM}} \end{bmatrix} \quad \text{(D3)}$$

where $\alpha_{nM} = K_{xM} x_n + N_M \theta_n$ and $E_{nM} = E_{nM}(K_{M,\mu}^{\sigma} r_n)$ are consistent with the notation in Appendix A.

Since in most cases considered in this program, the duct microphones were located on the duct wall, and because of the simplification achieved in the ensuing analysis, in what follows, the microphones will be considered to be restricted to the duct wall. With this assumption, $E_{nM} = E_{nM}(K_{M,\mu}^{\sigma} b)$. That is, the E-functions are independent of microphone location. The determinant of the matrix H can then be expressed as:

$$\det \underline{H} = \left\{ \prod_{M=1}^{N} E_M \right\} \Delta_{n,n} \quad \text{(D4)}$$

where $\Delta_{n,n}$ is the NxN determinant of $\underline{H}$ with the E-functions factored out. The elements of the determinant are unit vectors. Similarly, the determinant of the co-factor transposed corresponding to the H_{nM} element, can be expressed as:

$$C_{Mn} = (-1)^{n+M} \frac{\prod_{M=1}^{n} E_M}{E_M} \Delta^{(M,n)}_{n-1,n-1} \quad \text{(D5)}$$

where $\Delta^{(M,n)}_{n-1,n-1}$ is the (N-1) x (N-1) determinant of the transposed co-factor of the nth row and mth column of the matrix H. The elements of this determinant are also unit vectors.

An element g_{MN} in the inverse matrix Q is defined by the ratio of the determinant of the co-factor transposed and the determinant. Thus, using the preceding relations (D4) and (D5) the modulus of the element g_{MN} becomes, after some simplifying:

$$g_{MN} = \frac{1}{E_M} \frac{\Delta^{(M,N)}_{N-1,N-1}}{\Delta_{N,N}} \tag{D6}$$

Combining equations (D1) and (D2) and using equation (D6) for g_{MN}:

$$\frac{\sigma A_M}{A_M} = \frac{\sigma B}{A_M} \sqrt{\sum_{n=1}^{N} \frac{1}{E_M^2} \frac{|\Delta^{(M,n)}_{N-1,N-1}|^2}{|\Delta_{N,N}|^2} \cos^2(\beta_{Mn} + \psi_n - \phi_M)} \tag{D7}$$

In order to obtain an order-of-magnitude analysis of equation (D7), the phase angles of the unit complex vectors in the two determinants Δ_{NN} and $\Delta^{(M,N)}_{N-1,N-1}$ and the phase angles $(\beta_{Mn} + \psi_n - \phi_M)$, denoted by η_{MN}, will be assumed statistically independent and uniformly distributed in $[0, 2\pi]$. Also, the total number of modes given by N will be assumed sufficiently large so that a reliable statistical analysis can be conducted. Although in fact the phase angles of the determinant and β_{MN} are determined once a set of microphone locations has been fixed, it is conjectured that if N is large, these angles will probably cover the range $[0, 2\pi]$ in a reasonably uniform manner for most cases considered. Experience from the program conducted under this contract indicates that the above assumptions are good. A comparison of the order-of-magnitude results from this Appendix with the exact values for the influence coefficients, shown in Figures 3.5-1 and 3.5-2, demonstrates that the order-of-magnitude results of this section are representative of the exact values.

Now, the determinant $\Delta_{N,N}$, consisting entirely of unit complex vectors can be expanded formally and written in the form;

$$\Delta_{N,N} = \sum_{j=1}^{N!} e^{i\gamma_j} \tag{D8}$$

Similarly

$$\Delta^{(M,n)}_{N-1,N-1} = \sum_{j=1}^{(N-1)!} e^{i\lambda_j} \tag{D9}$$

where δ_j is assumed to be independent of n so that the expressions for the determinant can be taken out of the summation over n in equation (D7). Substituting (D8) and (D9) into equation (D7) and squaring each side, the expected value of the variance of A_m can be written as:

$$\frac{E_x\{\sigma_A^2\}}{A_M^2} = \frac{\sigma_B^2}{A_M^2 E_M^2}\left[E_x\left\{\sum_{j=k=1}^{(N-1)!} e^{i(\delta_j-\delta_k)}\right\} \times E_x\left\{\frac{1}{N!\sum_{j=k=1}^{} e^{i(\gamma_j-\gamma_k)}}\right\} \times E_x\left\{\sum_{n=1}^{N}\cos^2\eta_{Mn}\right\}\right] \tag{D10}$$

The three expected value expressions in the RHS of equation (D10) will be considered separately recalling that all the γ_j, δ_j and η_{Mn} are statistically independent and uniformally distributed in $[0, 2\pi]$.

$$E_x\left\{\sum_{j=k=1}^{(N-1)!} e^{i(\delta_j-\delta_k)}\right\}$$

$$= E_x\left\{\sum_{j=1}^{(N-1)!} e^{0}\right\} + \sum_{j\neq k}^{(N-1)!}\int_0^{2\pi}\frac{1}{4\pi^2} e^{i(\delta_j-\delta_k)}\, d\delta_j\, d\delta_k$$

$$= (N-1)!$$

$$E_x\left\{\frac{1}{N!\sum_{j=k=1}^{} e^{i(\gamma_j-\gamma_k)}}\right\} \tag{D11}$$

$$= \frac{1}{(2\pi)^{N!}}\int_0^{2\pi}\cdots\int \frac{d\gamma_1\, d\gamma_2 \cdots\cdots d\gamma_{N!}}{\left\{N! + \sum_{j\neq k}^{N!} e^{i(\gamma_j-\gamma_k)}\right\}}$$

$$= \frac{1}{(2\pi)^{N!}}\int_0^{2\pi}\cdots\int \frac{d\gamma_1\, d\gamma_2 \cdots\cdots d\gamma_{N!}}{N! + \sum_{\substack{j\neq k\\ j,k\neq 1}}^{N!} e^{i(\gamma_j-\gamma_k)} + e^{i\gamma_1}\sum_{j=2}^{N!} e^{-i\gamma_j} + e^{-i\gamma_1}\sum_{j=2}^{N!} e^{i\gamma_j}}$$

Now, it was shown in Appendix E that $E_x\{|\sum_{j=1}^{N} e^{i\alpha_j}|^2\} = N$ for large N and with α_j, uniformly distributed in $[0, 2\pi]$. Thus, the denominator can be expanded, yielding for large N:

$$E_x\left\{\frac{1}{N!}\sum_{\substack{j,k=1\\ j\neq k}}^{N} e^{i(\gamma_j-\gamma_k)}\right\} = \frac{1}{(2\pi)^{N!}}\int_0^{2\pi}\int \frac{d\gamma_1 d\gamma_2 \cdots d\gamma_{N!}}{N!} \sum_{\substack{j,k=1\\ j\neq k\\ j,k\neq 1}}^{N!} e^{i(\gamma_j-\gamma_k)}\left[1 - e^{i\gamma_1}\sum_{j=2}^{N!} e^{-i\gamma_j}\right]$$

$$- e^{-i\gamma_1}\sum_{j=2}^{N!} e^{i\gamma_j} + O\left\{\frac{(N-1)!}{[N!]^2}\right\} d\gamma_1$$

$$= \frac{1}{(2\pi)^{N!-1}}\int_0^{2\pi}\cdots\int \frac{d\gamma_2 d\gamma_3 \cdots d\gamma_{N!}}{N!} + \sum_{\substack{j\neq k\\ j,k=2}}^{N!} e^{i(\gamma_j-\gamma_k)} + O\left[\frac{1}{N!^3}\right]$$

Continuing this process, for all N! integrations yields:

$$E_x\left\{\frac{1}{N!}\sum_{\substack{j,k=1\\ j\neq k}}^{N} e^{i(\gamma_j-\gamma_k)}\right\} = \frac{1}{N!} + O\left(\frac{1}{N!^3}\right) \qquad \text{(D12)}$$

$$E_x\left\{\sum_{n=1}^{N}\cos^2\eta_{Mn}\right\} = \frac{1}{2\pi}\int_0^{2\pi}\sum_{n=1}^{N}\cos^2\eta_{Mn}\, d\eta_{Mn}$$

$$E_x\left\{\sum_{n=1}^{N}\cos^2\eta_{Mn}\right\} = \frac{N}{2} \qquad \text{(D13)}$$

Substituting (D11), (D12) & (D13) in (D10):

$$\frac{E_x\{\sigma_{A_M}^2\}}{A_M^2} = \frac{\sigma_B^2}{A_M^2 E_M^2}\,\frac{(N-1)!\,\frac{N}{2}}{N!}$$

or

$$\frac{E_x\{\sigma_{A_M}^2\}}{A_M^2} = \frac{1}{2}\,\frac{\sigma_B^2}{A_M^2 E_M^2} \qquad \text{(D14)}$$

Equation (D14) relates the expected variance of the modal calculation with the variance associated with the errors in acoustic pressure amplitude measurement. In a similar manner, similar expressions can be obtained for the other three influence coefficients associated with measurement errors. They are:

$$\begin{aligned} \lambda\{\sigma_{A_{mn}}^2\} &= \frac{B_n^2 \sigma_\psi^2}{A_{ij}^2} \\ \lambda\{\sigma_{\phi_{mn}}^2\} &= \frac{\sigma_\beta^2}{A_{ij}^2 E_{ij}^2} \\ \lambda\{\sigma_{\phi_{ij}}^2\} &= \frac{B_n^2 \sigma_\psi^2}{A_{ij}^2 E_{ij}^2} \end{aligned} \qquad \text{(D15)}$$

where

$$B_n^2 = \sum_{n=1}^{N} B_n^2$$

If probe microphones had been used, the expressions (D14) and (D15) would be much more complicated. However, for cases where [illegible] are the same order-of-magnitude, the above expressions can be used to represent the order-of-magnitude although the approximation is not as good as the case for just wall mounted microphones.

ANALYSIS OF MICROPHONE LOCATION ERRORS

Six influence coefficients [illegible] express the error in the calculated modal amplitudes and phases due to errors in the knowledge of microphone locations. The partial derivative from equation (3.2-18).

[illegible] (D16)

will be used to illustrate the order-of-magnitude analysis. The analysis for the other five influence coefficients is similar. The combined standard deviation for axial location errors at all microphone locations while assuming all other errors are zero is:

(D17)

Substituting (D16) in (D17) and using the result (see equation (3.2-13):

Again, the microphones will be assumed restricted to the wall so that $E_{ns} = E_s$ Squaring and taking the expected values of each side (assuming as before that the η_{mns} are statistically independent and uniformly distributed in $[0, 2\pi]$):

(D18)

In a similar manner, expressions for the remaining five influence coefficients are:

(D19)

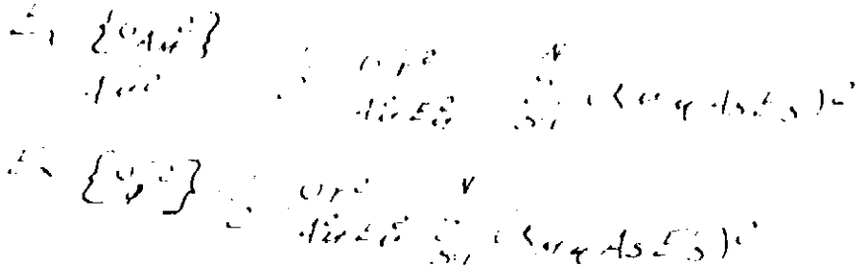

where

The expressions given by (D14), (D15), (D18), and (D19) represent order-of-magnitude estimates of the expected variances of modal amplitude and phase, due to the five possible error types represented by the variances associated with microphone location and pressure measurement errors. These variances are used in section 3.5 to determine the utility and required experimental accuracy of the modal calculation method.

APPENDIX F

ANALYSIS FOR THE STANDARD DEVIATION OF THE ERROR IN PRESSURE MEASUREMENT DUE TO EXTRANEOUS MODES

If the total number of modes propagating in a fan inlet duct is N_P and the number of modes used in the modal calculation is N, then the number of extraneous modes is $(N_P - N)$. If the contribution to the total measured pressure amplitude and phase at any given location of the nth mode are A_n and ϕ_n respectively, for n = 1, 2, . . . N_P, the resultant of the total acoustic field at that point can be written as:

$$B e^{i\psi} = \sum_{n=1}^{N_P} A_n e^{i\phi_n} \tag{F-1}$$

The resultant due to the modes included in the calculation is:

$$b e^{i\beta} = \sum_{n=1}^{N} A_n e^{i\phi_n} \tag{F-2}$$

and the resultant due to the extraneous modes is:

$$c e^{i\gamma} = \sum_{n=N+1}^{N_P} A_n e^{i\phi_n} \tag{F-3}$$

Thus, at the given location

$$B e^{i\psi} = b e^{i\beta} + c e^{i\gamma} \tag{F-4}$$

The square of the amplitude of the total sound field, B^2, can be obtained by separating the complex functions into real and imaginary parts and by trigonometrical manipulation, thus,

$$B^2 = b^2 + c^2 + 2bc \cos\beta \cos\gamma + 2bc \sin\beta \sin\gamma \tag{F-5}$$

Expressions for $R \cos\delta$ and $R \sin\delta$ can be obtained from the real and imaginary parts of equation (F-3) and R^2 can be obtained as follows:

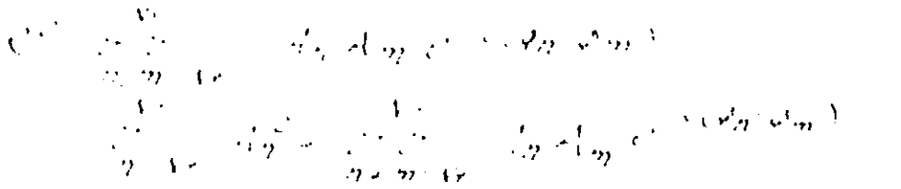

Equation (F-4) then becomes:

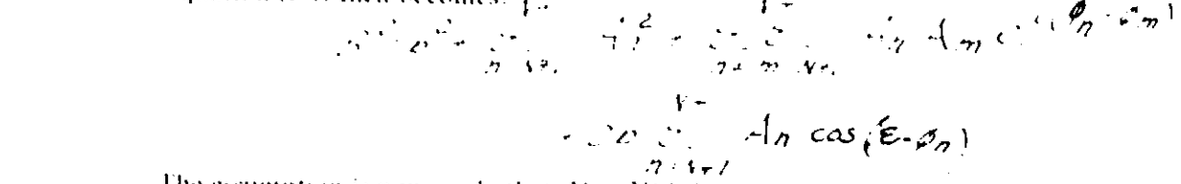

$$= b^2 + \sum_{n=N+1}^{N_T} A_n \cos(\xi - \phi_n) \qquad \text{(F-6)}$$

The assumption is now made that $(N_T - N)$ is large and that at any duct location the phases of the extraneous modes can be considered to be uniformly distributed in $[0, 2\pi]$ and can be treated as statistical variables. If the amplitudes of the extraneous modes are also considered as statistical variables with mean $\bar{A}_{N+M}$ and a probability distribution function P_{An}, and if the A_n and ϕ_n are assumed to be statistically independent, an expected value for $(B^2 - b^2)$ can be obtained, which can be considered as the variance in the amplitude measurement error due to the contribution to the sound field of all the extraneous modes. That is $\sigma_B^2 = E_x\{B^2 - b^2\}$, where the operator $E_x\{\ \}$ denotes that the expected value is to be taken.

The assumptions used in this analysis can be justified on the basis that for typical turbofan engine inlets, the total number of duct modes is very large and thus the number of modes omitted from the modal calculation $(N_T - N)$ also will be large. The amplitudes and phases of these modes — although, strictly speaking deterministic — can be considered to be statistically independent variables because there is generally no simple reason for specific extraneous modes to favor particular amplitudes and the phases of these modes change at different rates as new locations are considered.

Taking the expected values of equation (F-6):

$$\sigma_B^2 = E_x\left\{\sum_{n=N+1}^{N_T} A_n^2 + \sum_{n\neq m=N+1}^{N_T}\sum A_n A_m e^{i(\phi_n - \phi_m)} + 2b\sum_{n=N+1}^{N_T} A_n \cos(\xi - \phi_n)\right.$$

which from the assumptions stated earlier becomes:

$$\sigma_B^2 = \frac{V_r}{n \neq m} \int_{-\infty}^{\infty} A_n \cdot A_n \cdot dA_n +$$

$$\frac{V_r}{n \neq m} V_r \iint \iint A_n \cdot A_m \cdot A_n \cdot A_m e^{i(\phi_n - \phi_m)} \cdot dA_n \cdot dA_m d\phi_n d\phi_m$$

$$\frac{1}{n \neq m} \frac{1}{V_r} \iint A_n \cdot A_n \cos(\phi_n - \phi_n) \cdot dA_n \cdot d\phi_n$$

Since the last two terms integrate to zero (because of the uniformly distributed phase),

$$\sigma_B^2 = \frac{1}{n \neq m} \overline{A^2}_{FM}$$

$$\sigma_B = \frac{1}{n \neq m} \overline{A^2}_{FM}$$

where $\overline{A^2}_{FM}$ is the mean square amplitude of these extraneous modes.

Thus, the standard deviation in the acoustic amplitude measurement error due to the contribution of extraneous modes is:

$$\sigma_B = \frac{1}{n \neq m} \overline{A^2}_{FM}$$

This expression for σ_B due to extraneous modes is used in the main body of the report to obtain order-of-magnitude estimates of the effect on the modal calculation method of a large number of extraneous modes.